Chem Soc Rev

REVIEW ARTICLE

View Article Online
View Journal | View Issue

Cite this: *Chem. Soc. Rev.*, 2023, **52**, 5255

Insights into the solvation chemistry in liquid electrolytes for lithium-based rechargeable batteries

Peitao Xiao, *[a] Xiaoru Yun,[a] Yufang Chen,[a] Xiaowei Guo,[b] Peng Gao,[c] Guangmin Zhou *[d] and Chunman Zheng *[a]

Lithium-based rechargeable batteries have dominated the energy storage field and attracted considerable research interest due to their excellent electrochemical performance. As indispensable and ubiquitous components, electrolytes play a pivotal role in not only transporting lithium ions, but also expanding the electrochemical stable potential window, suppressing the side reactions, and manipulating the redox mechanism, all of which are closely associated with the behavior of solvation chemistry in electrolytes. Thus, comprehensively understanding the solvation chemistry in electrolytes is of significant importance. Here we critically reviewed the development of electrolytes in various lithium-based rechargeable batteries including lithium–metal batteries (LMBs), nonaqueous lithium-ion batteries (LIBs), lithium–sulfur batteries (LSBs), lithium–oxygen batteries (LOBs), and aqueous lithium-ion batteries (ALIBs), and emphasized the effects of interactions between cations, anions, and solvents on solvation chemistry, and functions of solvation chemistry in different types of electrolytes (strong solvating electrolytes, moderate solvating electrolytes, and weak solvating electrolytes) on the electrochemical performance and redox mechanism in the abovementioned rechargeable batteries. Specifically, the significant effects of solvation chemistry on the stability of electrode–electrolyte interphases, suppression of lithium dendrites in LMBs, inhibition of the co-intercalation of solvents in LIBs, improvement of anodic stability at high cut-off voltages in LMBs, LIBs and ALIBs, regulation of redox pathways in LSBs and LOBs, and inhibition of hydrogen/oxygen evolution reactions in LOBs are thoroughly summarized. Finally, the review concludes with a prospective outlook, where practical issues of electrolytes, advanced *in situ*/*operando* techniques to illustrate the mechanism of solvation chemistry, and advanced theoretical calculation and simulation techniques such as "material knowledge informed machine learning" and "artificial intelligence (AI) + big data" driven strategies for high-performance electrolytes have been proposed.

Received 28th February 2023

DOI: 10.1039/d3cs00151b

rsc.li/chem-soc-rev

1. Introduction

Over the past three decades, lithium-ion batteries (LIBs) have overwhelmingly dominated the field of rechargeable batteries since their first commercialization based on $LiCoO_2$||graphite by Sony in the 1990s. The success, in turn, spurred worldwide research on novel electrochemistry to meet the increasing demands for storage systems with high energy/power density, low cost and intrinsic safety.[1,2] Consequently, various metal–sulfur batteries[3–6] and metal–air batteries,[7,8] LIBs with silicon, lithium metal anodes or high-voltage cathodes, have been extensively investigated to increase the energy density, rechargeable batteries with aqueous or solid-state electrolytes have also been explored to improve their intrinsic safety,[9,10] and sodium or potassium-based batteries have been studied to reduce the cost.[11–13] As the media to transport ions, electrolytes are indispensable and ubiquitous in all rechargeable batteries. Moreover, electrolytes are sandwiched between positive and negative electrodes, which directly interact with cathodes and anodes, determining the stability of electrode–electrolyte

[a] *College of Aerospace Science and Engineering, National University of Defense Technology, Changsha, Hunan, 410073, China. E-mail: xiaopt@nudt.edu.cn, xpt_fdu@126.com, zhengchunman@nudt.edu.cn*
[b] *College of Computer, National University of Defense Technology, Changsha, Hunan, 410073, China*
[c] *College of Materials Science and Engineering, Hunan Joint International Laboratory of Advanced Materials and Technology of Clean Energy, Hunan Province Key Laboratory for Advanced Carbon Materials and Applied Technology, Hunan University Changsha, Changsha, Hunan, 410082, China*
[d] *Tsinghua-Berkeley Shenzhen Institute & Tsinghua, Shenzhen International Graduate School, Tsinghua University, Shenzhen 518055, China. E-mail: guangminzhou@sz.tsinghua.edu.cn*

interfaces and the corresponding electrochemical performance. Thus, compatible electrolytes are urgently demanded and required for novel electrodes. This is the reason why the number of peer-reviewed articles about electrolytes has exponentially increased since 1990, especially after 2010, as shown in Fig. 1a.

As one of the key components in rechargeable batteries, electrolytes play a much more important role than just as the media to transport ions between electrodes. As shown in Fig. 1b, the energy level of the lowest unoccupied molecular orbital (LUMO) of electrolytes is lower than the Fermi level of anodes, that is, electrolytes in contact with anodes are prone to be reduced, leading to the formation of solid–electrolyte interphases (SEIs) on the surface of anodes. Similarly, electrolytes are susceptible to oxidation, leading to the construction of a cathode–electrolyte interphase (CEI) because of the higher energy level of the highest occupied molecular orbital (HOMO) of electrolyte than that of cathodes. The stability of the electrode–electrolyte interphase (EEI, including the SEI and CEI) is pivotal in manipulating the electrochemical stable potential window (ESPW) and cycling lifespan. Since the concept of the "SEI" was proposed by Pelad in 1979, tremendous attention has been attracted toward its functions and mechanism.[14–16] Researchers have gradually realized that the EEI is highly related with the cation's solvation structures in the electrolytes. Moreover, Xu precisely identified that the de-solvation process of Li^+ in LIBs is the rate-determining step during the electrochemical process, highly affecting the electrochemical kinetics, especially at low temperatures,[17,18] implying the significance of solvation chemistry in electrolytes for high-performance batteries.

Electrolytes are usually composed of salts, solvents, and/or functional additives. For example, in the case of common electrolytes in LIBs, when they are dissolved in solvent, lithium salts dissociate into cations (Li^+) and anions, and solvation sheaths of Li^+ (Li^+–solvent complexes) form simultaneously due to the stronger interaction between Li^+ and solvents than that of Li^+ and anions, which shuttle between the cathode and

Peitao Xiao

Peitao Xiao received his BS degree and MS degree from Tianjin University in 2010 and 2013, respectively, and PhD degree from Fudan University in 2019. Then he worked as a research engineer at Envision AESC and postdoc fellow at Tsinghua University. Now he is an assistant professor at the National University of Defense Technology. His research interests include rechargeable batteries with high energy density and intrinsic safety.

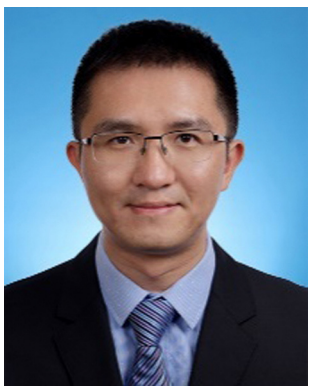

Guangmin Zhou

Guangmin Zhou is an associate professor at Tsinghua Shenzhen International Graduate School, Tsinghua University. He received his PhD degree from the Institute of Metal Research, Chinese Academy of Sciences in 2014 under the supervision of Prof. Hui-Ming Cheng and Prof. Feng Li, and then worked as a postdoc fellow at UT Austin with Prof. Arumugam Manthiram during 2014–2015. After that, he was a postdoc fellow at the Department of Materials Science and Engineering at Stanford University with Prof. Yi Cui from 2015 to 2019. His research mainly focuses on the development of advanced energy-storage materials and devices, and battery recycling.

Chunman Zheng

Prof. Chunman Zheng obtained his BS and PhD degrees from the National University of Defense Technology in 2000 and 2006, respectively. Then he joined the faculty of the National University of Defense Technology in 2007. He was a visiting scholar at the University of St. Andrew in 2012 and is currently a Head Professor of material science and engineering. Professor Zheng's current research interests include new electrode materials, high-performance energy storage devices, power supplies, and systems for extreme environments.

Peng Gao is currently an assistant professor at the College of Materials Science and Engineering at Hunan University in China. He received his MS degree in materials science from Tianjin University, China, in 2013 and PhD degree in materials science and engineering from the New York State College of Ceramics, Alfred University, USA, in 2018. His current research interests include 2D materials synthesis and defect engineering for enhanced electrochemical energy storage, and synchrotron-based in situ characterization (XRD, XAFS, X-ray total scattering, and PDF analysis) for in-depth understanding of charge storage mechanisms.

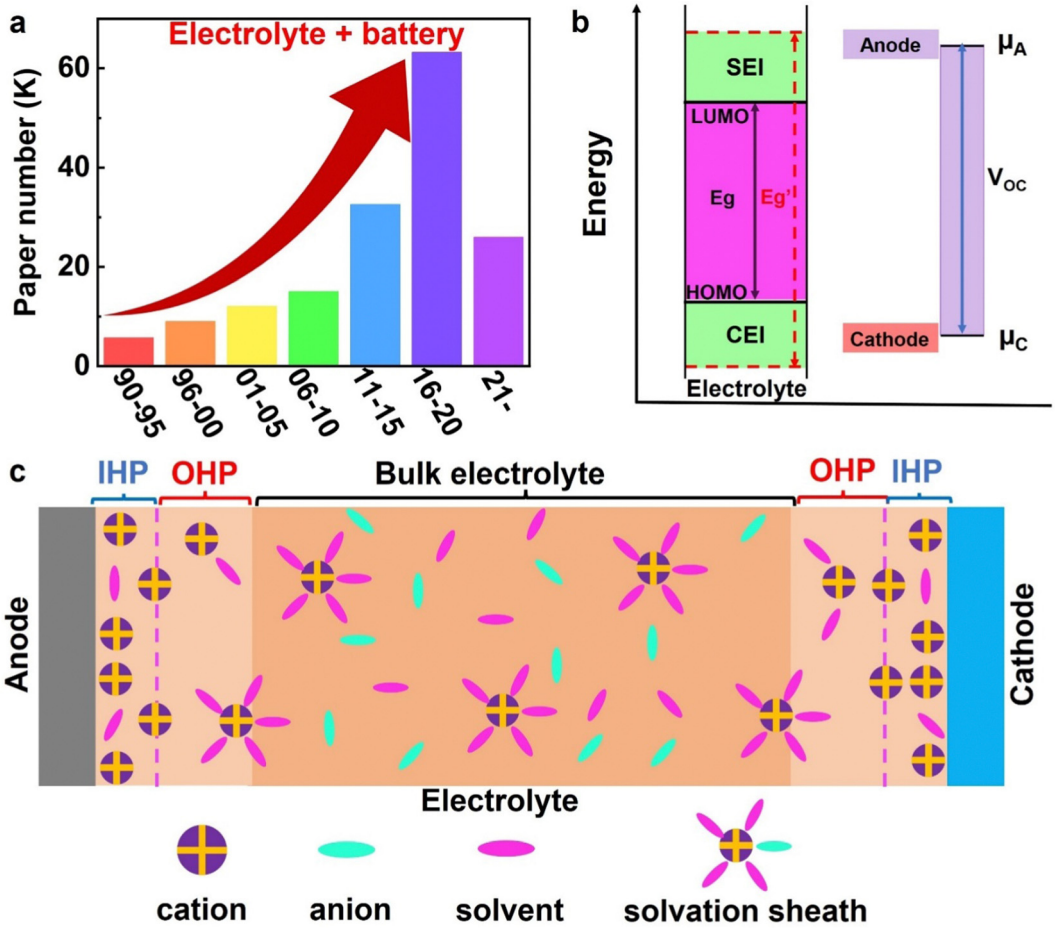

Fig. 1 (a) Number of peer-reviewed papers about electrolytes published from 1990. (b) Representative energy levels of molecular orbitals for different components in rechargeable batteries. (c) Illustration of the distribution of cations, anions, and solvents, and the corresponding electrochemical processes in electrolytes during the electrochemical process.

anode during the electrochemical process. As shown in Fig. 1c, the solvated cations firstly transport, as Li^+ solvation sheaths, in the bulk electrolyte to electrodes. Secondly, the Li^+ solvation sheath moves into the outer layer of the double electrical layer (outer Helmholtz plane, OHP), followed by the de-solvation of Li^+. Because the thickness of the inner layer in the double electrical layer (inner Helmholtz plane, IHP) is smaller than the size of the Li^+ solvation sheath, only single ions or solvent molecules exist in the IHP.[19] Thirdly, ions or solvents adsorbed on the surface of electrodes are preferably decomposed to form the EEI. Finally, Li^+ transfers through the EEI, either depositing on the surface of the anode, or moving into the electrodes.[20–22]

Fully understanding the interactions of cations, anions, and solvents is the prerequisite to regulate the solvation chemistry in liquid electrolytes. Typically, cation–solvent, cation–anion, anion–solvent, and solvent–solvent interactions co-exist in the electrolytes (Fig. 2). Moreover, there are other types of interactions, such as the interactions between discharge or charge intermediates and solvents in lithium–sulfur (LSBs) or lithium–oxygen batteries (LOBs) and solvent–solvent interactions in aqueous zinc-ion batteries. These interactions are highly related with the expansion of ESPW, manipulation of kinetics, regulation of the reaction mechanism and suppression of side reactions in the batteries (Fig. 2). For instance, the relative affinity intensity of cation–solvent to cation–anion determines the salt solubility, that is, when cation–solvent interaction is significantly stronger than that of cation–anion, salt dissolves easily in the solvent. Generally, the larger the relative interaction intensity of cation–solvent to cation–anion complexes, the higher the solubility of lithium salts, and the larger the transfer number of cations. More importantly, the relative interaction intensity of these two complexes determines the solvation structures of Li^+ (solvent-separated ion pairs, SSIPs; contact ion-pairs, CIPs; or ion aggregates, AGGs).[23,24] The interaction between cations and solvents strengthens the oxidation stability and weakens the reduction stability of the solvents, while further incorporation of anions into the cation–solvent complex has the opposite effect, which significantly influences the interfacial stability, and the corresponding ESPW and cycling lifespan.[25,26] Besides, the interaction between cations and solvents or anions in the solvation structure highly influences the de-solvation process and the

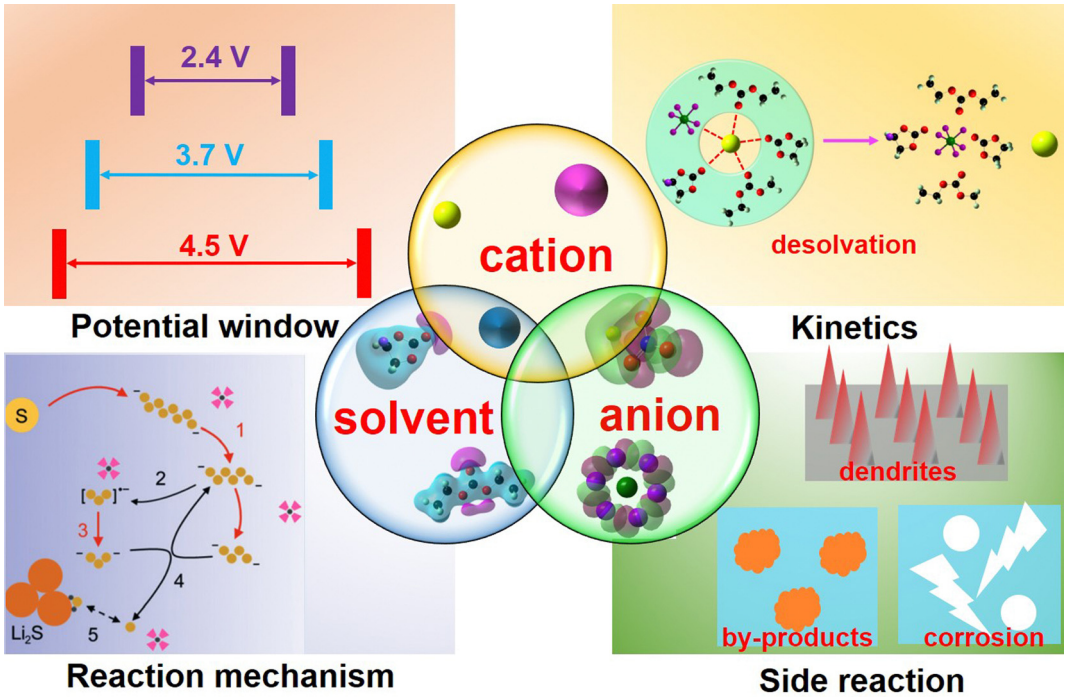

Fig. 2 Illustration of the interaction types in the electrolytes, and their relations with ESPW, kinetics, reaction mechanism,[30] and side reactions.

corresponding electrochemical kinetics. Therefore, these interactions determine both the properties of bulk electrolytes and interfacial behavior, concomitantly, the performance of rechargeable batteries.

Many strategies have been deliberately designed to improve the electrochemical performance by tailoring the solvation chemistry in electrolytes. For instance, Suo *et al.* first proposed the concept of "salt in solvent" electrolyte by increasing the ratio of salt to solvent, in which the solvation structure of Li^+ was completely different from that in conventional dilute electrolyte. As a result, the "salt in solvent" electrolyte in LSBs not only supressed the formation of lithium dendrites, but also inhibited the "shuttle effect" of lithium polysulfides.[27] Fan *et al.* regulated the cation–solvent interaction by incorporation of fluorinated solvents, substantially broadening the ESPW (5.4 V *vs.* Li^+/Li) and operating temperature range (from −95 to 70 °C) in lithium–metal batteries (LMBs).[28] Antisolvents were also adopted to tune the solvation chemistry of the aqueous electrolyte on a molecular level in zinc-ion batteries, resulting in dendrite-free deposition and enhanced Zn reversibility.[29]

Up to now, substantial progress has been made in the fundamental research on electrolytes, and there are excellent reviews on functional electrolytes. These reviews partially summarize the development of electrolytes in one specific type of battery, and one specific type of electrolyte in various battery systems,[23,31] or comprised of comprehensive overviews of the electrolyte development over a specific period.[32,33] To our best knowledge, a comprehensive review focus on fundamental understanding and strategies of regulating solvation chemistry in different types of electrolytes is lacking. An in-depth understanding of the fundamental mechanism of solvation chemistry and a comprehensive overview of the regulation strategies in different electrolytes not only provide a timely and critical overview of the latest development in this filed, but also shed light on the design of novel electrolytes for next-generation batteries based on solvation chemistry regulation.

In this review, we particularly focus on the fundamental scientific understanding of solvation chemistry, strategies for regulating solvation chemistry in different electrolytes, and perspectives in designing advanced electrolytes based on solvation chemistry. Five representative types of lithium-based rechargeable batteries, including LMBs, nonaqueous LIBs, LSBs, LOBs, and aqueous LIBs are chosen in this review; since the main challenges in those five different battery systems are different, the emphases of solvation chemistry and regulating strategies in those five battery systems are also different. Other metal-based (Na, K, Zn, *etc.*) battery systems are not involved because these electrochemical systems may face similar challenges and adopt analogous strategies to their corresponding lithium-based battery systems. For instance, LSBs are adopted to represent sodium/potassium–sulfur batteries,[34–36] LMBs represent sodium/potassium metal batteries,[37–39] and aqueous LIBs represent other aqueous batteries.[10,40–42]

2. Criteria for classifying solvation chemistry in electrolytes

Among these different interactions, cation–solvent and cation–anion interactions are two dominant factors greatly influencing the solvation chemistry in electrolytes. In conventional electrolytes using solvents with moderate solvating ability, defined as

"moderate solvating electrolyte" (MSE), the interaction between cations and solvent moderately outstrips that between cations and anions. Likewise, "strong solvating electrolyte" (SSE) is the one using a strong solvating solvent, in which the interaction between cations and solvent far exceeds that of cation–anion, while "weak solvating electrolyte" (WSE) refers to that in which the cation–solvent interaction is relatively weak, but still stronger than that of cation–anion. It is worth noting that there are no absolute parameters to classify these three types of electrolytes, we usually fix lithium salts or solvents to define whether the electrolytes are MSE, SSE, or WSE. Although there are no specific parameters or absolute criteria to discriminate these three types of electrolytes, some parameters such as the dielectric constant and donor/acceptor number are vital to illustrate the solvating power of the solvents in electrolytes.

2.1. Dielectric constant

Dielectric constant (DC, donated as ε) of a material is the ratio of its permittivity to that of vacuum. DC is an important parameter to measure the chemical polarity of solvents, which indicates their ability to dissociate lithium salts, that is, in electrolytes using the same lithium salt, cation–solvent interactions increase with the improvement of solvents' DC, enhancing the solubility of lithium salts and resulting in more mobile conductive ions in the electrolyte. This is one of the reasons why ethylene carbonate (EC, DC: 89.78) has been the main solvents for decades in commercial LIBs. The DCs of typical solvents are listed in Table 1. It is clearly shown that DCs of cyclic carbonate are much higher than those of linear carbonates or ethers. It is noted that the viscosity (η) of solvents with high DC is also high, which inhibits the mobility of conductive Li^+. Thus, solvents with high DC and those with low DC and small viscosity are usually mixed as the solvents in electrolytes.

2.2. Donor number

The Gutmann donor number (DN), based on the heat of reaction between the compound dissolved in 1,2-dichloroethane and antimonic(v) chloride, is the measure of the strength of solvents as Lewis bases. When the DN of the solvent exceeds that of anions, lithium salt is prone to dissociation due to the strong Lewis base–acid interactions between cations and solvent. For instance, lithium nitrate ($LiNO_3$) hardly dissolves in carbonate, while it has a higher solubility in ether with a higher DN (Table 1).[43] Therefore, regulating the DN of the solvents is an effective way to tailor the solvation chemistry in electrolytes.

2.3. Relative solvating power and other emerging parameters

Although both DC and DN are two prevalent parameters used to illustrate the solvating ability of different solvents to dissociate lithium salts, controversy still exists: solvents have high a DC but a low DN.[45] For example, in the case of EC and 1,2-dimethoxyethane (DME), compared with DME, EC has a higher DC and lower DN, which may lead to confusion when choosing solvents to tailor the solvation chemistry. Therefore, an unambiguous parameter is highly desired for different solvents. Amine *et al.*, using internally referenced diffusion-ordered

Table 1 Properties of the typically used solvents in electrolytes

Solvents	Molecular formula	T_m (°C)	T_b (°C)	η (cP) 25 °C	ε 25 °C	DN (kcal mol^{-1})
Ethylene carbonate (EC)	$C_3H_4O_3$	36.4	248	1.9 (40 °C)	89.78	16.4
Propylene carbonate (PC)	$C_4H_6O_3$	−48.8	242	2.53	64.92	15
Fluoroethylene carbonate (FEC)	$C_3H_3O_3F$	18	249	—	—	—
N-Methyl-2-pyrrolidinone(NMP)	CH_5H_9NO	−24	202	—	32	—
γ-Butyrolactone(γ-BL, GBL)	$C_4H_6O_2$	−43.5	204	1.73	39	18
Dimethyl carbonate (DMC)	$C_3H_6O_3$	4.6	91	0.59 (20 °C)	3.11	17.2
Diethyl carbonate (DEC)	$C_5H_{10}O_3$	−74.3	126	0.75	2.81	16
Ethyl methyl carbonate (EMC)	$C_4H_8O_3$	−53	110	0.65	2.96	—
Ethyl acetate (EA)	$C_4H_8O_2$	−84	77	0.45	6.02	17.1
1,3-Dioxolane (DOL)	$C_3H_6O_2$	−95	78	0.59	7.1	21.2
1,2-Dimethoxyethane (DME)	$C_4H_{10}O_2$	−58	84	0.46	7.2	20
Ethylene glycol diethyl ether (DEE)	$C_6H_{14}O_2$	−74	121	—	—	—
Tetraglyme	$C_{10}H_{22}O_5$	−30	275			
Tetrahydrofuran (THF)	C_4H_8O	−109	66	0.46	7.4	20
2-Methyltetrahydrofuran (2-Me-THF)	$C_5H_{10}O$	−137	80	0.47	6.2	12
Trimethyl phosphate (TMP)	$C_3H_9O_4P$	−46	197	—	21.26	23
Triethyl phosphate (TEP)	$C_6H_{15}O_4P$	−56.5	215	—	13.0	26
Dimethyl sulfoxide (DMSO)	C_2H_6OS	18	189	2.24	46.68	29.8
Water	H_2O	0	100	1	80.1	18
Acetonitrile (AN, ACN)	C_2H_3N	−43.8	81.65	—	36.64	14
Tetramethylene sulfone (TMS)	$C_4H_8O_2S$	27	285	10.3	44	14.8
Tris(2,2,2-trifluoroethyl)orthoformate (TFEO)	$C_7H_7F_9O_3$	—	144–146	—	1.97	—
1,1,2,2-Tetrafluoroethyl-2,2,3,3-tetrafluoropropyl ether (TTE)	$C_5H_4F_8O$	—	93.2	—	1.43	—
Bis(2,2,2-trifluoroethyl)ether (BTFE)	$C_4H_4F_6O$	—	62–63	—	0.7	—
1,2-(1,1,2,2-Tetrafluoroethoxy)ethane (TFEE)	$C_6H_6F_8O_2$	—	141	—	—	—
1*H*,1*H*,5*H*-Octafluoropentyl1,1,2,2-tetrafluoroethyl ether (OTE)	$C_7H_4F_{12}O$	—	133[44]	—	—	—
1,1,2,2-Tetrafluoro-1-(2,2,2-trifluoroethoxy)ethane	$C_4H_3F_7O$	—	56	—	—	—

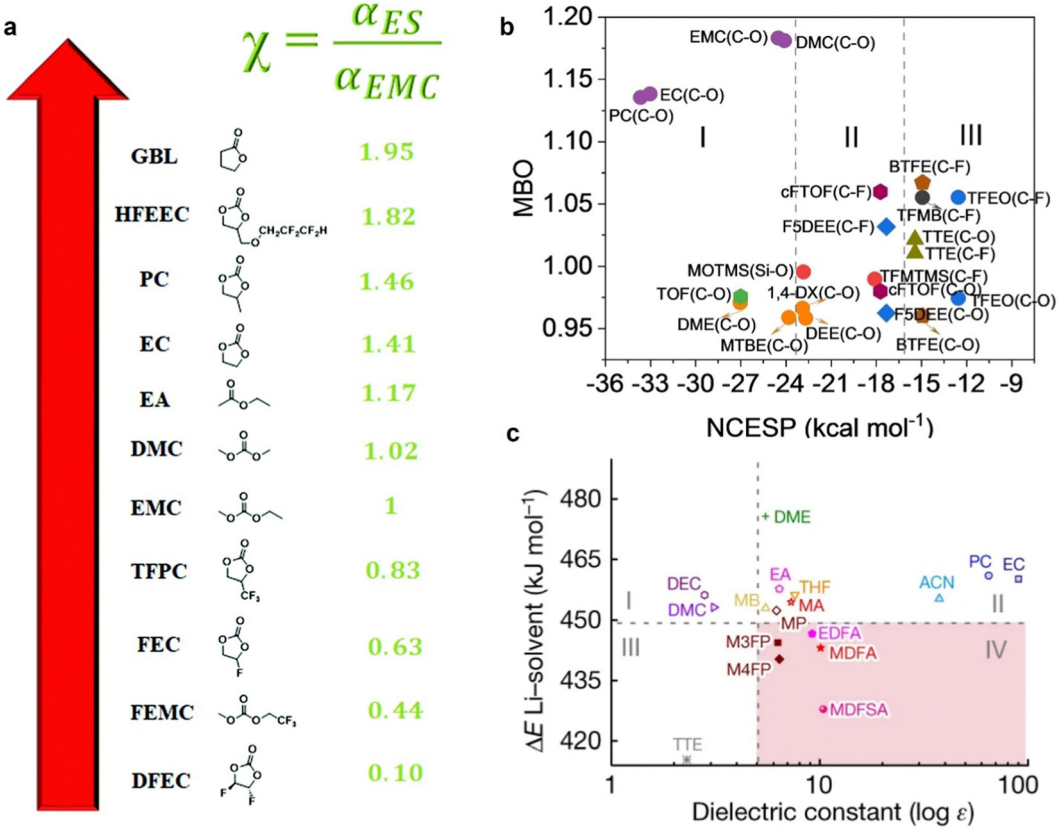

Fig. 3 (a) The relative solvating power of different solvents with EMC as the reference solvent. Reproduced with permission.[45] Copyright 2019 Royal Society of Chemistry. (b) Solvent diagram of the Mayer bond order (MBO) and negative center of electrostatic potential (NCESP). Reproduced with permission.[50] Copyright 2023 Wiley. (c) The solvent diagram of Li^+–solvent binding energy *versus* dielectric constant. Reproduced with permission.

nuclear magnetic resonance spectroscopy (IR-DOSY), defined the relative solvating power (χ) of individual solvent, which is the ratio of the coordination percentage of a test solvent to that of a reference solvent.[45–47] Unlike DC and DN, which are not sensitive to steric hindrance or denticity and thus not directly correlated with the solvating ability precisely, the relative solvating power is an unequivocal parameter to exhibit the solvating power of solvents, as shown in Fig. 3a. Compared with EMC, fluorinated solvents such as 4-(trifluoromethyl)-1,3-dioxolan-2-one (TFPC), FEC, and methyl-(2,2,2-trifluoroethyl)-carbonate (FEMC) exhibit weaker solvating power, while solvents including GBL, PC, EA, *etc.* exhibit stronger solvating ability. Moreover, the relative solvating power of EC is 1.41, while that of FEC and di-fluoroethylene carbonate (DFEC) is 0.63 and 0.1, respectively, implying that solvating power of individual solvent decreases with the increase in the fluorination degree.

Besides these parameters obtained by experiments, other parameters derived from theoretical calculation or simulation, including surface electrostatic potential, binding energy between different components,[48] positive maximum of the electrostatic potential energy,[49] negative center of electrostatic potential,[50] have also been widely adopted recently to investigate the affinity between ions and solvents.

These above-discussed parameters are all widely adopted to evaluate the ability of solvents to solvating Li^+, that is, to assess the intensity of cation–solvent interactions. Because of the small radius of Li^+ as a strong Lewis acid, the interactions between Li^+ and anions are very strong in most of the simple lithium compounds, such as LiF, Li_2O, and Li_2CO_3, which have poor solubility, especially in organic electrolytes, making them unsuitable as lithium salts.[33] There are only a few lithium compounds with complex anions used as lithium salts, including lithium hexafluorophosphate ($LiPF_6$), lithium tetrafluoroborate ($LiBF_4$), lithium bis(fluorosulfonyl)imide (LiFSI), lithium bis(trifluoromethylsulphonyl)imide (LiTFSI), lithium bis(oxalate) borate (LiBOB), lithium difluoro(oxalato)borate (LiDFOB), lithium difluorophosphate (LiDFP), $LiNO_3$, *etc.* In these lithium salts, different anions exhibit completely disparate interactions with lithium ions, that is, the cation–anion interactions are different in various lithium salts. For instance, the intensity of cation–anion interaction in LiFSI is much lower than that in $LiNO_3$, and this is the reason why LiFSI is prone to dissolution in organic solvents compared to $LiNO_3$. However, there is usually only one type of lithium salt, or only one kind of lithium salt dominates in electrolytes, that is, the interactions of cation–anion in electrolytes are usually stable, while those of cation–solvents vary dramatically. Therefore, the following sections mainly focus on regulation of cation–solvent interactions and their effects on solvation chemistry and the corresponding electrochemical performance.

In this section, although parameters such as the dielectric constant or donor number are widely used to evaluate the solvating power of solvent or anions, sometimes controversial conclusions are obtained from these parameters of solvents. For instance, compared with DOL, EC has a higher value of DC (89.78) but a lower DN (16.4 kcal mol^{-1}), which makes it difficult to evaluate the order of the solvating power for these two molecules. Then, the relative solvating power (the solvating ability ratio of a test solvent to a reference solvent) was proposed. Recently, other parameters such as NCESP and Li^+–solvents binding energy have also been adopted to evaluate the solvating ability of different solvents (Fig. 3b and c). Although these parameters are only used to assess the solvating power for several solvents, they demonstrate the possibility of designing a unified parameter to evaluate the solvating power of all the commonly used solvents in electrolytes. The development of a sophisticated and standard parameter to evaluate the solvating power of electrolytes is more intriguing, although it is a highly challenging task to precisely classify the electrolytes based on the solvating ability.

3. Strategies for regulating the solvation chemistry in LMBs

Owing to the ultrahigh specific energy (3860 mA h g^{-1}) and extremely low redox potential (−3.04 V *vs.* standard hydrogen electrode) of lithium metal, lithium metal batteries were first developed by M. Stanley Whittingham in 1970s. However, their further commercial application had been impeded by the safety issues induced by lithium dendrites.[51] Recently, lithium metal batteries have been revitalized to overcome the limited energy density of commercial LIBs. To further improve the energy density and strengthen their adaptability of extreme environments, high-voltage lithium metal batteries with wide operating temperature ranges are highly needed. Besides the extensive investigations on the regulation of cathodes, anodes, and separators, significant breakthroughs in the development of high-performance electrolytes have also been achieved.[52]

3.1. Moderate solvating electrolytes in LMBs

There are two prevalent types of electrolytes, that is, carbonate-based and ether-based electrolytes in moderate solvating electrolytes for LMBs. Carbonate-based electrolytes are typically composed of 1 M (mol L^{-1}) $LiPF_6$ in EC/DMC/EMC/DEC solvents, while there are usually 1 M LiTFSI or LiFSI in DOL/DME in ether-based electrolytes.

In the moderate solvating carbonate-based electrolytes, EC has a relatively high DC of 89.78, which is beneficial for the dissociation of $LiPF_6$ due to the stronger interaction between Li^+ and EC than that between Li^+ and PF_6^-, leading to the formation of solvent separated ion pairs (SSIPs), as shown in Fig. 4a.[53] In the SSIPs, solvents dominate the primary solvation sheath of Li^+, while most anions are excluded from the first solvation sheath. It is well known that the solvents or anions in the inner solvation sheath of Li^+ are prone to reduction on the surface of the anode, or oxidized by the high-voltage cathode, forming SEIs and CEIs, respectively. The carbonate-based MSEs dominated with SSIPs usually lead to inferior electrochemical performance in LMBs. First, at the lithium metal anode, carbonate solvents are preferred to be reduced, forming the fragile SEI composed of both insoluble components like Li_2CO_3 and partially soluble semi-carbonates and polymers.[15,54,55] These components possess inferior mechanical properties and poor ion conductivity, resulting in the formation of lithium dendrites, especially at high current densities or low temperatures. During the long-term discharge–charge process, some dendrites grow large enough to penetrate the separator, leading to short-circuits or safety issues; during the stripping process, some may lose contact with bulk lithium metal, resulting into the formation of "dead lithium".[20] Second, the electrochemical kinetics are highly associated with the transport of Li^+, including solvated Li^+ in bulk electrolyte, de-solvation of Li^+ near the electrodes, diffusion of Li^+ through electrode–electrolyte interphases, and Li^+ diffusion in the electrodes (Fig. 1c), among which Li^+ de-solvation is the rate-determining step.[56,57] The relative strong interaction of Li^+–solvents severely slows down the de-solvation of Li^+, which further exacerbates at low temperatures. Moreover, EC has a high melting point ($\sim$36.4 °C) and high viscosity. Although the introduction of EMC, DMC, or DEC can reduce the melting point and viscosity, the electrochemical performance using carbonate-based electrolytes deteriorates severely when the temperature drops to sub-zero, resulting into a limited operating temperature range.[58–60] Third, although compared with moderate solvating ether-based electrolytes, EC-based electrolytes exhibit enhanced anodic stability, their anti-oxidation ability gradually declines with the increase in cut-off voltages when at voltages $>$4.3 V *vs.* Li^+/Li.[61–63] The CEI derived from the oxidation of carbonate also cannot stand up with high voltages, leading to consistent decomposition of electrolytes.[64–66] Finally, it is noteworthy that these factors are highly related, and have synergistical effects on the electrochemical performances. For instance, the fragile SEI cannot suppress the formation of lithium dendrites, and in turn, the dendrites and the large volume variation during the lithium plating/stripping process break the SEI, followed by reformation of a new inhomogeneous and thick SEI, worsening the Li^+ diffusion in the SEI due to which the lithium dendrites and kinetics would be further aggravated.

In moderate ether electrolytes, SSIPs still dominate the electrolytes, because the binding energy between Li^+ and $TFSI^-$ or Li^+ and FSI^- is smaller than that between Li^+ and PF_6^-, while DME or DOL has a higher DN than EC. Although the Li||Cu cells using ether electrolytes show higher Coulombic efficiency (CE) than those using carbonate electrolytes,[33] the fragile SEI induced by the reduction of ethers cannot effectively suppress lithium dendrites.[27] Moreover, the high de-solvation energy barrier restricts the electrochemical performance at low temperature, and the low boiling points significantly worsen the high-temperature performance. Meanwhile, moderate solvating ether-based electrolytes have a narrow ESPW because of the poor oxidation resistance of ethers ($\leq$4.0 V *vs.* Li^+/Li).[27,67]

Since both the moderate solvating carbonate and ether electrolytes cannot meet the requirements of high-voltage lithium metal batteries with wide operating temperature ranges, researchers gradually turn their attention to novel weak solvating electrolytes.

3.2. Weak solvating electrolytes in LMBs

By manipulating the relative binding energy of Li^+–solvent and Li^+–anion, weak solvating electrolytes with unique solvation structures (CIPs and AGGs) and de-solvation behavior can be obtained. The peculiar solvation chemistry endows these weak electrolytes with excellent compatibility with the lithium metal anode, improved oxidation stability, and superior environmental adaption at extreme high/low temperatures, which are widely demonstrated in the recent reports (Fig. 4b and Tables 2, 3). In order to regulate the relative binding energy of Li^+–solvent and Li^+–anion, various types of electrolytes have been developed. Generally, there are three effective strategies to design weak solvation chemistry: increase the concentration of lithium salts, reduce the Li^+–solvent binding energy, and strengthen the Li^+–anion binding interaction. In WSEs, anions, instead of solvents, dominate the primary solvation sheath of Li^+, leading to the formation of contact ion pairs and aggregates. As mentioned above, the components in the primary solvation sheath are easily reduced or oxidized on the surface of anodes and cathodes, inducing an anion-derived inorganic-rich SEI and CEI, respectively. The properties of typical inorganic compounds are summarized in Fig. 5. These inorganic-rich electrode–electrolyte interphases possess not only excellent mechanical properties and ion conductivity, but also highly enhanced oxidation stability at high cut-off voltages.[68] For instance, LiF has a high bandgap (8.9 eV), large shear modulus (48.6 GPa),[15] high interfacial energy (73.28 meV $Å^{-2}$), and excellent anodic stability ($\sim$6.5 V *vs.* Li^+/Li), effectively ameliorating the compatibility with both the lithium metal anode and high-voltage cathodes. Furthermore, combined with the modified solvents with wide liquid temperature ranges, low viscosity, and small de-solvation energy barriers, the weak solvating electrolytes also exhibit satisfying performance at both low and high temperatures.[69,70]

3.2.1. Highly concentrated electrolytes (HCEs) in LMBs. One of the most effective and facile strategies of designing weak solvating electrolytes is to increase the salt concentration, that is, improve the molar ratio of cations/anions to solvents, which are usually denoted as HCEs. In conventional electrolytes (moderate solvating electrolytes), there are plenty of solvents available to fully solvate Li^+ because of the low salt/solvent ratio, and free solvents distributed outsides the Li^+ solvation sheath, forming SSIPs dominated solvation structures. However, in the WSEs such as HCEs, not enough solvents are available to solvate Li^+. Instead, due to the high salt/solvent ratio, the anions exist in the primary solvation sheath of Li^+ because of the improvement of the overall Li^+–anion affinity, and there are no free solvents in the electrolytes, leading to the

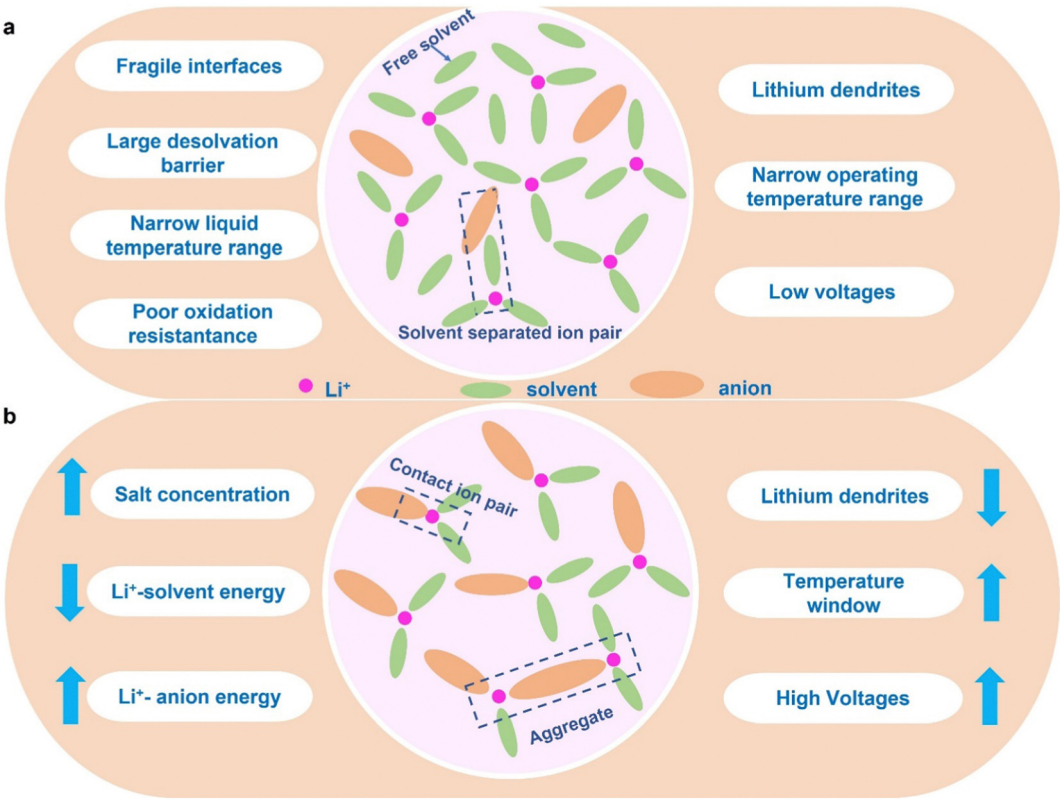

Fig. 4 (a) Schematic illustration of the solvation structure of Li^+ in moderate solvating electrolytes, and their drawbacks in LMBs. (b) Schematic illustration of the solvation structure of Li^+ in weak solvating electrolytes, and their mechanism in lithium metal batteries.

Table 2 Summary of the high-voltage performance in LMBs using different electrolytes

No.	Electrolytes	Cathodes	High-voltage performance: Cut-off voltages (V)	High-voltage performance: Capacity retention/cycles	SEI	CEI	Ref.
HCE							
1	3 M LiTFSI in G4	LCO	4.2	90%/50	—	—	83
2	5 M LiFSI + 0.16 M NaFSI in EMIm-FSI	LCO NCM811	4.3 4.4	81%/1200 94%/200	Robust SEI composed of LiF, Li_2SO_4, Li_2SO_3, Li_2S, Li_2CO_3, Li_2O, Li_3N, and $-CF_3$	F-riched CEI (LiF, NaF, Li_2CO_3, S-based species, and organic compounds) (5–10 nm)	159
3	10 M LiFSI in EC : DMC (1 : 1)	NCM622	4.6	86%/100	LiF-rich SEI	Fluorine-rich interphase (LiF, CF_x, and S–F)	82
4	7 M LiFSI in FEC	$LiNi_{0.5}Mn_{1.5}O_4$	5.0	94.26%/150	LiF, Li_2O, Li_2CO_3	LiF	84
5	LiFSI : DMC (1 : 1.1)	$LiNi_{0.5}Mn_{1.5}O_4$	5.2	95%/100	LiF	—	85
6	4.6 M LiFSI + 2.3 M LiTFSI in DME	NCM622	4.4	88%/300	A TFSI-dervied SEI (LiF, Li_2O, Li_2S, CF_3)	A uniform anion (FSI, TFSI)-derived CEI	86
7	5 M LiFSI in DME	NCM111	4.5	>95%/100	—	FSI-derived CEI ((LiF, Li_xSO_y, Li_xNO_y) with a thickness of 4–9 nm.	87
8	3.25 M LiTFSI/$LiNO_3$-SL	NCM811	4.4	99.5%/200	LiF-Li_xNO_y-rich SEI	denser CF_x-rich CEI after introducing $LiNO_3$	88
9	2 M LiTFSI + 2 M LiODFB in DME	NCM111	4.3	80%/500	Polymeric SEI layer with B–F, B–O, LiF	Polycrystalline CEI with a thickness of 4 nm.	160
10	3.1 M $LiPF_6$ in EC/EMC	NCM811	4.6	77%/500	—	$LiM_xF_yO_z$, $Li_xPF_yO_z$, $LiPF_6$	161
LHCEs							
1	2.5 M LiTFSI in PC : HFE(1 : 2 by volume)	LNMO	5.0	95.1%/45	—	—	104
2	1.2 M LiFSI in DMC : BTFE (1 : 2 by mol)	NCM111	4.3	80%/700	A robust FSI-derived SEI layer (rich in LiF and/or Li_2O)	—	95
3	1.2 M LiFSI in TEP : BTFE (1 : 3 by mol)	NCM622	4.4	>97%/600	A robust FSI-derived ''LiF-rich'' SEI	—	96
4	1 M $LiPF_6$ in FEC/FEMC/HFE (2 : 6 : 2, by weight)	NCM811 LCP	4.4 5.0	90%/450 93%/1000	LiF-rich (90%) SEI	F-rich CEI	102
5	LiFSI-3TMS-3TTE	LNMO	4.9	—	LiF-derived SEI (Li_xN, LiF, N-SO_x)	—	97
6	LiDFOB : EC/DMC : BTFE (0.51 : 1.1 : 2.2 by mol)	NCM111	4.3	84%/100	DFOB-derived robust SEI (LiF, Li_2O)	—	98
7	1.2 M LiFSI in DME : TFEO (1.2 : 3 by mol)	NCM811	4.4	80%/300	Amorpous FSI-derived SEI with a thickness of 10 nm.	LiF-rich CEI (~5 nm)	99
8	1.28 M LiFSI-FEC/FEMC–D2	LNMO	5.0	93.7%/>1000	LiF-rich SEI	LiF-rich CEI	28
9	LiFSI-1.2DME-3TTE	NCM811	4.5	90%/250	LiF-rich SEI	LiF-rich CEI	101
10	1 M LiFSI in DME : HFE(1 : 4 by volume)	NCM811	4.4	80%/303[a]	Anion-derived LiF-rich SEI (LiF, Li_xN); dilute further reduced the decomposition of solvents	LiF-rich CEI (with a thickness of 2 nm); dilute further reduced the decomposition of solvents	106
11	1LiFSI-1.1DME-2.2TFMB	NCM811	4.4	80%/260[b]	Anion-diluent pairing-derived homogenous and robust inorganic SEI (LiF, Li_2O, Li_3N)	A uniform and thin CEI of 3.15 nm	53
12	1LIFSI-1.5DMC-2BTFE + 2.0 wt% TPFPB	NCM532	4.3	80%/194[a]	Improved anion-derived SEI by anion acceptors (LiF, Li_2S, Li_2O/Li_2CO_3, Li_3N)	—	108
13	LiFSI-1.5DMC-1.5TTE	NCM622	4.6	83.5%/100	LiF-rich SEI	—	162
14	1.6 M LiFSI in FEC-DME-HFE	NCM532	4.3	80%/200	An inorganic-rich SEI with high F content (LiF, Li_2O, Li_2CO_3)	—	163
15	LiFSI-DME-3TTE	LCO	4.55	87.6%/200	Anion-derived SEI (LiF, N-SO_x, Li_2SO_x, Li_2S_n, Li_2S)	F-enriched CEI (atomic ratio of F 38%)	164
16	0.3 M LiDFOB + 0.2 M $LiBF_4$ in DEC/FEC/FB (3.5 : 1.5 : 5 by volume)	LCO	4.6	85.6%/120	LiF-rich SEI with a thickness of 9 nm	F-rich CEI with a thickness of 6 nm (LiF, B–F, C–F)	165

Table 2 (*continued*)

No.	Electrolytes	Cathodes	High-voltage performance: Cut-off voltages (V)	High-voltage performance: Capacity retention/cycles	SEI	CEI	Ref.
17	LiFSI–DMAC–HFE (1.0 : 1.3 : 2, by mole)	NCM532	4.3	80%/105[b]	LiF, Li_3N-rich SEI	—	166
18	1 M Li^+ de-solvated LiTFSI-DOL-DME (in ZIF67)	NCM811	4.4	94.6%/200 77.8%/800	—	No CEI	112
19	1 M LiTFSI-PC (in CuBTC)	LCMO NCM811	5.3 4.4	95.4%/1250 90%/400	—	Thin CEI	110
20	1 M $LiPF_6$-EC-DEC with MIL-100(Al)	NCM111	4.8	82%/50	MOF-involved SEI	—	167
21	1.59 M LiFSI in TFEP : FMP (2 : 1 by volume)	LNMO	5.0	95.5%/90	—	—	168
WSEs based on weakly-polar solvents							
1	0.2 M LiTFSI in FM: CO_2	LCO	4.2	96.7%/100	A highly ceramic-like SEI composed primarily of LiF and Li_2CO_3	Little or no CEI	115
2	1.2 M LiTFSI, 1 M AN in FM	NCM622	4.5	~89%/200	Inorganic-rich SEI by decomposition of FM, CO2, and TFSI (LiF, Li_2CO_3)	A ceramic-like CEI composed primarily of LiF, Li_2CO_3, and S–O, N–O species	117
3	2.5 M LiFSI + 0.2 M $LiPF_6$ in FSA	NCM622	4.3	89%/200	LiF, Li_2S_2/Li_2S -rich SEI	LiF-rich CEI	118
4	1 M LiFSI in DMTMSA	NCM811	4.7	88.1%/100	Inorganic-rich SEI including LiF, Li_2S_2/Li_2S	CEI consists of more LiF-like inorganic components and less organic components	119
5	1 M LiFSI in DMTMSA	LCO	4.6	85%/100	Inorganic-rich SEI including LiF, Li_2S_2/Li_2S	CEI consists of more LiF-like inorganic components and less organic components	120
6	4 M LiFSI in DEE	NCM811	4.4	80%/182[a]	SEI composed of inner inorganic layer (FSI-derived) and outer organic layer	—	122
7	1 M LiFSI in FDMB	NCM532	4.2	90%/420[b]	An ultrathin SEI (~6 nm) rich in F, S and O	—	125
8	1.2 M LiFSI/F5DEE	NCM811	4.4	80%/270[b]	A thin inorganic-rich SEI (~12 nm) (LiF and Li_2O)	CEI with high C and F content	126
9	LiFSI/1.6Cl-DEE/3TTE	NCM811	4.6	88%/200[b]	Anion-derived SEI (LiF, LiCl, N-SO_x, SO_x, S_n^{2-} component)	CEI riched in LiF and LiCl with a thickness of 8 nm	129
10	2 M LiFSI-cFTOF	NCM811	4.3	100%/110[b]	Uniform and compact LiF-rich SEI	LiF-rich CEI	127
11	2 M LiFSI-DTDL	NCM811	4.3	84%/200[b]	FSI-derived inorganic SEI (LiF and S-F compositions, and rich in N and S contents)	LiF-rich CEI	128
12	1 M $LiPF_6$-FEC-BTC	NCM811	4.8	85.7%/100	Robust LiF-rich SEI	LiF-rich CEI with a thickness of 4.1 nm	130
13	1 M $LiPF_6$-DFEC/DEC	NCM811	4.5	91%/300	Robust LiF-rich SEI	Fluorine-rich CEI	131
14	0.95 M LiFSI in TFEP/FEMC	LNMO	4.9	70%/200	LiF-rich SEI	—	133
15	1 M $LiPF_6$ in TFMP/FEC	NCM811	4.5	80%/200	Fluorine-rich interphase	Fluorine-rich interphase	132
WSEs based on strong Li^+–anion affinity							
1	1.5 M LiBF4 in FEC/DME	LCO	4.6	55.5%/160	BF_4^--derived inorganic-rich SEI (LiF)	BF_4^--derived inorganic-rich CEI (LiF, $LiBO_2$)	141
SSEs							
1	$LiPF_6$-FEC-DMC-$LiNO_3$-DMSO	NCM811	4.3	75%/200	Inorganic-rich SEI (LiF, Li_2O, Li_3N, Li_2CO_3, and LiN_xO_y)	—	145
2	$LiPF_6$-FEC-EMC-$LiNO_3$-TPPB	LCO	4.6	89.8%/160	A multilayer SEI (~30 nm) with a robust Li_2O crystal layer (also including LiF, Li_3N)	F- and B-containing CEI with a thickness of about 5nm	158

Table 2 (*continued*)

No.	Electrolytes	Cathodes	High-voltage performance: Cut-off voltages (V)	High-voltage performance: Capacity retention/cycles	SEI	CEI	Ref.
3	$LiPF_6$-FEC-EMC-$LiNO_3$-$Sn(OTF)_2$	NCM811	4.3	80%/200[b]	Metal–organic hybrid SEI layer derived from the Sn^{2+}–NO_3^- solvation structure ($LiNO_2$, LiN_xO_y and Li_2O)	Amorphous CEI layer (~6.8 nm) derived mainly from Sn^{2+}–NO_3^- coordination-solvation structure	146
4	$LiPF_6$-EC-EMC-$LiNO_3$-$In(OTF)_3$	NCM811	4.3	80%/160[b]	wavy SEI with inorganic-rich components (Li_2O, Li_3N, and LiN_xO_y)	—	147

Note: [a] Represents cells with thin lithium. [b] Represents full cells with specific N/P ratio.

formation of CIPs and AGGs dominated solvation structures.[72] In the HCEs, it is commonly accepted that the LUMO of the Li^+ solvation structure shifts from the energy level of solvents to that of anions, leading to the formation of anion-derived electrode–electrolyte interphases. The first HCE can be dated back to 1985 when J. R. Dahn adopted saturated solution of $LiAsF_6$ in PC to address the co-intercalation of PC in Li||ZrS_2 cells.[73] Subsequently, concepts of "polymer in salt",[74] "solvent in salts",[27] and "water in salts"[10] were successively proposed, stimulating the overwhelming investigation of HCEs.

On the one hand, the anion-derived SEI in HCEs effectively inhibit the formation of lithium dendrites, improving Li depositing/stripping efficiency and cycling stability.[75,76] Jeong and co-workers first investigated the effect of HCEs in LMBs, and found that HCEs (3.27 mol kg^{-1} $LiN(SO_2C_2F_5)_2$ in PC) induced a thinner SEI, and could improve the cycling stability. However, the CE of Li deposition/stripping is below 90%,[77] Suo *et al.*[27] investigated the highly concentrated LiTFSI (7 M) in DME : DOL (1 : 1 by volume), and found that, compared with other LiTFSI-based electrolytes, the HCEs could largely improve the lithium depositing/stripping efficiency, but the CE was as low as ~71%. The striking progress was made by Qian and co-workers in 2015. By using 4 M LiFSI in DME, lithium dendrites can be effectively suppressed (Fig. 6a and b). Meanwhile, the Li||Cu cells exhibited an average CE of 99.1% at a current density of 0.2 mA cm^{-2}, and 98.4% at a current density as high as 4 mA cm^{-2} during 1000 cycles (Fig. 6c). Li||Li cells showed remarkable long-term cycling stability (>6000 cycles) at 10 mA cm^{-2}.[78] LiFSI–TEP (1 : 1.5, by mol),[79] LiFSI/TEP (1 : 2, by mol)/FEC/LiBOB[80] and 1 : 2.5 LiFSI/sulfolane (by mol)[81] with plating/striping CEs of 99.3% for 350 cycles, 99%, and 98% for 400 cycles at 1 mA cm^{-2}, respectively, were also reported.

On the other hand, the unique solvation structures of Li^+ in HCEs improve the anodic stability, expanding the ESPWs (Table 2). In 2009, Tamura *et al.* first reported enhanced cycling stability of Li||LCO cells with a cut-off voltage of 4.2 V using an ether-based HCE (3 M LiCTFSI in tetraethylene glycol dimethyl ether, G4).[83] In 2011, Yoshida *et al.* first illustrated, using DFT calculations, that solvents coordinated with Li^+ in HCEs showed better anodic stability than free solvents due to the downshifts of the energy level of the HOMO (Fig. 7a–c).[67] Later in 2014, Yamada *et al.* clarified that the anodic stability in HCEs resulted from an anion-derived SEI instead of a solvent-derived SEI because of the higher energy level of the LUMO (Fig. 7d–f).[24] In 2018, Fan *et al.* reported a HCE with salt (LiFSI) concentration as high as 10 M in DMC or EC/DMC. Due to the anion-derived LiF-rich SEI and F-rich CEI, this electrolyte demonstrates outstanding compatibility with both the lithium meal anode and high-voltage cathode. As a result, Li||Cu cells exhibited a CE of ~99.3%, and Li||NCM622 cells showed excellent cycling stability with a capacity retention of 86% after 100 cycles with a cut-off voltage of 4.6 V *vs.* Li^+/Li (Fig. 6d).[82] But Suo *et al.* found that high concentration of LiFSI (11 M) in DMC would deteriorate the capacity, while a relatively lower concentration (7 M LiFSI in DMC) would cause severe Al corrosion when the voltage is higher than 4.7 V *vs.* Li^+/Li. By replacing DMC with FEC, the electrolyte composed of 7 M LiFSI in FEC not only endowed the Li||Cu cells with a CE as high as 99.6% after 400 cycles, but also enabled the $LiNi_{0.5}Mn_{1.5}O_4$ (LNMO)||Li cells work stably with a capacity retention of 94.26% after 150 cycles in 3.3–5.0 V.[84] Wang *et al.* proposed a 1 : 1.1 LiFSI/DMC (molar ratio) electrolyte, achieving a capacity retention of 95% for the LNMO cathode with a cut-off voltage of 5.2 V (*vs.* Li^+/Li) after 100 cycles.[85] Alvarado and co-workers reported 4.6 M LiFSI + 2.3 M LiTFSI in DME with excellent anodic stability (a capacity retention of 88% for NCM622 with a cut-off voltage of 4.4 V after 300 cycles) and stable Li plating/stripping performance (98.6% during 200 cycles at 0.5 mA cm^{-2}).[86] Ren *et al.* further improved the anodic stability of HCEs in ether solvent by adopting a 5 M LiFSI in DME.[87] Recently, novel HCEs have been developed for high-performance LMBs. Fu *et al.* reported that 3.25 M LiTFSI/$LiNO_3$-TMS not only had a Li metal CE of 98.5%, but also exhibited an enhanced decomposition potential (5.4 V *vs.* Li^+/Li) and a capacity retention rate of 99.5% after 200 cycles in Li||NCM811 cells with a cut-off voltage of 4.4 V (Fig. 7g–i).

3.2.2. Localized highly concentrated electrolytes (LHCEs) in LMBs. Although HCEs can effectively achieve a stable Li stripping/plating behavior with high CE, and greatly enhance the anodic stability, they show inferior wettability, poor ionic conductivity, and high cost, which inhibit their further practical application in next-generation rechargeable batteries. To address these issues, inert solvents (dilutes) with low viscosity and a wide liquid temperature range, which cannot dissolve

Table 3 Summary of the high/low temperature performance in lithium batteries using different electrolytes

No.	Electrolytes	Anode/cathode	High/low temperature performance				Key mechanism	Ref.
			HT (°C)	Retention (%)/cycles	LT (°C)	Retention (%)/cycles		
1	1.28 M LiFSI FEC/FEMC-D2	Li/NCA	70	(170 mA h g^{-1})	−85	(96 mA h g^{-1})	• Tame the affinity between solvents and Li^+ • Fluorinated electrolytes	28
2	LiFSI-1.5DMC-1.5TTE	Li/NCM622	60	84.6%/100	—	—	• Alter solvation structure of Li^+ by introduction of counter-solvent, forming LiF-rich SEI	162
3	LiFSI-DME-3TTE	Li/LCO	55	81.3%/200	−30	(∼150 mA h g^{-1})	• *In situ* construction of both stable SEI and CEI in LHCEs	164
4	LiFSI-DME-FB	Li/S	—	—	−20	58%/300	• Alter solvation behavior and interfacial chemistry by introduction of fluorobenzene.	105
5	LiFSI-DME-5BTFE	Li/NCM811	23	94.9%/200	−40	99.1%/200	• Introduction of cation/anion pairs	109
6	1 M LiTFSI in EA:DCM (1:4 by volume)	Li/PI	20	(121 mA h g^{-1})	−70	(84 mA h g^{-1})	• Design of co-solvent electrolytes, combining advantages of LHCEs and solvents with low viscosity and low melting points	90
7	0.2 M LiTFSI in FM:CO_2	Li/LCO	25	(133 mA h g^{-1})	−60	(80.6 mA h g^{-1})	• Adoption of liquified gas electrolytes with low viscosity • Stable SEI	115
8	1.2 M LiTFSI, 1 M AN in FM	Li/NCM622	55	(∼220 mA h g^{-1})	−60	(∼90 mA h g^{-1})	• Adoption of liquified gas electrolytes with low viscosity • Stable SEI	117
9	1 M LiFSI in DEE	Li/SPAN	23	(∼623 mA h g^{-1})	−60	(∼474 mA h g^{-1})	• Tailoring electrolyte solvation with weak Li^+/solvent binding	124
10	1 M $LiPF_6$-FEC-BTC	Li/NCM811	55	88.4%/100	−30	(143.5 mA h g^{-1})	• Design electrolytes by fluorination of commercial solvents for stable F-rich SEI/CEI and low de-solvation barriers	130
11	1 M $LiPF_6$-DFEC/DEC	Li/NCM811	20	91%/300	−30	(93 mA h g^{-1})	• Ion-dipole strategy by regulating the fluorination degree of solvating agents	131
12	1 M $LiPF_6$ in TFMP/FEC	Li/NCM811	23	80%/200	−60	(134 mA h g^{-1})	• Construction of stable fluorine-rich interphases in the all-fluorinated electrolyte	132
13	1 M $LiPF_6$ in EC-DEC with TPPO and $LiNO_3$	Li/LFP	70	80%/50	−15	99.5%/100	• Construction of a robust and ionic conductive Li_3N-rich SEI • Stable CEI	143
14	LiFSI + $LiNO_3$ in FEC-TEGDME	Li/LFP	90	91.5%/100	—	—	• Construction of a high resistant SEI	156
15	0.8 M LiTFSI-0.2 M LiODFB in ADN:EC (1:1)	Li/LTO	120	87.9%/1000	−20	95.1%/100	• Manipulation of competitive decomposition in electrolyte with adiponitrile for a stable and inorganic-rich SEI layer	142
16	LIFSI:EMC (1:1.1 by mol)	Graphite/LNMO	40	>90%/100	25	>95%/100	• Adoption of HCEs with stable lithium salts	85
17	1.4 M LiFSI in DMC-EC-TTE (2:0.2:3 by mol)	Graphite/NCM811	60	94.9%/100	−30	(160.7 mA h g^{-1})	• Adoption of HCEs for excellent EEIs	169
18	4 M LiFSI in DMC	Graphite/NCM622	100	66%/100[a]	−20	∼75%/100	• Adoption of HCEs for highly thermal stable solvation structure and the robust and Li^+-conductive passivation interphase	170
19	6.5 M LiTFSI in FEC	Li/S	90	(981.5 mA h g^{-1})/100	−10	99.2%/50	• Flame-retardant HCEs with LiF-rich SEI	171
20	1 M LiFSI-Me_2O-TFE-PFE	Li/NCM622	55	>80%/50	−60	(71 mA h g^{-1})	• Design of fire-extinguishing, recyclable liquefied gas electrolytes	114
21	LiFSI:$LiNO_3$:TEGDME (1:1:2.3 by mol)	Li/LFP	100	89%/50	25	98.5%/150	• Design of a thermal stable electrolyte based on stable solvation structure using multiple ion–dipole interaction	172

Note: [a] Represents cells with thin lithium.

lithium salts, but have good miscibility with solvating solvents in HCEs, are widely used.[89,90] Different from the Li^+ solvation structures in conventional electrolytes (Fig. 8a) and highly concentrated electrolytes (Fig. 8b), Li^+–anion–solvent clusters in LHCEs (Fig. 8c) are well preserved, and the non-solvating dilute solvents are distributed outside the Li^+ solvation sheath. On the one hand, these non-solvating solvents significantly lower the viscosity, improve the wettability, and broaden the operating temperatures, resulting into enhanced electrochemical kinetics; on the other hand, unlike in HCEs, the non-solvating diluents further enhance the Li^+–solvent and Li^+–anion interactions in the solvation structure of Li^+ by isolating the Li^+–anion–solvent clusters.[89,91]

The pioneering work on LHCEs was carried out by Watanabe's group. In 2013, they first used 1,1,2,2-tetrafluoroethyl 2,2,3,3-tetrafluoropropyl ether (TTE) as the diluent to design the LHCEs (LiTFSI/G4/TTE, 1:1:4 by mol) to ameliorate the "shuttle effect" of lithium polysulfides in LSBs.[92] In 2015, the same group systemically investigated the ion–ion/solvent interactions and their effects on the solvation structure of Li^+, and found that LiTFSI-G3-HFE (1:1:4.46, molar ratio) not only had high anodic stability and low corrosion of Al in high-voltage

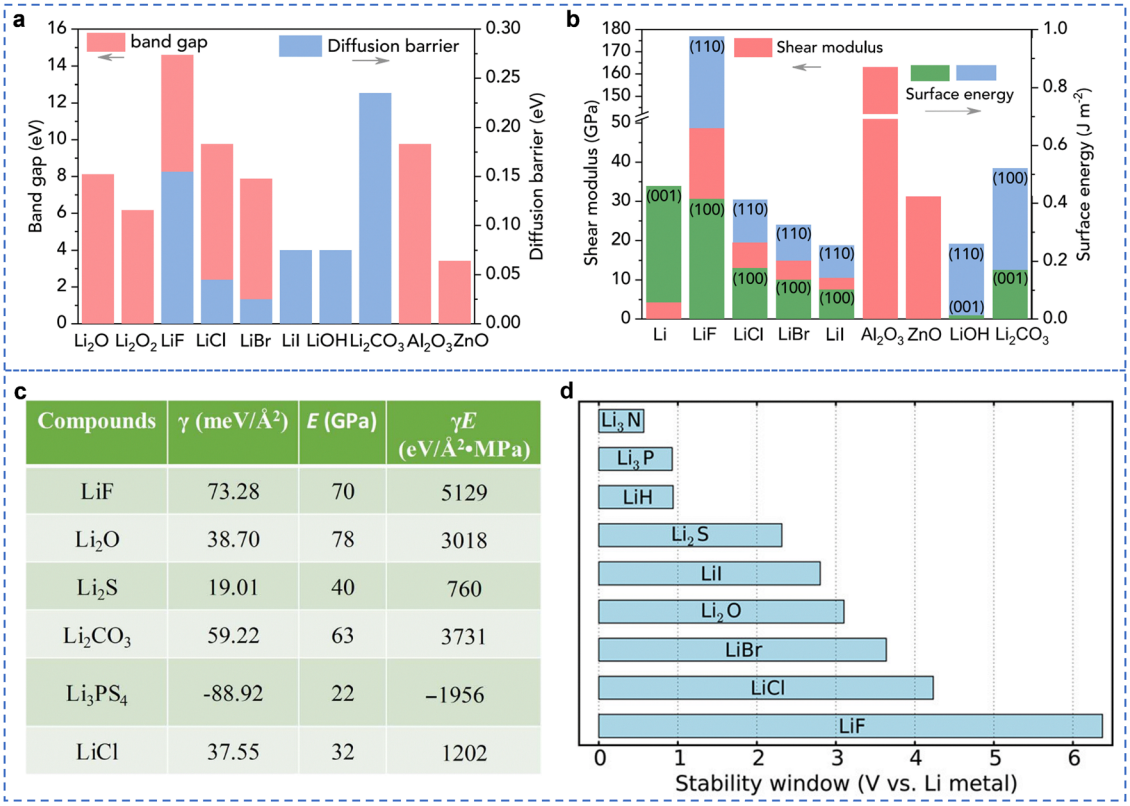

Compounds	γ (meV/Å²)	E (GPa)	γE (eV/Å²•MPa)
LiF	73.28	70	5129
Li_2O	38.70	78	3018
Li_2S	19.01	40	760
Li_2CO_3	59.22	63	3731
Li_3PS_4	-88.92	22	−1956
LiCl	37.55	32	1202

Fig. 5 Properties of typical inorganic components in SEI. (a) Band gap and diffusion barrier and (b) shear modulus and surface energy of components in the SEI. Reproduced with permission.[15] Copyright 2021 Cell Press. (c) Interfacial energy (γ) and bulk modulus (*E*) of different SEI components. Reproduced with permission.[71] Copyright 2018 AAAS. (d) Calculated stability window of different lithium binary compounds. Reproduced with permission.[61] Copyright 2021 Royal Society of Chemistry.

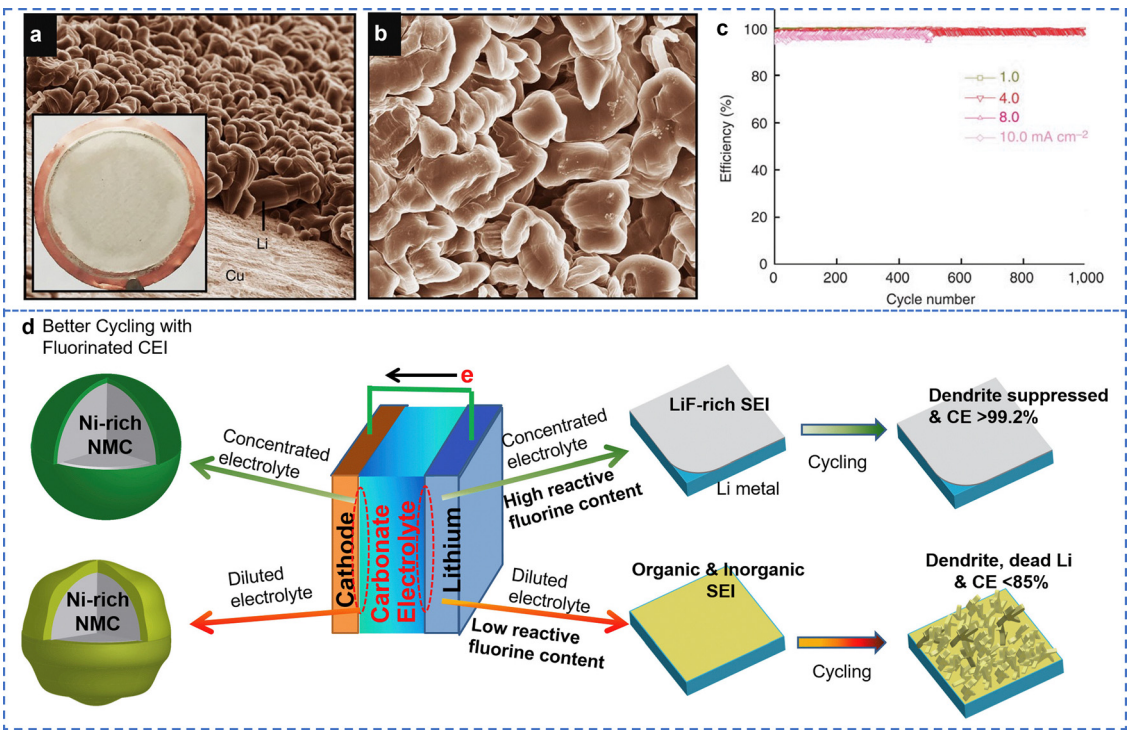

Fig. 6 (a and b) Scanning electron microscopy (SEM) images of the morphologies of Li metal after plating on the Cu substrate in 4 M LiFSI-DME, and (c) CE of Li deposition/striping in 4 M LiFSI-DME at different current densities. Reproduced with permission.[78] Copyright 2015, Nature Publishing Group. (d) Schematic illustration of the effect of 10 M LiFSI in EC/DMC on a Li-metal anode and Ni-rich cathode. Reproduced with permission.[82] Copyright 2018 Elsevier Inc.

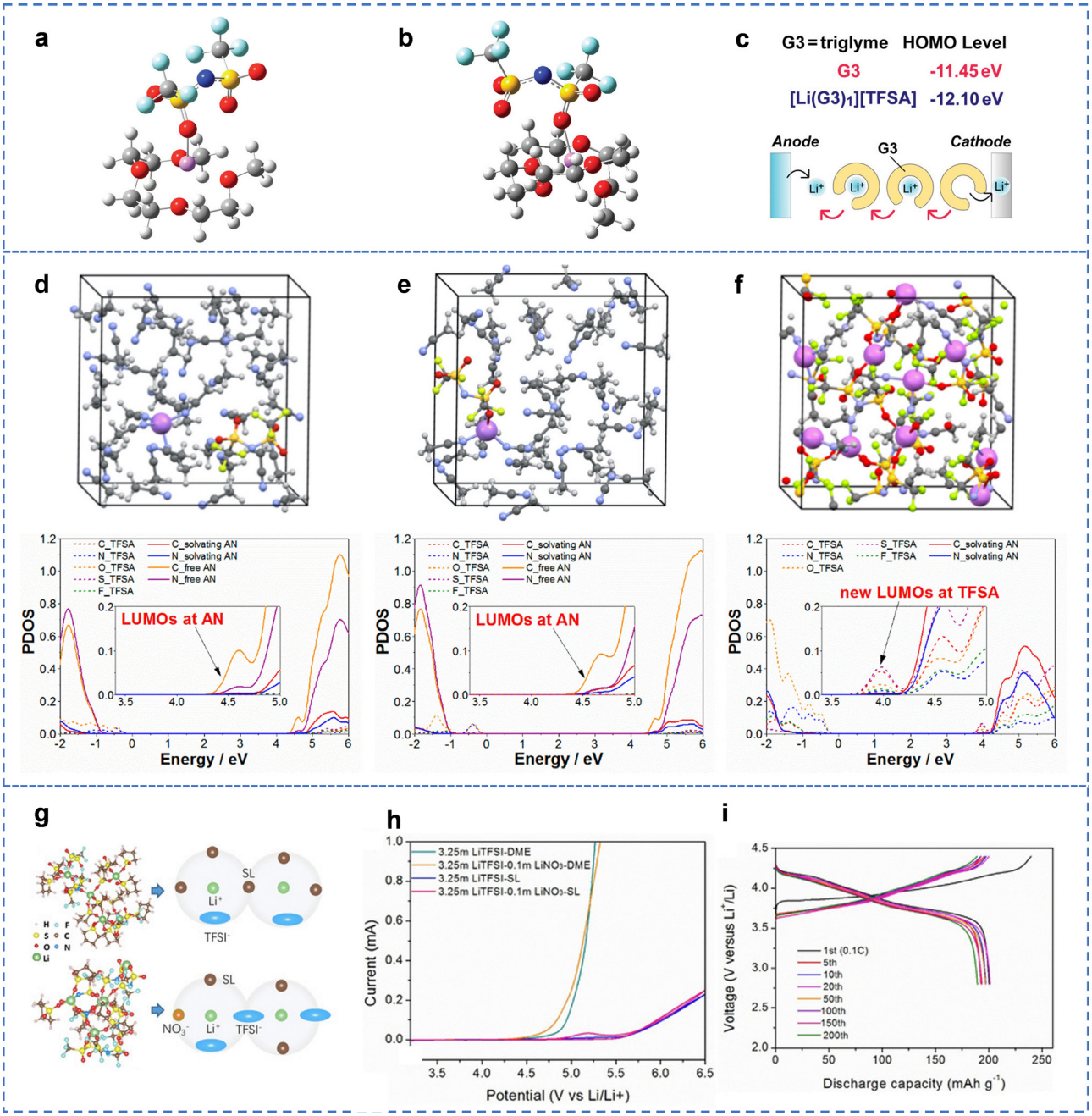

Fig. 7 Optimized structures of (a) $[Li(G3)_1][TFSA]$ and (b) $[Li(G4)_1][TFSA]$, and (c) the energy levels of different electrolytes. Reproduced with permission.[67] Copyright 2011 American Chemical Society. Supercells used and projected density of states (PDOS) obtained in quantum mechanical DFT-MD simulations on (d and e) dilute (1LiTFSA/43-AN) and (f) super-concentrated (10-LiTFSA/20-AN) LiTFSA/AN solutions. The illustrated structures are the snapshots in equilibrium trajectories. For a dilute solution, both situations of LiTFSA salt (*i.e.*, (a) full dissociation and (b) CIPs) were considered. Insets in the PDOS profiles are magnified figures of the lowest energy-level edge of the conduction band. Reproduced with permission.[24] Copyright 2014 American Chemical Society. (g) Typical Li^+ solvation structures of different electrolytes from MD simulation. (h) Linear sweep voltammetry curves (LSV) for different electrolytes at a scanning rate of 1 mV s^{-1}. (i) Charge/discharge curves of Li||NMC811 cells. Reproduced with permission.[88] Copyright 2020 Wiley.

lithium batteries, but also suppressed the co-intercalation of Li^+/G3 in graphite in LIBs and inhibited the solubility of polysulfides in LSBs.[93] In the same year, they further explored the effects of non-polar solvents on the conductivity and viscosity of the LHCEs, and found that LiTFSI-G4-toluene or LiTFSI-G4-HFE possessed huge potential as novel LHCEs.[94]

Subsequently, Zhang *et al.* and Wang's group further made significant contribution to the development of LHCEs in LMBs. In 2018, Zhang's group demonstrated that LHCE, 1.2 M LiFSI in DMC/bis(2,2,2-trifluoroethyl)ether (BTFE) (1 : 2 by mol), not only suppressed the lithium dendrites with a high stripping/plating CE of 99.3%, but also had a capacity retention of 80%

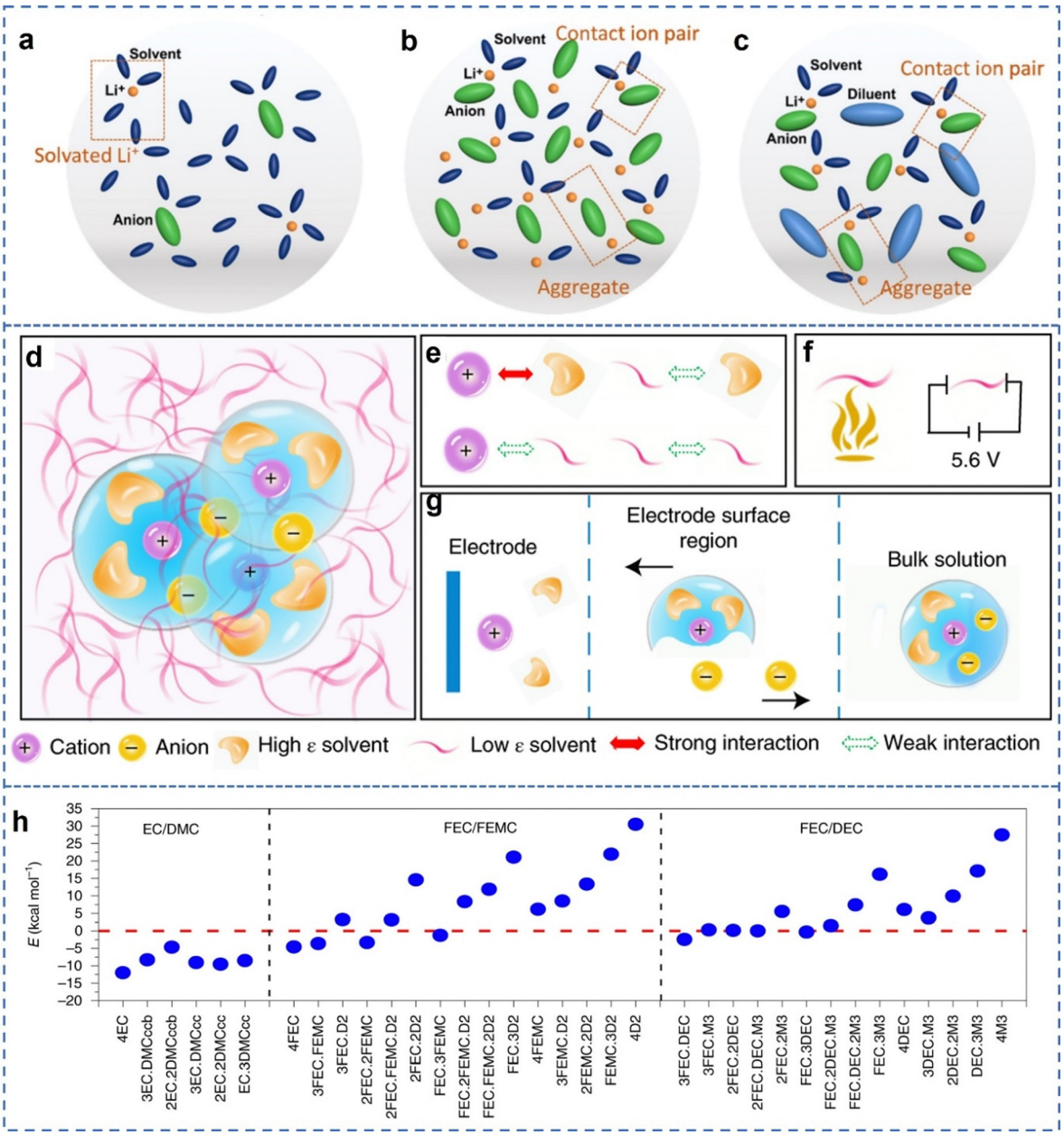

Fig. 8 Solvation structure of (a) conventional electrolyte, (b) HCE and (c) LHCE. Reproduced with permission.[89] Copyright 2021 The Electrochemical Society. (d) Schematic diagram of electrolyte; the transparent blue spheres indicate the Li^+ solvation structure. (e) The affinities between the solvents and Li^+. (f) The non-flammable electrolyte and its excellent anodic stability. (g) Schematic illustration of the electrochemical process at the electrode–electrolyte interface. (h) The calculated Li^+ de-solvation energy with different solvents. Reproduced with permission.[61] Copyright 2021 Royal Society of Chemistry.

after 700 cycles for NCM111 with a upper cut-off voltage of 4.3 V *vs.* Li^+/Li.[95] They also examined the fire-retardant electrolyte, 1.2 M LiFSI in triethyl phosphate (TEP)/BTFE (1 : 3 by mol), and found that this LHCE not only enabled stable and dendrite-free lithium metal anodes with a high CE of 99.2%, but also retained 97% capacity after 600 cycles in NCM622 with a cut-off voltage of 4.4 V *vs.* Li^+/Li.[96] In the same year, Zhang and collaborators explored the sulfone (tetramethylene sulfone, TMS)-based LHCE using TTE as the dilute solvent, (LiFSI-3TMS-3TTE), which not only addressed the viscosity and wettability issues of sulfones, but also achieved stable performances of both lithium metal anodes and 5 V LNMO cathodes.[97] A LHCE of LiFSI-EC/DMC-BTFE with additives of LiODFB was also investigated in Li||NCM333 cells.[98] In 2019, they used tris(2,2,2-trifluoroethyl)-orthoformate (TFEO) as the diluting solvent to construct a novel LHCE, 1 M LiFSI in DME : TFEO (1.2 : 3 by mol), and found that the unique monolithic SEI effectively minimized the dendritic Li formation, Li loss and volumetric variation. Moreover, this new LHCE strongly inhibited the structural degradation of Ni-rich cathodes, resulting in

an improved capacity retention of 80% after 300 cycles in Li||NCM811 cells with a cut-off voltage of 4.4 V *vs.* Li^+/Li.[99] In 2021, they investigated the solvation structures of TFEO-based electrolytes (LiFSI-DME-TFEO) with different compositions, and demonstrated that the Li||NCM811 cells using the optimized electrolytes retained 80% capacity after 200 cycles under practical conditions.[100] Using time-of-flight secondary ion mass spectroscopy (TOF-SIMS), in-depth X-ray photoelectron spectroscopy (XPS), and transmission electron microscopy (TEM), they further comprehensively investigated the components of the anion-derived interphase in LiFSI-1.2DME-3TTE, and emphasized the effects of F-rich interphases on both anodic and cathodic stability in high-voltage Li||NCM811 cells.[101]

In 2018, Wang's group reported another non-flammable LHCE composed of 1 M $LiPF_6$ in FEC/FEMC/HFE (2 : 6:2, by weight), which could endure a much aggressive cathode, achieving a capacity retention of 90% after 450 cycles and 93% after 1000 cycles in NCM811 with a cut-off of 4.4 V and 5 V $LiCoPO_4$ (LCP), respectively.[102] In 2019, they developed an ''omnipotent'' electrolyte by addition of non-polar tetrafluoro-1-(2,2,2-trifluoroethoxy) ethane (D2) into 4.2 M LiFSI-FEC/FEMC (1.28 M LiFSI-FEC/FEMC-D2). As shown in Fig. 8d, this electrolyte exhibits the typical Li^+ solvation structure of LHCEs. Due to the different affinities between the solvents and ions, this electrolyte not only showed superior anodic and cathodic stability, but also exhibited non-flammability and all-temperature resistance (Fig. 8e–g). As a result, this electrolyte delivered high ionic conductivity in a wide temperature range from −125 to + 70 °C, and $LiNi_{0.8}Co_{0.15}Al_{0.05}O_2$ (NCA)||Li cells exhibited remarkable capacities from −85 to 70 °C. More importantly, they not only investigated the effects of components and structures of the anion-derived SEI or CEI on the anodic and cathodic stability, but also systemically explored the influence of Li^+ solvation/de-solvation energy barriers on the kinetics performance, especially the kinetics at low temperature (Fig. 8h).[28]

Besides the excellent reports discussed above, Zhang's group further systemically investigated the effects of different diluents and solvating solvents on the Li^+ solvation structure, electrolyte–electrode interphase, and the final electrochemical performances.[91,103] BTFE (D1), TTE (D2), bis(2,2,2-trifluoroethyl) carbonate (BTFEC, D3), tri(2,2,2-trifluoroethyl) borate (TFEB, D4), and TFEO (D5) were chosen as the representative diluents, with which LiFSI and DME were mixed to obtain different LHCEs. It is shown that the distance between Li^+ and anions or solvents is derived from the radical distribution, which is calculated based on the results of molecular dynamics simulation. It is clearly shown that anions and DME solvent are tightly attracted by Li^+ in the first solvation sheath within a radius of 2 Å, implying the strong affinity between Li^+ and DME/FSI^-; BTFE (D1), TTE (D2), TFEB (D4), and TFEO (D5) are barely coordinated with Li^+ (>4.5 Å), demonstrating that these four diluents do not participate into the solvation sheath of Li^+. BTFEC (D3), as an exception, although not in the first solvation shell, is still coordinated with Li^+ (~3.25 and 3.75 Å). Surprisingly, the cycling stability of Li||NCM811 cells using different LHCEs follows the order: LHCE-TFEO > LHCE-TTE > LHCE-BTFE > LHCE-BTFEC > SOA electrolyte > LHCE-TFEB. The authors then thoroughly carried out various characterization studies and concluded that the electrochemical performances were highly associated with both the solvation structures associated with diluents and the intrinsic physical and chemical properties of these diluents.[103] They also explored the effects of a series of polar solvents (TMS, TEP, DMC, and DME) in LHCEs and demonstrated the synergistic effects of lithium salts and polar solvents on the inner solvation sheath regulation and the corresponding electrochemical performances.[91]

In addition to the above significant reports, there are other excellent research studies on LHCEs that have contributed to refining the electrochemical performance of LMBs. In 2017, Doi *et al.* found that a mixture of 2.5 M $LiBF_4$/PC : HFE (2 : 1 by volume) endowed LNMO with a high capacity retention of 95.1% with an upper cut-off voltage of 5 V *vs.* Li^+/Li.[104] In 2020, Jiang adopted fluorobenzene (FB) with low density and low cost as a diluent to obtain LHCE (Fig. 9a). Since FB can inhibit the decomposition of DME and increase the content of LiF in SEI, this designed LHCHs could efficiently suppress the formation of lithium dendrites.[105] In 2021, Lu's group first examined the use of LiODFB as the lithium salt in LHCE (1 M LiODFB in 1DME: 2HFE) and discovered that a SEI containing polyether/coordinated borate (Fig. 9b) was constructed, enabling improved Li reversibility and enhanced cycling performance of NCM811 with a high cut-off voltage of 4.6 V *vs.* Li^+/Li.[106] Wang *et al.* first explored the non-flammable ionic liquid (*N*-methyl-*N*-propyl-piperidinium bis(fluorosulfonyl)imide, PP_{13}-FSI)-based LHCE (Fig. 9c) and found that the diluent largely decreased the viscosity of the pure ionic liquid electrolyte and greatly improved the ionic conductivity and wetting ability, resulting in excellent Li reversibility with high CE (99.4% over 800 cycles) and stable LMBs.[107] Zhu *et al.* used fluorinated aromatics (trifluoromethoxybenzene, TFMB and benzotrifluoride, BZTF, Fig. 9e) as the diluents to design new LHCEs. They found that, unlike the typical LHCEs, the diluent–anion interaction in these LHCEs facilitated the formation of a robust and homogenous SEI, which enabled excellent Li reversibility with an ultrahigh CE of 99.8%, and stable cycling performance of practical Li||NCM811 cells.[53] Li *et al.* also investigated the effects of anion–solvent interaction on the SEI and electrochemical performance. They introduced 2 wt% tris(pentafluorophenyl)borane (TPFPB), as an anion acceptor in LHCE (LiFSI-1.5DMC-2BTFE, by mol), and revealed that the introduction of TPFPB strengthened the Li^+–FSI^- interaction and promoted the decomposition of FSI^-, leading to the formation of a Li_2S-rich SEI, which further improved the electrochemical performance of Li||NCM532 cells (Fig. 9d).[108] Li *et al.* systematically investigated the influence of LHCEs on the electrochemical performance at low temperatures, and found that the LHCE (LiFSI in DME: 5BTFE) largely enhanced the Li stripping/plating efficiency with CEs of 98.9, 98.5, and 96.9% at −20, −40, and −60 °C, respectively, and enabled the stable cycling performance of Li||NCM811 cells with negligible capacity retention at −20 and −40 °C.[109]

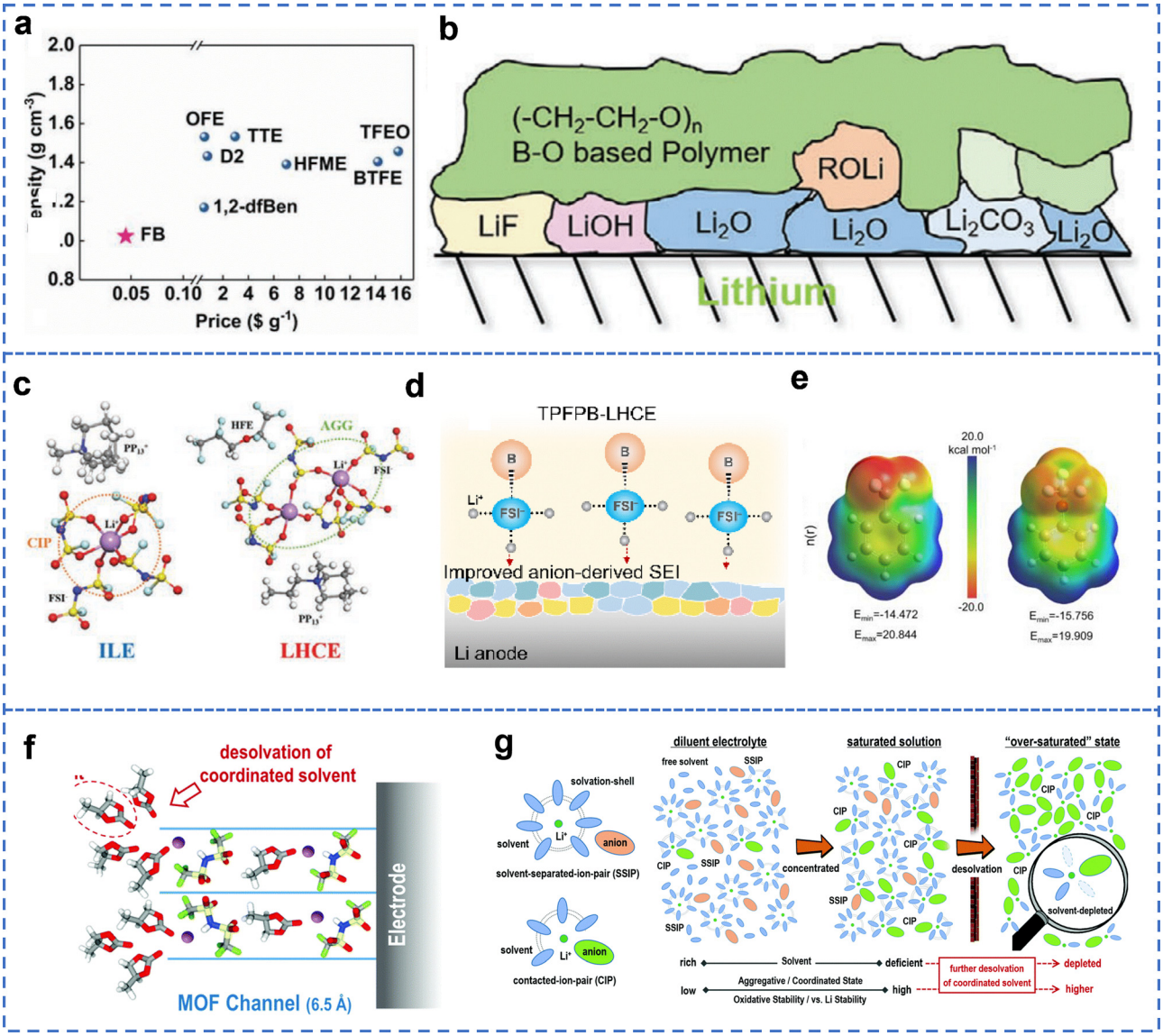

Fig. 9 (a) The comparison of the density and cost of FB with other cosolvents. Reproduced with permission.[105] Copyright 2020 Wiley. (b) Schemes of the high-efficiency polyether-like SEI in 5 M LiDFOB/DME/HFE. Reproduced with permission.[106] Copyright 2021 Wiley. (c) Li^+ coordination structure in LHCEs derived from MD simulation. Reproduced with permission.[107] Copyright 2021 Wiley. (d) Schematic illustration of the electrolyte structure of FSI^- and the correspondingly formed SEI in TPFPB-LHCE. Reproduced with permission.[108] Copyright 2021 Wiley. (e) Electrostatic potential diagrams of TFMB and BZTF. Reproduced with permission.[53] Copyright 2021 American Chemistry Society. (f) Schematic illustration of the configuration achieved inside MOF channels, and (g) the proposed design idea of further depleting solvent molecules within the Li^+ solvation sheath. Reproduced with permission.[110] Copyright 2020 Royal Society of Chemistry.

Recently, Zhou and co-workers designed an intriguing electrolyte (de-solvated electrolyte or ''over-saturated'' electrolyte) which is composed of conventional electrolytes and metal organic frameworks (MOFs) with unique pore structures.[111] As shown in Fig. 9f, compared with conventional electrolytes, Li^+ is completely desolvated and the solvents are ''frozen'' with MOFs in the ''desolvated electrolyte''. As a result, ultra-stable Li||NCM811 cells were achieved with a capacity retention of 77.8% after 800 cycles and 94.6% after 200 cycles.[112] In the same year, they designed an ''over-saturated'' electrolyte by addition of 1 M LiTFSI-PC in Cu-1,3,5-benzene tricarboxylate. As shown in Fig. 9g, most of the coordinated solvents in the solvation sheath of Li^+ are depleted from Li^+ due to the confining effect of MOFs, leading to an ''over-saturated'' state near the electrodes. The ''over-saturated'' electrolyte provided a capacity retention of 90% after 400 cycles for Li||NCM811 in the range of 2.7–4.4 V and 94.5% after 1250 cycles for Li||LCMO in the range of 3–5.3 V.[110]

3.2.3. WSEs based on weakly-polar solvents in LMBs. Decreasing the polarity of the solvents is another effective strategy to construct weak solvating electrolytes.[113] Compared with increasing the concentration of lithium salts, choosing solvents with low polarity or decreasing the polarity through molecular design is a more straightforward way to weaken the

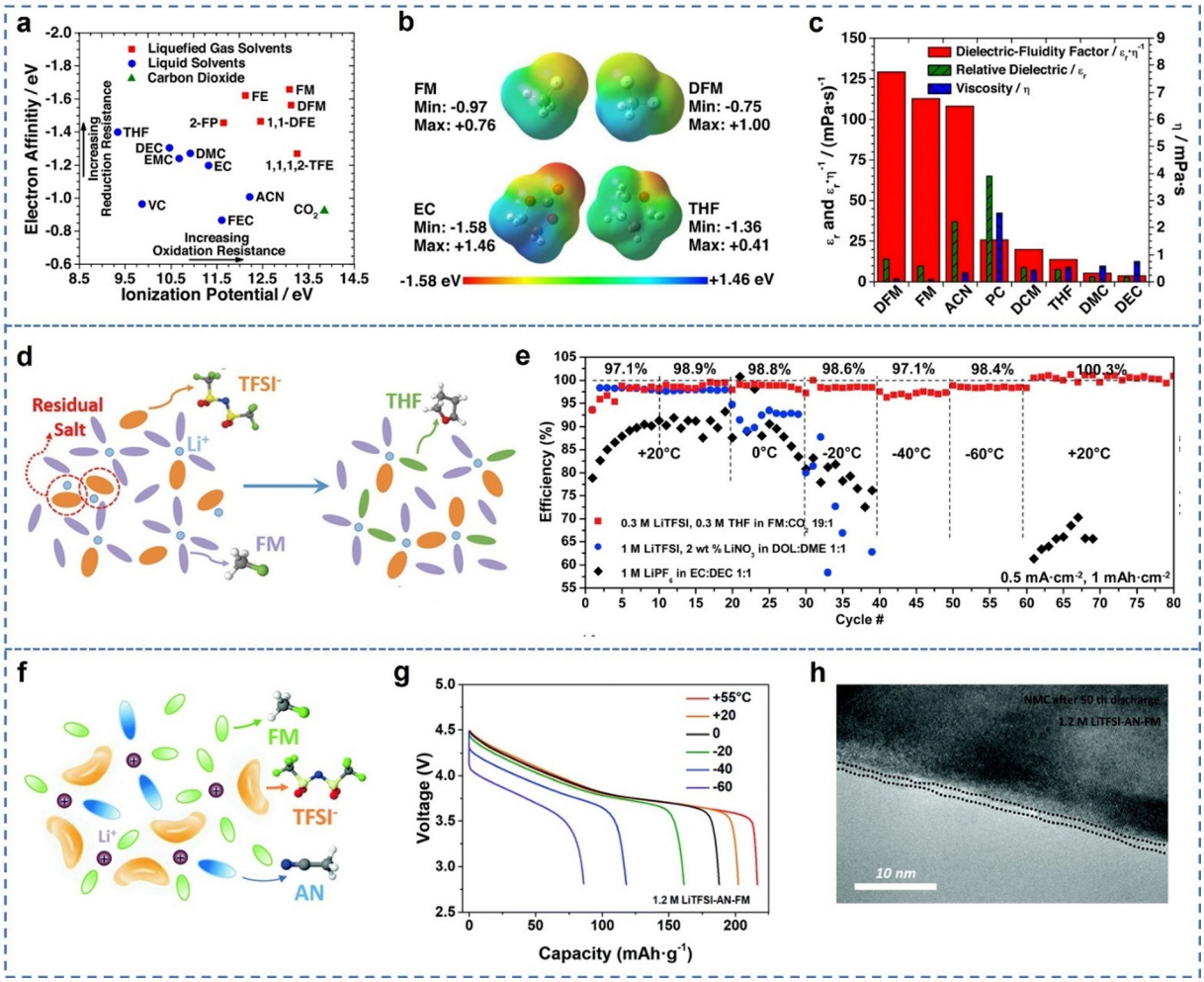

Fig. 10 (a) The electron affinity and ionization potential of different solvents. (b) Electrostatic potential maps of different solvents. (c) Dielectric-fluidity factor, relative dielectric, and viscosity of different solvents. Reproduced with permission.[115] Copyright 2017 AAAS. (d) Schematic of the solvation sheath of Li^+ with the addition of THF. (e) The Li plating/stripping CE using different electrolytes at various temperatures. Reproduced with permission.[116] Copyright 2019 Elsevier. (f) Schematic illustration of the solvation sheath of Li^+ with the addition of AN. (g) Discharge curves of Li-NMC cells at different temperatures using 1.2 M LiTFSI-AN-FM. (h) Cryo-TEM (transmission electron microscope) images of NMC particles after the 50th discharge in 1.2 M LiTFSI–AN–FM. Reproduced with permission.[117] Copyright 2020 Royal Society of Chemistry.

Li^+–solvent affinity. The decreased binding ability between Li^+ and solvents strengthens the affinity of Li^+ and anions; thus more anions appear in the Li^+ solvation sheath, forming CIPs and AGGs dominated solvation structures, which further lead to anion-derived electrode–electrolyte interphases, which are vital to the electrochemical performance of the LMBs.

One of the representative examples of WSEs using solvents with low polarity is the striking liquified gas electrolytes, which were first proposed by Meng's group in 2017.[114] From the calculated results shown in Fig. 10a, it is clearly shown that the liquified gas solvents have both high ionization potential and electron affinity, that is, excellent reductive and oxidative stability, which are also demonstrated by the electrostatic potentials in Fig. 10b. Although, compared with conventional solvents, these liquified gas solvents such as fluoromethane (FM) and difluoromethane (DFM) have a lower dielectric constant (10–15), their viscosities are significantly lower than those of conventional solvents. Consequently, the ratios of the dielectric constant to viscosity of liquified gas solvents are substantially larger than those of conventional electrolytes (Fig. 10c), which implies that the potential for high ionic conductivities in these liquified gas electrolytes. Moreover, the low viscosity at ultra-low temperatures is beneficial for the low-temperature electrochemical performance. To verify the above speculation, 0.2 M LiTFSI in $FM:CO_2$ (19 : 1), in which the addition of CO_2 was used for stable SEI construction, was prepared as an electrolyte for 4 V class LMBs. The liquified gas electrolyte demonstrates superior electrochemical performance in lithium metal anodes and LCO cathodes at ultra-low temperatures.[115] The Li stripping/plating CE in the liquified gas electrolyte is about 97%, which cannot meet the requirements in LMBs. In order to further improve the performance of liquified gas electrolytes in LMBs, THF with a high dielectric constant was introduced as a cosolvent, obtaining the novel liquified gas

electrolyte (0.3 M LiTFSI, 0.3 M THF in FM: CO_2). The introduction of THF could effectively address the issues of limited salt dissolution and high polarization, leading to an alternative solvation sheath, high conductivity, and improved transference number (Fig. 10d). Therefore, a high CE of 99.6% was achieved during 500 cycles at 0.5 mA cm^{-2}. More inspiringly, a high CE of 98.4% was achieved at a temperature as low as −60 °C (Fig. 10e).[116] Furthermore, in 2020, they adopted AN, due to its high dielectric constant, good oxidation stability, and low viscosity, as a cosolvent to improve the FM-based liquified gas electrolytes. The deliberately designed electrolyte (1.2 M LiTFSI, 1 M AN in FM, Fig. 10f) exhibited superior ionic conductivity (>4 mS cm^{-1}) in the temperature range from −78 to 75 °C. Besides its excellent performance in lithium metal anodes, this electrolyte also exhibited substantially improved performance in Li||NCM full cells (Fig. 10g), which was ascribed to the homogeneous and robust CEI formed on the surface of the cathodes.[117]

Physical/chemical properties of solvents are closely related with not only the environmental conditions (temperature or pressure), but also their molecular composition and configuration. Thus, designing solvents with specific properties through a ''bottom–up'' molecular design is pivotal in electrolyte engineering. Li's group synthesized various solvents inspired by the molecular structures of anions in lithium salts. In 2020, they came up with a novel ''FSI-inspired'' organic solvent, dimethylsulfamoyl fluoride (FSA) by imitating the anion in LiFSI and developed a new ''full fluorosulfonyl'' (FFS) electrolyte composed of 2.5 M LiFSI and 0.2 M $LiPF_6$ in FSA (Fig. 11a). Due to the weak affinity between FSA and Li^+ and the similar structure of FSA with FSI^-, a LiF-rich FFS-derived SEI was formed, leading to not only compact and flat Li deposition, but also stable cycling performance in Li||NCM622 cells with a capacity retention of 89% after 200 cycles.[118] In 2021, they further synthesized *N*,*N*-dimethyltrifluoromethane sulfonamide (DMTMSA) by imitating the ''$TFSI^-$'' anion and developed a novel sulfonamide-based electrolyte composed of 1 M LiFSI in DMTMSA. Because the low polarity, lithium salt has a low solubility in DMTMSA, in which the weak Li^+–solvent interactions strengthen the affinities between Li^+ and anions, leading to an FSI^-derived SEI, making the sulfonamide-based electrolyte compatible with the lithium metal anode. Meanwhile, the weak ability to solvate salts and the intrinsic anodic stability, combined with LiF-rich inorganic components inside the CEI derived from the electrolyte, synergistically suppress the dissolution of transition metal, microcracks and phase transformation in the cathode, and the Al corrosion of current collector (Fig. 11b). As a result, the sulfonamide-based electrolyte significantly improved the cycling stability of NCM811 with an ultra-high cut-off voltage of 4.7 V *vs.* Li^+/Li (Fig. 11c, d).[119] Li||LCO cells using the sulfonamide-based electrolyte also demonstrated a capacity retention of 85% after 100 cycles with a cut-off voltage of 4.6 V *vs.* Li^+/Li (Fig. 11e). DFT results showed that the energy of the oxidation reaction between DMTMSA and highly de-lithiated LCO was much smaller than that of EC, clearly explaining the highly enhanced anodic stability of the sulfonamide-based electrolyte, especially at ultra-high voltages (Fig. 11f).[120]

Ethers such as DOL and DME, usually have low viscosity, low melting points and excellent compatibility with lithium metal, but poor anodic stability. Bao's group have performed excellent works on ether modification.[121] They replaced the methoxy groups in DME with ethoxy groups, obtaining 1,2-diethoxyethane (DEE). Compared with DME, DEE retains the ethylene glycol groups while having terminal alkyl groups with increased steric hinderance, which significantly affects its solvating ability. Thus, in LiFSI–DEE electrolyte, the weak Li^+–DEE interaction, in turn, enhanced the Li^+–anion affinity, leading to the formation of an anion-rich inner solvation sheath. Consequently, the new electrolyte facilitates the anion-derived SEI, suppresses Al corrosion, and promotes anodic stability. Li||NCM811 cells (50 μm thin Li) using 4 M LiFSI in DEE achieved a capacity retention of 80% after 182 cycles at a high cut-off voltage of 4.4 V *vs.* Li^+/Li.[122] The reduced Li^+–DEE interactions not only promote the anodic stability, but also facilitate the de-solvation of Li^+, largely ameliorating the charge-transfer resistance, especially at low temperature.[123] As a result, Li||Cu cells using 1 M LiFSI in DEE delivered a high CE of 98.4% at −60 °C, and Li||SPAN full cells retained 76% of their room-temperature capacity at −60 °C.[124] However, the wide application of 1 M LiFSI in DEE was severely impeded by its moderate anodic stability. Instead, another alternative strategy to further regulate the polarity of ether solvent has also been reported by Bao's group. In 2020, they first improved the length of the alkyl chain in the middle of DME, obtaining 1,4-dimethoxylbutane (DMB). Then the –H groups in the added alkyl chain were replaced with –F groups. In brief, two $-CF_2$ groups were added into the middle of DME, obtaining fluorinated 1,4-dimethoxylbutane (FDMB). It is worth noting that the addition of $-CF_2$ groups does not severely decrease the solvation ability due to distance between –F and –O groups. Both the longer alkyl chain and –F substitution strengthen the oxidative stability and alter the solvation structure of Li^+ in the presence of more anions. From the results of MD simulation, the average ratio of anions to solvent increases from 2.31 to 3.29, in consistence with the speculations. As a result, 1 M LiFSI in FDMB exhibited excellent Li compatibility and considerable high-voltage resistance, as evidenced by oxidation voltages >6 V *vs.* Li^+/Li. The NCM523 with thin Li delivered a capacity retention of 90% after 420 cycles.[125] However, 1 M LiFSI in FDMB showed high overpotential in Li||Li symmetric cells, implying its poor kinetics, indicating that the $-CF_2$ groups have an immoderate effect on the solvation ability of DME or DEE. Therefore, based on DME, they further thoroughly investigated the effect of the position and amount of –F groups on the electrolyte performance. The introduction of fully fluorinated $-CF_3$ with strong electron-withdrawing properties boosts the oxidative stability of the electrolyte; however, in turn, it induces weak solvation of lithium salts and reduced ionic conductivity. The interaction between Li^+ and partially fluorinated $-CHF_2$ groups is much stronger than that between Li^+ and $-CF_3$ due to intrinsic locally polar and more negatively

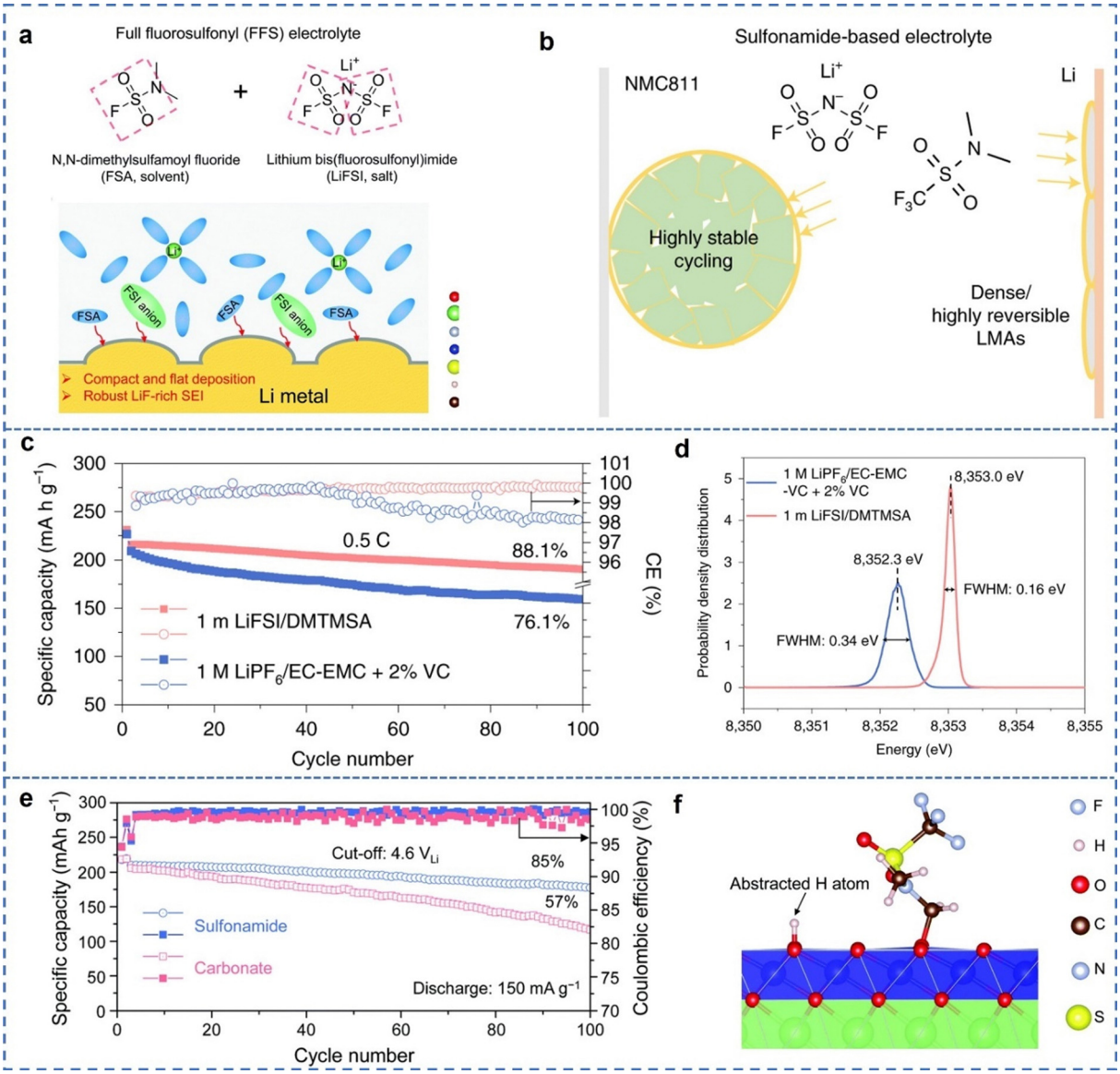

Fig. 11 (a) Schematic illustration of the solvation structure and derived SEI in electrolytes containing both solvent and lithium salt with fluorosulfonyl groups. Reproduced with permission.[118] Copyright 2020 Royal Society of Chemistry. (b) Schematic illustration of the function of the sulfonamide-based electrolyte in both the lithium metal anode and Ni-rich cathode. (c) Cycling performance of Li||NMC811 cells using different electrolytes. (d) Ni oxidation states of the cycled NMC811 cathodes with different electrolytes. (e) Cycling performance of Li||LCO cells with different electrolytes. (f) Relaxed structure and reaction energy of $DMCF_3SA$ derived from DFT. Reproduced with permission.[120] Copyright 2021 Royal Society of Chemistry.

charged nature of $-CHF_2$. By analysing the Li^+–solvent binding and solvation environment, it is found that partially fluorinated $-CHF_2$ is the optimal group for molecular design. In LiFSI/F5DEE, the content of AGGs is about 80.6%, which is lower than that in LiFSI/F6DEE and LiFSI/FDMB, but higher than that in LiFSI/F4DEE, LiFSI/F3DEE, and LiFSI/DEE. As a result, an ultrahigh CE of 99.9% in Li||Cu cells and a capacity retention of 80% in high-loading NCM811 with thin Li anode were achieved, respectively.[126]

In order to combine high redox stability with good ionic conductivity in ether-based electrolytes, Zhou *et al.* developed a novel solvent, 2-ethoxy-4-(trifluoromethyl)-1,3-dioxolane (cFTOF), by modifying triethyl orthoformate (TOF), *via* integrated ring-chain and fluorination processes (Fig. 12a). The novel molecule cFTOF, combined with low concentration lithium salts, results in dendrite-free and compact Li anodes and highly enhanced cycling stability in NCM811 paired with ultrathin Li foil.[127] Zhao and co-workers synthesized a new fluorinated ether, 2,2-dimethoxy-4-(trifluoromethyl)-1,3-dioxolane (DTDL) by combining linear ether and cyclic fluorinated segments (Fig. 12b and c). The spatial arrangement of electron-withdrawing $-CF_3$ groups not only increases the oxidation stability, but also prevents a significant decrease in its solvating ability by preventing direct attachment of the $-CF_3$ group to the O atoms. Therefore, DTDL exhibits high anodic stability and controlled solvating ability with Li^+. Consequently,

Li||Cu cells using 1 M LiFSI-DTDL exhibited a high CE of 99.2% during 500 cycles. More intriguingly, NCM811 paired with thin Li using 2 M LiFSI-DTDL delivered a capacity retention of 84% after 200 cycles.[128]

Besides fluorination, the introduction of chlorine functionality in ethers was also demonstrated to be an effective strategy by Tan *et al.* to boost the performance of ether-based electrolytes. On the one hand, the lower electronegativity of Cl atoms and smaller energy of the Cl–C bond, compared with the F-based counterparts, are beneficial to regulating the Li^+ solvation structure (the content of AGGs increased from 33.9% to 47%) and achieving an anion-derived SEI or CEI (LiF, LiCl-rich). An nnion-derived SEI can supress the formation of lithium dendrites, while an anion-derived CEI supresses the dissolution of transition metal (Ni, Co, and Mn). On the other hand, Cl, similar with other halogens, lowers the energy level of HOMO of molecules, enhancing the oxidative stability under high voltage (Fig. 12d). Consequently, LiFSI/1.6Cl-DEE/3TTE electrolyte exhibited a high Li CE of 99.2% and an excellent capacity retention of >88% after 200 cycles in 4.6 V NCM811 cells.[129]

Compared with conventional ether-based electrolytes, ester-based electrolytes possess better anodic stability. However, they are not compatible with either high-voltage (>4.3 V) cathodes and lithium metal anodes, severely hindering their application in high-voltage LMBs with high energy density. Through simple but effective molecular design of traditional esters, such as EC and DEC, desired Li^+ solvation structures and electrolyte–electrode interphases can be achieved, which enable not only significantly improved compatibility with the lithium metal anode and ultrahigh-voltage cathode, but also superior electrochemical kinetics in a wide temperature range. Recently, our group proposed a multiscale regulation strategy of "molecular

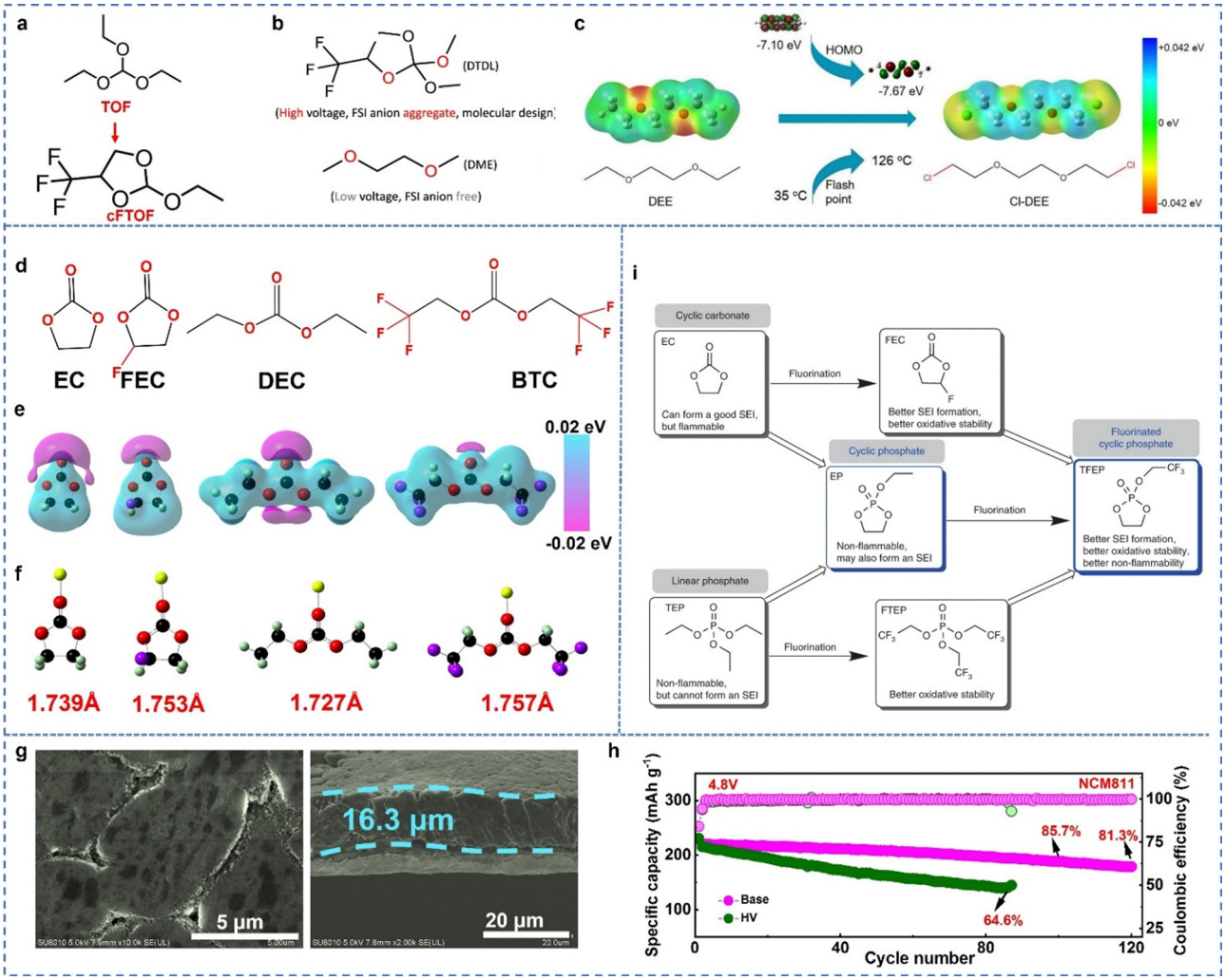

Fig. 12 (a) Molecular structures of TOF and cFTOF. Reproduced with permission.[127] Copyright 2022 Wiley. (b) Molecular structures of DME and DTDL. Reproduced with permission.[128] Copyright 2022 Nature Publishing Group. (c) Design schematic and molecular structures of DEE and Cl-DEE. Reproduced with permission.[129] Copyright 2022 Wiley. (d) Molecular structures and (e) the electrostatic potential (ESP) of different solvents. (f) Optimized structures of Li^+ with different solvents. (g) SEM images of deposited lithium using HV electrolyte. (h) Cycling performance of Li||NCM811 cells with a cut-off voltage of 4.8 V *vs.* Li^+/Li. (i) Design principle of the fluorinated cyclic phosphate solvent (TFEP). Reproduced with permission.[130] Copyright 2022 Royal Society of Chemistry.

structure-solvation behavior–stable interfaces-electrochemical performance'' based on the above design principles. As shown in Fig. 12d–f, fluoroethylene carbonate (FEC) and bis(2,2,2-trifluoroethyl) carbonate (BTC) are synthesized by replacing –H atoms with –F groups in both EC and DEC. Consequently, there is less negative charge in both BTC and FEC, indicating their relatively weaker binding with Li^+, which is corroborated by the smaller binding energies and larger distances between Li^+ and these different solvents. On the one hand, the weak binding energy between Li^+ and fluorinated solvents facilitates the desolvation process of Li^+, reducing the charge-transfer resistance and resulting in an improved performance, especially at low temperatures. Moreover, the presence of abundant –F groups in the solvents promotes the wetting ability, which also improves the electrochemical kinetics with lean electrolytes. On the other hand, the optimized Li^+ solvation structure induces the formation of LiF-rich electrode–electrolyte interphases, combined with the intrinsic oxidative stability of fluorinated solvent, resulting into stable cycling performance at ultra-high voltage. As shown in Fig. 12h, homogeneous and compact dendrite-free lithium was achieved in the fluorinated electrolytes. Meanwhile, NCM811 with an ultra-high voltage of 4.8 V *vs.* Li^+/Li exhibited 85.7% retention after 100 cycles (Fig. 12i).[130] Wang *et al.* investigated the influence of the amount of F atoms in EC-based solvent (EC, FEC, difluoro ethylene carbonate, DFEC) on the performance of lithium metal batteries. They found that the strength of Li^+–solvent interactions decreased with the increase in the fluorination degree. Therefore, the desolvation rate in DFEC-based electrolyte was six times high as that in EC-based electrolytes. Li||NCM811 cells displayed stable cycling performance and fast kinetics using DFEC-based electrolyte.[131] Chen *et al.* designed a new all-fluorinated ester electrolyte (1 M $LiPF_6$ in methyl 3,3,3-trifluoropionate (MTFP) and FEC) for high-voltage LMBs with excellent low-temperature performance. The all-fluorinated ester endowed Li||NCM811 cells with a cut-off voltage of 4.5 V, a high capacity retention of 80% after 250 cycles and a discharge capacity of 133 mA h g^{-1} at −60 °C.[132] In 2020, Zheng *et al.* designed a cyclic phosphate, 2-(2,2,2-trifluoroethoxy)-1,3,2-dioxaphospholane 2-oxide (TFEP), which combined the following advantages of other solvents: ability of forming a good SEI in cyclic EC, excellent oxidative stability in fluorinated molecules, and non-flammability of linear phosphate (Fig. 12g). As a result, a non-flammable electrolyte was obtained based on TFEP, which enhanced the cycling stability of a 4.9 V LNMO cathode with a capacity retention of 70% after 200 cycles.[133]

3.2.4. WSEs based on strong Li^+–anion affinity in LMBs. An ideal lithium salt for conventional LIBs should be able to dissociate completely, and the resulting solvated Li^+ ions have high mobility, allowing to achieve high ionic conductivities. However, due to the strong Lewis acid character and small ionic radius of Li^+, most of the lithium salts with simple anions, such as F^-, O^{2-}, N^{3-}, Cl^-, S^{2-}, and CO_3^{2-}, barely dissolve in organic solvents. Thus, complex anions composed a simple anion core and Lewis acid agents are designed to improve the dissolution of lithium salts in nonaqueous solvents.[33] For instance, ''PF_6^-'' can be viewed as a strong Lewis base (F^-) neutralized by Lewis acid (PF_5). Similarly, ''BF_4^-'' is composed of F^- and BF_3, which weakens the interactions between Li^+ and anions, improving the solubility of lithium salts in organic solvents. For example, in the case of LiFSI, the weak binding ability of Li^+ with FSI^- substantially enhanced its solubility, allowing its wide usage in HCEs or LHCEs. However, reducing the binding energy of anions with Li^+ inevitably introduces a significant amount of solvents into the inner solvation sheath of Li^+, which is not beneficial for the formation of ideal electrode–electrolyte interphases. Therefore, precisely regulating the affinity of Li^+ and anions not only maintains the dissolubility of lithium salts, but also makes the manipulation of Li^+–anion interaction possible.[19,134,135] For instance, the order of the dissociation constant for some typical lithium salts is LiFSI > $LiAsF_6$ > $LiPF_6$ > $LiClO_4$ > $LiBF_4$ > LiTFSA, implying that the affinities between Li^+ and the corresponding anions follows the opposite order,[32] highly affecting the solvation structure of Li^+ and stability of electrode–electrolyte interphases.[136–138] It is worth noting that in these lithium salts suitable for rechargeable batteries, the binding energy between Li^+ and solvents is larger than that between Li^+ and anions, ensuring the dissolubility of lithium salts and the favourable ionic conductivity.

Zhang's group introduced $LiNO_3$ into 2 M LiFSI–DME electrolytes to investigate the effects of $LiNO_3$ on the solvation sheath of Li^+, the SEI structure, and the corresponding electrochemical performance. Due to the strong interaction between Li^+ and NO_3^-, NO_3^- was successfully introduced into the inner Li^+ solvation sheath, which was proven by MD simulation and Raman spectroscopy. Moreover, NO_3^- in the primary solvation sheath tamed the interaction between Li^+ and FSI^-, resulting in the polarization of FSI^-, which, combined with the reduction of NO_3^-, led to the formation of an inorganic-rich SEI. This work provided a new insight into the effect of different anions on high-performance LMBs.[139] Wang *et al.* adopted lithium trifluoroacetate (LiTFSA) as the substitute for $LiPF_6$. Due to the strong affinity between Li^+ and $TFSA^-$, the introduction of LiTFSA significantly altered the Li^+ solvation structure, leading to the formation of a stable LiF, Li_2O-abundant SEI and a fast de-solvation process. As a result, the LiTFSA-based electrolyte designed *via* the anion-tuned strategy significantly suppressed the formation of lithium dendrites and highly improved the cycling performance of the NCM622 cathode.[140] Recently, Jiang *et al.* presented a novel WSE by regulating the anion rather than the solvent (1.5 M $LiBF_4$ in FEC/DME). Due to the strong affinity between Li^+–BF_4^-, anion derived B, F-rich SEIs/CEIs were obtained, enhancing the high-voltage (4.6 V) Li||LCO full cells with cycling stability.[141]

Besides these WSEs discussed above, Zheng found that in 0.8 M LiTFSI–0.2M LiODFB in ADN : EC (1 : 1), the solvation structure of Li^+ changed significantly with the increase in operating temperatures, that is, AGGs and CIPs increased with the improvement of temperature. Due to this unique temperature-dependant property of the Li^+ solvation structure,

LMBs utilizing this electrolyte demonstrated a temperature range from −20 to 150 °C.[142]

3.3. Strong solvating electrolytes in LMBs

Although WSEs have been extensively investigated and widely used in LMBs, the introduction of additional polar solvents (or non-solvents) with strong solvating ability is another alternative strategy for designing ideal electrolytes for LMBs. Unlike the strategies in WSEs, the highly polar solvents (or non-solvents) with strong solvating ability are usually used to dissociate salts to manipulate the Li^+ solvation structure with specific anions or cations. A typical example is the introduction of $LiNO_3$ into carbonate-based electrolytes. NO_3^- has a low energy level of the LUMO, making it prone reduction on the surface of lithium metal. The reduction of NO_3^- induces the construction of robust and highly conductive SEI rich in Li_3N and Li_2O, suppressing the formation of lithium dendrites and homogenous and compact deposition of lithium even at high current densities (Fig. 13b).[149] However, compared with other complex anions, the simple NO_3^- anion has stronger binding ability with Li^+, allowing $LiNO_3$ to barely dissolve in the conventional carbonate-based electrolytes.[150] Therefore, strong Lewis bases or acids with enhanced binding ability with Li^+ or NO_3^-, respectively, are highly needed for successful introduction of $LiNO_3$ or NO_3^- into the primary solvation sheath.[151] There are two ways to dissociate $LiNO_3$, that is, addition of a strong Lewis base to attract Li^+, or a strong Lewis acid to attract NO_3^- to weaken the interaction between Li^+–NO_3^-, as shown in Fig. 13a, which are known as cation receptors or anion receptors, respectively.[32]

Cation receptors, such as TMU, DMSO, ethylene glycol diacetate, crown ether, tetra-ethylene glycol dimethyl ether, tris(pyrrolidinophosphine)oxide (TPPO), tetramethylurea (TMU), and GBL, are widely used as strong solvating solvents.[88,143–145,152–157] Since the donor number is an important parameter to measure the strength of the solvents as a Lewis base, it is widely adopted to choose or design appropriate solvents as cation receptors. For example, NO_3^- has a DN of 21.1 kcal mol^{-1}, which is much higher than those of EMC and EC, resulting in extremely low solubility of $LiNO_3$ in conventional carbonate-based electrolytes.[152] Wang's group chose SL and DMSO as the solubilizer to dissolve $LiNO_3$ (Fig. 13c and d). Because of the strong affinities between SL or DMSO and Li^+, $LiNO_3$ is prone to dissolution into the electrolyte with the introduction of NO_3^- into the Li^+ solvation sheath. The NO_3^- in the Li^+ solvation sheath tends to undergo reduction on the surface of lithium metal when the solvated Li^+ approaches the anode, forming an inorganic-rich (Li_3N, Li_2O, and LiF) SEI, achieving a high Li plating/stripping CE of 99.55% and a capacity retention of 75% after 200 cycles in the NCM811 cathode.[145] Our group deliberately chose TPPO and TMU as the strong solvating solvents for the introduction of $LiNO_3$ into the conventional carbonate-based electrolyte. Similarly, both the electrolytes significantly enhanced the stable Li stripping/plating process. More importantly, these two solvents, as Lewis bases, can coordinate with PF_5, preventing the formation of HF, and thus preventing the deterioration of the cathode and CEI, and avoiding metal ion dissolution and consistent electrolyte decomposition, leading to ultra-stable cycling performance in 4 V LMBs, especially at high temperatures.[143,157]

Anion receptors, such as copper fluoride (CuF_2), tris(pentafluorophenyl)borane (TPPB), indium(III) tri-fluoromethane sulfonate ($In(OTf)_3$), and tin tri-fluoromethane sulfonate ($Sn(OTf)_2$) are also used to address the issue of dissolubility of $LiNO_3$.[19,146,147,158] Lu's group investigated the effects of different anion receptors on the Li^+ solvation sheath and the corresponding electrochemical performance of LMBs. First, they designed a new electrolyte by addition of TPPB and $LiNO_3$ in 1M $LiPF_6$-FEC-EMC and found that the addition of TPPB can significantly increase the dissolubility of $LiNO_3$ in carbonate-based electrolytes with a new Li^+ solvation structure. As a result, a robust SEI and F-, B-containing CEI were successfully constructed, leading to a high Li CE of >98.5% over 300 cycles at 1 mA cm^{-2}, and a capacity retention of 89.8% after 160 cycles for a 4.6 V LCO.[158] $Sn(OTf)_2$ was also used as a solubilizer to coordinate and solvate NO_3^- from $LiNO_3$ in 1 M $LiPF_6$-EC-DEC. A unique Sn^{2+}–NO_3^- solvation structure was obtained, leading to the formation of a metal–organic hybrid SEI layer, resulting in a high Li CE of 98.14% during 150 cycles and a capacity retention of 80% after 200 cycles in high-loading NCM811 paired with a thin Li anode (Fig. 13e).[146] Similarly, *via* addition of $In(OTf)_3$, a wavy SEI with high ionic conductivity was constructed derived from In^{3+}–NO_3^- solvation structures, significantly improving the Li stripping/plating CE, promoting compacted deposition, and enhancing the cycling performance of high-capacity NCM811 with a thin lithium anode (Fig. 13f).[147] Xu *et al.* systemically investigated the interfacial chemistry of anion/cation receptors in electrolyte near the lithium metal using a combined theoretical and experimental model, which afforded a fundamental understanding of the strong solvating electrolytes, and shed light on the further design of ideal electrolytes in LMBs (Fig. 13g).[148] The electrochemical performance of high-voltage LMBs, focussing on the properties of SEI/CEI and LMBs with wide operating temperature ranges and strategies adopted are summarized in Tables 2 and 3, respectively.

In high-voltage LMBs, WSEs show great potential as ideal electrolytes because the weak Li^+–solvent interactions endow them with not only excellent anodic and cathodic stability induced by an anion-derived EEI, but also enhanced kinetics because of the low de-solvation barriers. There is both solid theoretical and experimental evidence demonstrating the key roles of the anion-derived inorganic-rich SEI in WSEs in strengthening the compatibility of electrolytes with both high-voltage cathodes and lithium anodes. However, there are several paradox or controversial issues regarding the kinetics. First, the extent to which the weak interaction of Li^+–solvents is beneficial to the performance of LMBs is not fully understood. Does reducing the interaction of Li^+–solvents always lead to better cycling stability and kinetics? Obviously, if the interaction of Li^+–solvents decreases to a point where the solvents are not capable of dissociating enough lithium salts, the ionic

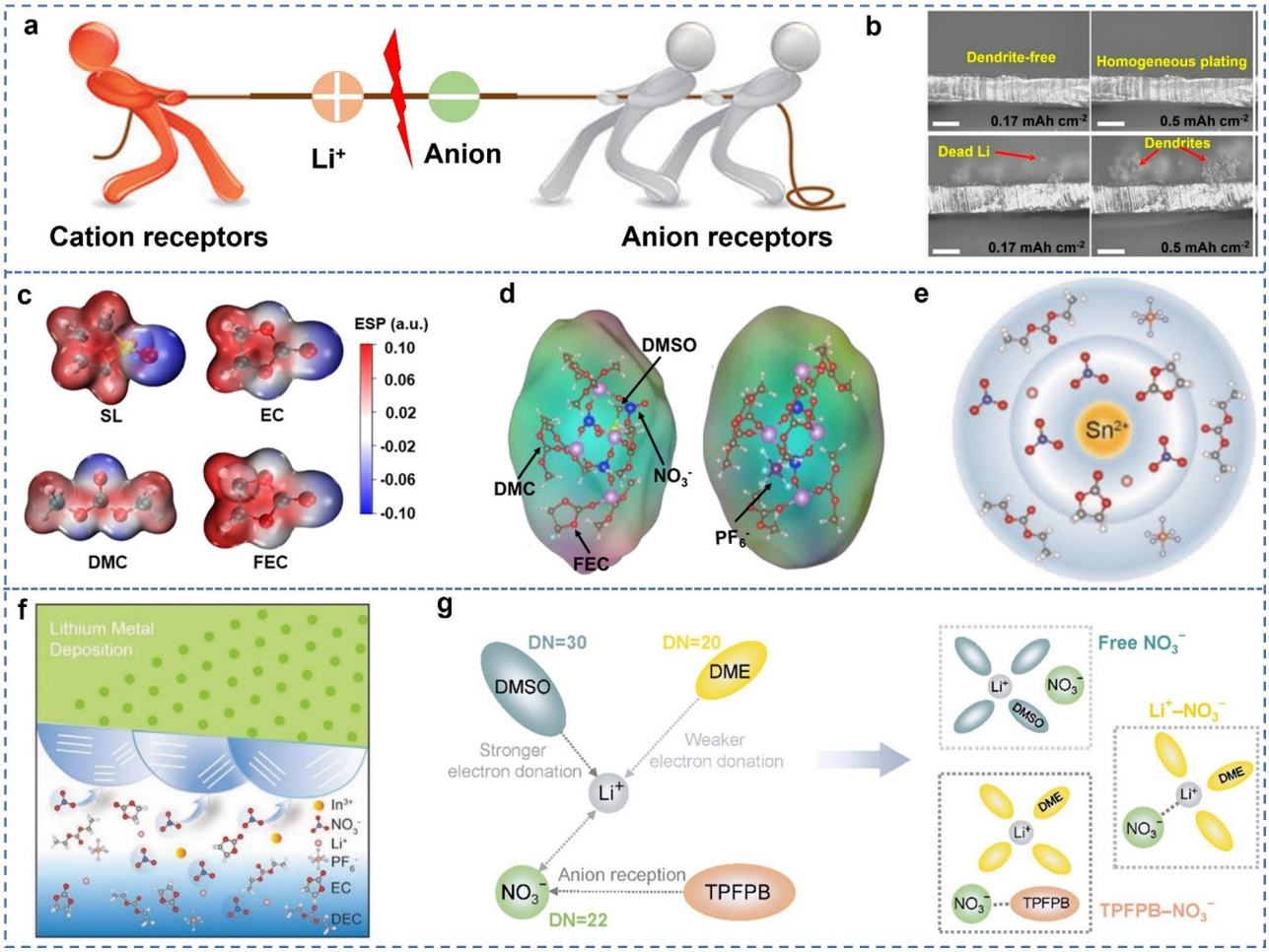

Fig. 13 (a) Schematic illustration of the functions of cation/anion receptors on the lithium salts. (b) SEM images of deposited Li in electrolytes with or without $LiNO_3$. Reproduced with permission.[143] Copyright 2021 American Chemical Society. (c) Electrostatic potential of SL, EC, DMC, and FEC molecules. Reproduced with permission.[144] Copyright 2021 American Chemical Society. (d) Representative Li-solvation structure in electrolytes with or without $LiNO_3$. Reproduced with permission.[145] Copyright 2020 Wiley. (e) Schematic illustration of the solvation sheath structure in the designed electrolyte. Reproduced with permission.[146] Copyright 2020 Wiley. (f) Schematic illustration and the proposed formation mechanism of the wavy SEI.[147] Reproduced with permission. Copyright 2020 Wiley. (g) The interaction between NO_3^- and solvent and cation/anion receptors. Reproduced with permission.[148] Copyright 2021 Wiley.

conductivity and the corresponding electrochemical kinetics would be severely compromised. Is there an ideal range in which the interaction between Li^+ and solvents is strong enough to dissociate enough lithium salts, while weak enough to achieve fast de-solvation of Li^+ and the construction of excellent EEIs? Second, there are several reports in which LMBs using WSEs exhibit superior low temperature performance but high overpotential in Li||Cu cells, both of which are highly associated with the kinetics.[124,173] The electrochemical kinetics are highly related with the ionic transport in bulk electrolyte, de-solvation process of Li^+ near the electrodes, and ion diffusion through the EEI and in the electrode. Does the ionic conductivity of bulk electrolyte play a key role in Li||Cu cells, while the de-solvation process dominates the low temperature process? These are intriguing but important questions which need to be addressed because understanding the underlying mechanism is the prerequisite for electrolyte design.

With LMBs, one must consider their practical issues such as energy density and cycling life. It is worth noting that the constant reactions occurring between lithium metal and electrolyte are inevitable due to the ultrahigh activity of lithium. Compared with LIBs, a high E/C ratio is needed to achieve a long cycling life. The N/P ratio is another important parameter which affects not only the energy density, but also the long-term cycling stability.[174] In anode-free LMBs (N/P = 0) with improved energy density, the constant reactions between Li and electrolytes progressively consume the limited Li inventory in the cathode, leading to a poor cycling life. If the N/P ratio is too high, the excess of lithium reacts with the limited electrolyte, leading to the depletion of electrolyte and an increase in cell impedance, resulting in the sudden failure of LMBs. Therefore, besides designing novel electrolytes, choosing appropriate E/C and N/P ratios, and adopting other strategies to protect Li are also quite important for the practical application of LMBs.

4. Strategies of regulating solvation chemistry in LIBs

Although LMBs received great attention before 1980s due to their high specific capacity and low redox potential, their commercial applications are still plagued by the notorious lithium dendrite issues. Instead, LIBs have overwhelmingly dominated the energy storage field for more than three decades since their first commercialization in 1990s.[33] Graphite or silicon-based materials, and EC-based solution, as anodes and electrolytes, respectively, are widely used in commercial LIBs. Despite their prevalence, the further development of high-performance of LIBs still faces huge challenges, such as the co-intercalation of solvents in graphite and the electrochemical performance at high-voltage or low/high temperatures. This section mainly summarizes the recent progress in addressing the above issues by regulating the solvation chemistry of electrolytes.

4.1. Moderate solvating electrolytes in LIBs

Compared with EC, PC has a wider liquid temperature range (T_m −48.8 °C, T_b 242 °C, Table 1), high anodic stability, and a comparable dielectric constant, which make it suitable as a solvent in LIBs. However, in 1970, Dey *et al.* found that PC constantly decomposed on graphite, leading to the disintegration of graphite induced by the co-intercalation of PC with Li^+ into graphite (Fig. 14).[175] It was not until 1990 that Dahn *et al.* investigated the Li^+ intercalation into graphite using PC/EC cosolvents and found that the SEI derived from the decomposition of EC could effectively suppress the co-intercalation of PC with Li^+ into graphite, after which EC has been widely adopted as a solvent in the electrolytes for commercial LIBs.[176] In 2003, Abe *et al.* also found that some other solvents such as DMSO, DMM, DEM, and DEE could undergo

co-intercalation with Li^+ into graphite, while other solvents such as 2-MeTHF and DBE could not.[177] It seems that in a moderate solvating electrolyte, the introduction of a robust SEI, whether derived from solvents or additives, is significantly important to avoid the co-intercalation of solvents into graphite.[32,33] Moreover, EC-based moderate solvating electrolytes usually show inferior anodic stability at high voltage and poor kinetics, especially at low temperatures.

4.2. Weak solvating electrolytes in LIBs

4.2.1. HCEs and LHCEs in LIBs. To address the issues in the moderate solvating electrolytes, HCEs or LHCEs have been deliberately designed.[178,179] In 2003, Jeony *et al.* first found that the phenomenon of co-intercalation of PC with Li^+ in graphite could be avoided just by increasing the concentration of lithium salts. As shown in Fig. 15a and b, compared with the conventional electrolyte, 2.72 M bis(perfluoroethylsulfonyl) imide (LiBETI)/PC electrolyte has fewer free PC molecules, successfully suppressing the co-intercalation of PC in graphite.[180] In 2010, Yamada *et al.* first reported the role of the Li^+ solvation structure in inhibiting the co-intercalation of solvents in graphite. Based on DMSO-based electrolyte, they found that increasing the concentration of lithium salts or the addition of co-solvents significantly reduced the DMSO in the solvation structure of Li^+, suppressing the co-intercalation of DMSO with Li^+ in graphite, leading to reversible Li^+ intercalation in graphite.[181,182]

In 2004, the same group investigated the electrochemical performance of graphite in AN-based electrolytes. As shown in Fig. 15c and d, when the concentration of LiTFSI in AN increased from 1 M to 4.2 M, the free anions almost disappeared and all participated into the primary solvation sheath of Li^+, forming CIPs or AGGs. As a result, the energy level of the LUMO in the concentrated electrolyte shifted from that of AN to that of anions (Fig. 15e). The anion-derived SEI was pivotal to the cathodic stability in AN-based electrolytes. This is the first report illustrating that the ideal SEI is derived from anions due to the changes in the Li^+ solvation sheath in LIBs.[24] The high reversibility of intercalation/deintercalation of Li^+ in graphite has also been demonstrated in SL-based HCEs.[184] In 2018, Ming *et al.* investigated the role of the SEI in inhibiting the co-intercalation of solvents with Li^+ in graphite. As shown in Fig. 15f, a robust SEI constructed during the first cycle in EC/DEC-based electrolytes could successfully maintain high reversibility of graphite but failed in conventional dilute ether-based electrolytes. They also discovered that the stable graphite anode in highly concentrated ether-based electrolytes also show severe exfoliation when discharged again in dilute ether-based electrolyte. Given these above phenomena, they concluded that the solvation sheath of Li^+ plays a more important role than the SEI in maintaining the reversibility of graphite in LIBs and proposed that the Li^+–solvent interactions weaken on increasing the concentration of lithium salts or introducing additional anions, significantly altering the Li^+ solvation structure, therefore avoiding the co-intercalation of solvents in graphite (Fig. 15g).[183] This report provides a new insight into the mechanism of electrolyte in stabilizing graphite in LIBs. It is worth noting that the above viewpoint is controversial due to the following reasons: first, the SEI is highly related with the Li^+ solvation structure, that is, regulating the Li^+ solvation structure alters the components and the structures of the SEI, leading to different electrochemical behaviors of graphite; second, increasing lithium salts weaken the Li^+–solvent interaction, facilitating the de-solvation of Li^+ and suppressing the co-intercalation of solvents with Li^+ into graphite; but these speculation cannot clearly explain the reason why the convention dilute EC/PC electrolyte (for example, 1 M $LiPF_6$ in EC/PC) can avoid the co-intercalation of solvents. In our viewpoint, both the SEI and the binding energy of Li^+–solvents play key roles in graphite stability in LIBs because the Li^+-binding energy dominates the de-solvation process of Li^+ before intercalation into graphite and the SEI makes the co-intercalation of solvents with Li^+ difficult. Moreover, due to the complex nature of the electrochemical performance, the roles of the SEI and Li^+–solving interaction may be different in different electrolytes. Jiang *et al.* investigated the influence of a localized highly concentrated electrolyte on the electrochemical performance of LIBs and found that the electrolyte composed of 1.5 M LiFSI in

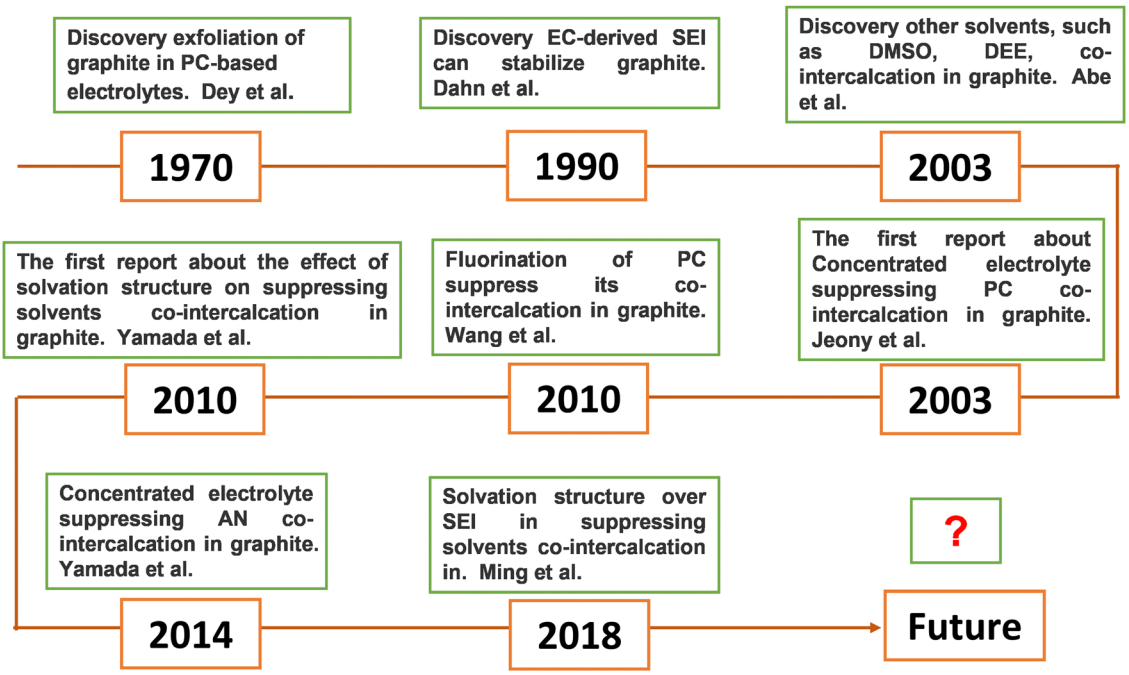

Fig. 14 The development of electrolytes in stabilizing graphite anodes.

DME/BTFE led to the formation of a uniform and robust FSI^--derived SEI, which not only significantly suppressed the co-intercalation of DME with Li^+ into graphite, but also significantly enhanced the rate performance, especially at a temperature as low as −20 °C.[185,186]

The solvation chemistry in highly concentrated electrolytes or localized highly concentrated electrolytes is also tamed to improve the high-voltage performance or kinetics in wide operating temperature ranges. Although EC-based electrolytes are widely used in 4 V-class LIBs, their anodic stability gradually declines with the increase in upper cut-off voltages when voltage >4.3 V *vs.* Li^+/Li or at high temperatures. The weak affinity between Li^+ and solvent in HCE or LHCEs alters the solvation structure of LI^+ from SSIPs to CIPs or AGGs, leading to an anodically stable and robust CEI, significantly enhancing the electrochemical performance at high cut-off voltages or high temperatures. Moreover, the electrochemical processes in LIBs are complex and there are more than ten processes of Li^+ migration during the charge or discharge process. Identification of the rate-limiting process is of great importance in regulating the electrochemical kinetics.[59,187–189] Li *et al.* investigated the factors affecting the kinetics in LIBS at different temperatures and found that the Li^+ de-solvation process was the rate-determining step in electrochemical processes at low temperatures.[59] In 2013, Yamada *et al.* designed a highly concentrated ether electrolyte composed of 3.6 M LiFSI in DME for LIBs. It was found that the ether-based HCE not only hindered the co-intercalation of DME into graphite, but also led to ultrafast intercalation of Li^+ in graphite, which significantly surpassed that in commercial EC-based electrolyte.[186] Later in 2015, Dahn *et al.* discovered that NCM422||graphite cells using EA-based HCE demonstrated a capacity retention of >95% at a cut-off voltage of 4.4 V *vs.* Li^+/Li, indicating that the EA-based HCE exhibited both excellent anodic and cathodic stability.[190] In 2016, Wang *et al.* reported a DMC-based HCE (LiFSI : DMC, 1 : 1.1 by mol) for high-voltage LNMO||graphite cells. Due to the unique solvation structure in the DMC-based HCE, the cells exhibited a capacity retention of >95% after 100 cycles with an ultrahigh cut-off voltage of 5.2 V *vs.* Li^+/Li and >90% after 100 cycles at high temperature (40 °C).[85] In 2018, a SL-based HCE (3.25 M LiFSI in SL) was prepared by Alvarado *et al.* for high-voltage LNMO||graphite cells. The high concentration of lithium salts reduced the Li^+–SL interaction, leading to an anion-dominated solvation structure of Li^+. Consequently, a LiF-rich SEI and a thin, conformal, and sulfur-based CEI were obtained. As a result, the co-interaction of SL in graphite was significantly suppressed and the LNMO||graphite full cells with a high cut-off voltage of 4.85 V showed 70% capacity retention after 1000 cycles.[184] Zhang *et al.* investigated the effects of LHCEs with different additives on the electrochemical performance for high-voltage LIBs in a wide operating temperature range. It was clearly shown that 1.4 M LiFSI in DMC-EC-TTE could significantly boost the cycling stability of 4.4 V NCM811||graphite cells with a capacity retention of 94.2% after 600 cycles, and widen the temperature range (−30–60 °C).[169] Jia *et al.* deliberately tuning the Li^+ solvation structure in LHCE with extra additives and found that the low-flammable LHCE composed of 1.44 M LiFSI in TMP-FEC-TTE could stabilize both the graphite anode and high-voltage cathode. As a result, 4.4 V NCM811||graphite cells demonstrated significantly improved cycling stability with a capacity retention of 85.4% after 500 cycles.[191] Wang *et al.* adopted an HCE composed of 4 M LiFSI in DMC to broaden the operating temperature range of −20 ~ 100 °C, which was attributed to the robust

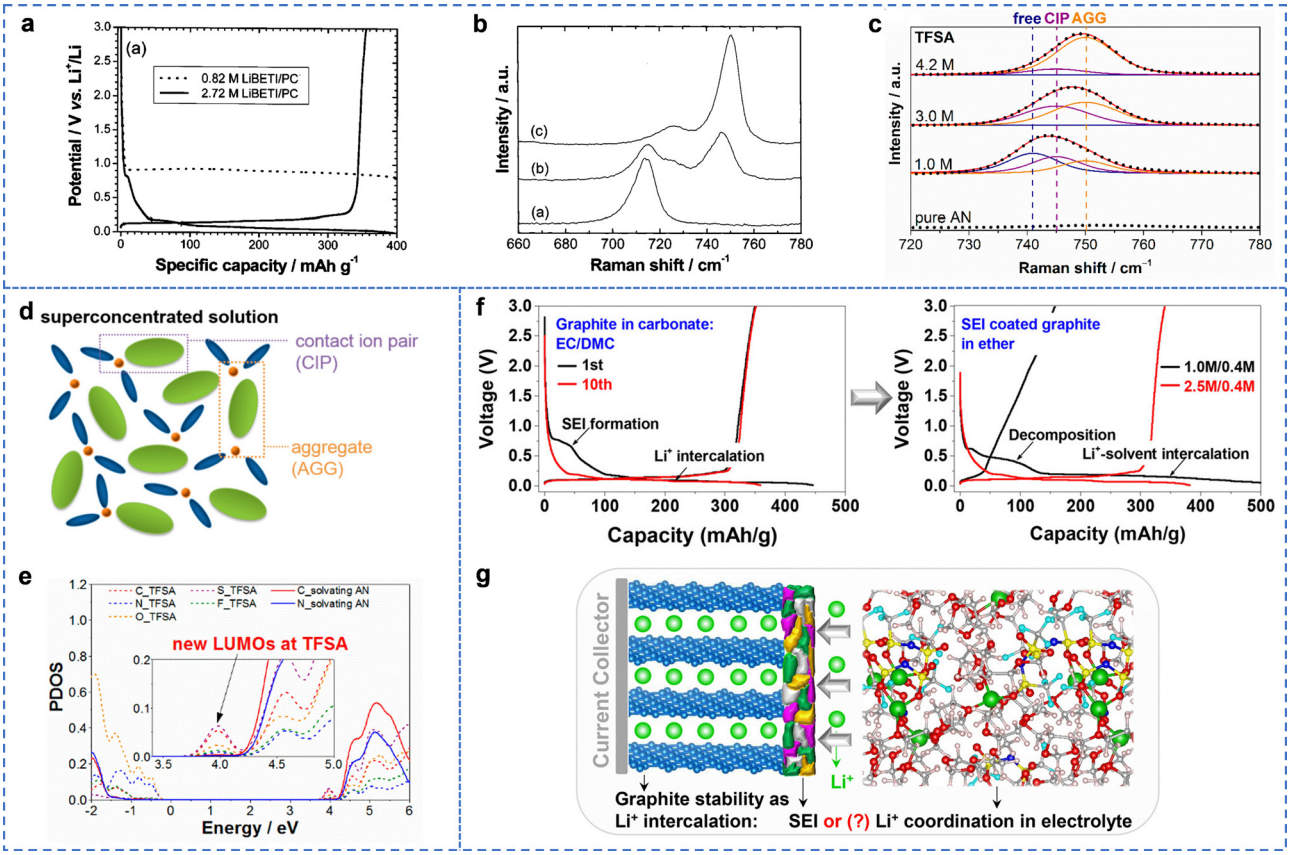

Fig. 15 (a) Charge–discharge curves in the first cycle of graphite in different electrolytes. (b) Raman spectra of PC, 0.82 M LiBETI/PC, and 2.72 M LiBETI/PC. Reproduced with permission.[180] Copyright 2003 the Electrochemical Society (c) Raman spectra of LiTFSI/AN in different electrolytes. (d) Schematic illustration of the Li^+ solvation structure in highly concentrated electrolyte. (e) Projected density of states (PDOS) of highly concentrated electrolytes. Reproduced with permission.[24] Copyright 2014 American Chemical Society. (f) Discharge–charge curves of graphite in carbonate-based electrolytes and in ether-based electrolytes. (g) Schematic illustration of the controversial issue for the reversibility of graphite in LIBs. Reproduced with permission.[183] Copyright 2018 American Chemical Society.

electrode–electrolyte interphases derived from decomposition of anions and the highly stable solvation sheath of the HCE itself.[170]

Besides the graphite anode, the effect of HCEs or LHCEs on silicon anodes was also widely investigated.[44] For instance, Jia *et al.* designed a LHCE (1.2 M LiFSI in TEP/FEC/BTFE, 1.2 : 0.13 : 4 by mol) for the Si/graphite anode. Because of the advantages of LHCE, a robust LiF-rich SEI was successfully constructed, which played a vital role in improving the cycling stability of Si anodes. As a result, Si/Gr||NMC333 full cells achieved a high capacity retention of >90% after 600 cycles.[192] Chen *et al.* further improved the cycling performance of neat Si anodes with a capacity retention of >90% after 400 cycles by constructing a LiF-rich SEI in 2 M $LiPF_6$ in THF: 2M-THF. Moreover, this electrolyte also endowed other alloy anodes, such as Al or Bi, with highly improved electrochemical performance.[193] 1.2 M LiFSI/0.05 M LiDFOB in DME/HFE/FEC (3 : 6:1 by vol) was also designed to ameliorate the cycling stability of the Si anode induced by huge volume variation. A LiF-rich SEI was also obtained in the LHCE, highly suppressing the capacity loss of Si anode with a capacity fading rate of 0.0615% per cycle during 200 cycles.[194]

4.2.2. Other weak solvating electrolytes in LIBs. Similar to the strategy in LMBs, designing weakly solvating solvents is also a facile way to regulate the solvation chemistry in WSEs. Reducing the affinity of Li^+–solvents promotes the binding ability of Li^+ with anions, leading to anion-dominated solvation structures, which is efficient in enhancing the electrochemical performance in LIBs.[195,196] One of the important ways to reduce the polarity of commercial solvents is appropriate substitution with electron-drawing atoms, such as F. In 2010, Wang *et al.* investigated the influence of the amount of F atoms in PC (monofluoropropylene carbonate, MFPC and trifluoropropylene carbonate, TFPC) on stable SEI formation in graphite. The strong electron withdrawing nature of $-CF_3$ groups enhanced the "ring-opening" reaction, leading to the formation of an excellent SEI in TFPC, while the electron donating $-CH_3$ group in PC suppressed the SEI formation. Therefore, they found that the formation capabilities of SEIs in MFPC/DMC and TFPC/DMC were the same with those in EC/DMC, while the formation ability of EC/PC/DMC was better than that of MFPC/PC/DMC, but poorer than that of TFPC/PC/DMC. This enlightening work first provided solid evidence about the effect of fluorination of carbonates on graphite anodes.[197] Later in

2017, a capacity retention of 81% after 200 cycles in 4.7 V NCM532||graphite cells in 1 M $LiPF_6$-FEC-FEMC was reported by Im *et al.*[198]

In 2020, Yao *et al.* adopted 1,4-dioxane (1,4-DX) with a dielectric constant of 2.2, as a non-polar solvent for WSEs. Due to the ultralow dielectric constant, 1,4-DX promoted the formation of anion-dominated Li^+ solvation structure with abundant AGGs and CIPs, resulting in an anion-derived EEI. Consequently, excellent cycling stability with a capacity retention of 92% after 500 cycles and superior electrochemical kinetics were obtained.[199] Methyl propionate (MP) was also used as a weakly solvating solvent for LIBs operating at low temperatures. Compared with conventional EC-based electrolytes, the MP-based electrolyte demonstrated superior electrochemical performance at temperatures as low as −40 °C due to the high ionic conductivity at low temperature, LiF-rich SEI, and fast Li^+ de-solvation process.[200] In 2021, Klein *et al.* designed a WSE composed of 1 M $LiPF_6$ in EMC by direct elimination of EC with high polarity from conventional electrolyte. Interestingly, the EC-free electrolyte endowed NCM532||graphite cells with a cut-off voltage of 4.5 V *vs.* Li^+/Li a better cycling stability.[201] Wu *et al.* also investigated the effect of weakly solvating EC-free electrolytes on the performance of LIBs. The WSE composed of 0.8 M LiFSI–0.1 M LiTFSI–0.6 M $LiPF_6$ in EMC exhibited 82.1% capacity retention after 200 cycles in 4.5 V NCM811||graphite full cells. Moreover, the WSEs also endowed these cells with enhanced intrinsic safety (Table 4).[202]

4.2.3. Strong solvating electrolytes in LIBs. There are only a few reports about the strong solvating electrolytes used to improve the performance of LIBs, one of which is the introduction of NO_3^- to strengthen Li^+–anion interactions. Wahyudi *et al.* found that the addition of NO_3^- altered the solvation structure with increased amount of AGGs and CIPs, effectively avoiding the co-intercalation of solvents.[203,204] Tezel *et al.* introduced an anion receptor, tris(hexafluoroisopropyl)borate (THFIPB) into the conventional electrolyte. Because of the strong solvent–anion interaction, the solvation structure was changed and a different inorganic-rich SEI was formed in graphite.[205]

In LIBs, EC-based electrolytes, instead of PC-based ones have been widely used due to the suppression of co-intercalation of solvent into graphite induced by the EC-derived SEI. To expand the application of LIBs (high-voltage, high/low temperature, and high power), other solvents including PC, DMSO, TEP, DOL-DME, have been further explored. Although the co-intercalation of these solvents has been effectively suppressed, the fundamental mechanism has not been fully understood. Several mechanisms such as the formation of SEIs and the presence of a unique solvation structure (weak Li^+–solvent interaction) have been proposed, as shown in Table 5. Are the SEI and unique solvation structure independently responsible for the stability of graphite? Or are they inter-related and synergistic? That is, both the SEI and the binding energy of Li^+–solvents play key roles in graphite stability in LIBs because the Li^+-binding energy dominates the de-solvation process of Li^+ before intercalation into graphite and the SEI makes the co-intercalation of solvents with Li^+ difficult. What is more, is it possible that the roles of the SEI and Li^+–solving interaction may be different in different

Table 4 Summary of the high-voltage performance in LIBs using different electrolytes

			High-voltage performance			
No.	Electrolytes	Cathode/anode	Cut-off voltages (V)	Capacity retention/cycles	Main mechanisms	Ref.
1	LIFSI : EMC (1 : 1.1 by mol)	LNMO/graphite	5.2	>95%/100	• HCEs inhibit the dissolution of both aluminium and transition metal	85
2	$LiPF_6$–LiFSi in EA (3 : 32 : 65)	NCM442/graphite	4.4	>95% /45 (40 °C)	• HCEs inhibit the decomposition of solvents	190
3	3.25 M LiFSI in SL	LNMO/graphite	4.85	70%/1000	• LiF-rich SEI effectively suppresses solvent co-intercalation thin, conformal, sulfur-based CEI slows down the decomposition at high voltage	184
4	1.4 M LiFSI in DMC–EC–TTE (2 : 0.2 : 3 by mol)	NCM811/graphite	4.4	94.2%/600	• A thinner but more robust and conductive SEI layer enriched with inorganic constituents that can protect the Gr anode • Enhanced CEI layer effectively protect the Ni-rich NMC cathode from electrolyte corrosion and suppress practice cracking during cycling	169
5	1.44 M LiFSI in TMPa–FEC–TTE (1.2 : 0.2 : 3.0 by mol)	NCM811/graphite	4.4	85.4%/500	• A thin SEI (~2 nm) derived from anion, additives and solvent, offer good protection against solvent co-intercalation and long-term cycling. • Stable CEI	191
6	1 M $LiPF_6$ in FEC/FEMC	NCM532/graphite	4.7	81%/200	• Stable inorganic-rich CEI	198
7	0.8 M LiFSI–0.1 M LiTFSI–0.6 M $LiPF_6$ in EMC	NCM811/graphite	4.5	82.1%/200	• Triple-salt, EC-free electrolyte forms effective CEI to stabilize cathodes • F-, N, and S-rich SEI enables stable cycling stability of anode	202

Table 5 Recent advances of the electrolytes designed for graphite stability in LIBs

No.	Electrolytes	Electrodes	Graphite stability	Ref.
1	1.0 M LiTFSI/0.4 M $LiNO_3$ in DOL/DME	Li/graphite	Unstable due to co-intercalation of solvent	183
2	1 M $LiClO_4$ in PC	Li/graphite	Unstable due to co-intercalation of solvent	33 and 175
3	LiFSI : TEP (1 : 5 by mol)	Li/graphite	Unstable due to decomposition of solvents	80
4	1 M LiTFSI in DMSO	Li/graphite	Unstable due to decomposition of solvents	182
5	2.5 M LiTFSI/0.4 M $LiNO_3$ in DOL/DME	Li/graphite	Stable due to unique solvation structure (weak Li^+–solvent interaction)	183
6	1 M $LiPF_6$ in PC + 6 wt% DTD	Li/graphite	Stable due to the unique solvation structure (weak Li^+–solvent interaction)	203
7	1 M $LiAsF_6$/PC/EC	Li/graphite	Stable due to SEI formation	176
8	2.72 M LiBETI in PC	Li/graphite	Stable due to SEI formation	180
9	LiFSI : TEP (1 : 2 by mol)	Li/graphite	Stable due to SEI formation	80
10	3.2 M LiTFSI in DMSO	Li/graphite	Stable due to SEI formation	182
11	$LiPF_6$ in PC: DEC + FEC	Li/graphite	Stable due to SEI formation	206

electrolytes? More sophisticated experiments are needed to address the above questions.[207]

5. Strategies of regulating solvation chemistry in LSBs

Due to the high specific capacity (1675 mA h g^{-1}), abundant resources, low-cost and environmental benign nature of sulfur, LSBs with an ultrahigh theoretic energy density of 2600 W h kg^{-1}, have attracted tremendous attention. However, several issues still exist, such as the poor conductivity of sulfur and its discharging products, the huge volume variation during the charge–discharge process, and especially the notorious shuttle effect of lithium polysulfides, which severely impede the commercial application of LSBs.[208] Generally, sulfur usually exists as cyclic S_8 due to the presence of strong atomic interactions.[209] During the discharge process, the solid S_8 is reduced, forming liquid lithium polysulfides (Li_2S_x, $2 \leq x \leq 8$), which are soluble in organic electrolytes; these liquid lithium polysulfides were further reduced, forming the final solid discharge product (Li_2S) (Fig. 16a). On the one hand, dissolution of lithium polysulfides facilitates the utiliztion of sulfur cathodes; on the other hand, the dissoluble lithium polysulfides shuttle between the cathode and anode, leading to low CE and rapid capacity fading. Therefore, there is an intractable trade-off about the dissoluble lithium polysulfides in this solid–liquid–solid transformation or dissolution-precipitation process: improving the solubility of polysulfides leads to high specific capacity and enhanced kinetics but aggravates the shuttling of lithium polysulfides; while decreasing the solubility of lithium polysulfides alleviates their shuttling, but results in inferior kinetics and low utilization of sulfur.[210] Moreover, a series of disproportionation reactions involving these polysulfides occur in the electrolyte, forming various polysulfides with different chain lengths. This complexity of the reactions in the electrolytes significantly affects the redox mechanism and the corresponding electrochemical performances.[211]

During the last few decades, great progress has been made in cathode design, separator modification, lithium metal anode protection, redox mechanism, and especially in electrolyte design because electrolytes play a pivotal role not only in suppressing the shutting effect of lithium polysulfides and lithium metal protection, but also in the redox process and mechanism.[211,212,215–222] Thus, in this section, we mainly summarize the recent development of electrolytes in LSBs and their effects on the corresponding electrochemical performances. Since the influence of electrolytes on lithium metal has been thoroughly summarized in the above section, we mainly focus on the role of electrolytes i aspects such as suppressing the shuttling effect of lithium polysulfides, the redox process, and electrochemical mechanism.[223]

5.1. Moderate solvating electrolytes in LSBs

Although the first generation of LSBs was proposed as early as 1960s, it was not until 2019 that LSBs attracted significant attention due to the publication of two important works.[4,224,225] The discovery of highly ordered mesoporous carbon, CMK-3, by Nazar *et al.* is widely considered as the landmark in LSBs. The conductive mesoporous carbon materials precisely confine sulfur in their channels, not only trapping polysulfides but also facilitating the redox reaction.[4] Aurbach *et al.* first investigated the functions of $LiNO_3$ in electrolyte for LSBs and found that it served as a critical component in preventing the shuttle effect.[224] These two reports significantly prompted the development of LSBs and spurred the extensive research interest worldwide.[226]

The most common electrolytes used in LSBs are composed of 1 M LiTFSI in DOL : DME (1 : 1 by volume) with the $LiNO_3$ additive (usually $\leq$ 0.5 M), which is the typical moderate solvating electrolyte in LSBs. The pioneering work focusing on polysulfides in solvents was performed in 1979 by Rauh *et al.*, in which almost 100% of the theoretical capacity was achieved by directly adopting lithium polysulfides in THF (its DN or DC is similar with that of DOL or DME) at 50 °C.[227] Barchasz investigated the discharge mechanism of LSBs in TEGDME-based electrolytes using high-performance liquid chromatography (HPLC), electron spin resonance spectroscopy, and UV-visible absorption, and proposed a three-step mechanism (Fig. 16b).[213] In 2013, Nazar *et al.* systemically investigated the evolution of sulfur speciation in 1 M LiTFSI in DOL/DME with 2 wt% $LiNO_3$ for LSBs using operando X-ray absorption near-edge spectroscopy (XANES) (Fig. 16c and d). The evolution of S K-edge XANES provided the first detailed and convincing evidence of the redox mechanism in LSBs, which

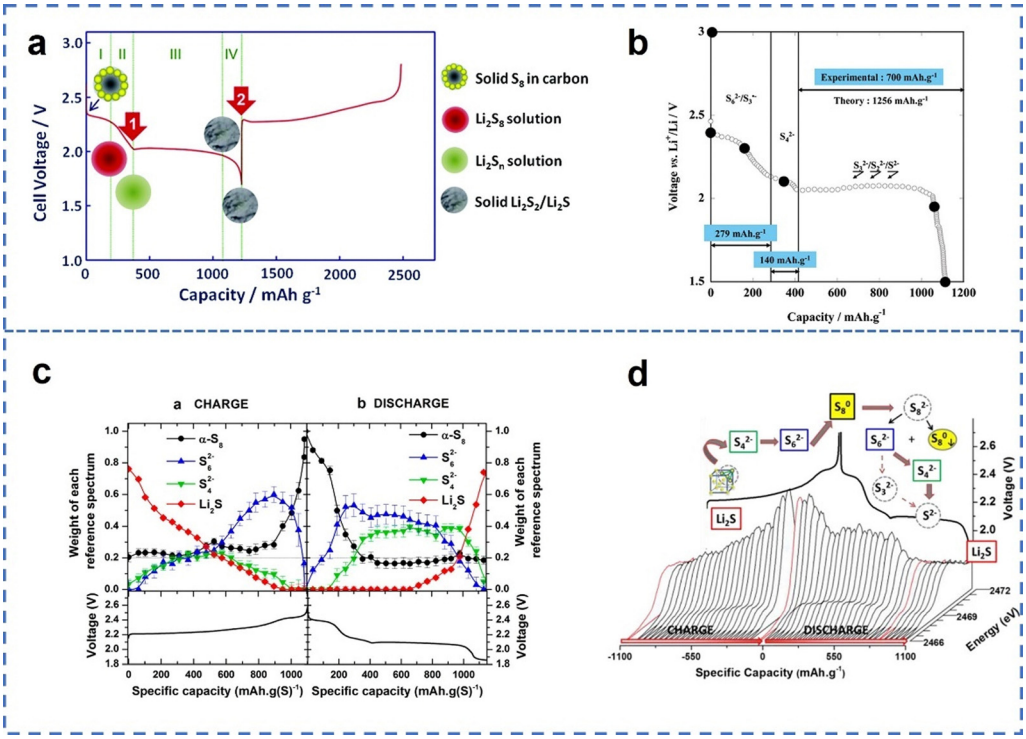

Fig. 16 (a) Typical discharge–charge curves in the first cycle of LSBs. Reproduced with permission.[212] Copyright 2013 Elsevier. (b) Proposed sulfur electrochemical mechanism in TEGDME-based electrolytes. Reproduced with permission.[213] Copyright 2012 American Chemical Society. (c) Weight of reference spectra for different compounds during the discharge–charge process derived from the sulfur K-edge XANES. (d) Evolution of sulfur K-edge XANES spectra during charge–discharge process and the proposed redox mechanism. Reproduced with permission.[214] Copyright 2013 American Chemical Society.

was significantly important in improving the electrochemical performance.[214]

Although great efforts have been devoted to the investigation of MSEs in LSBs, the development of high-performance LSBs still faces great challenges. Due to the moderate solvating ability of solvent, only limited polysulfides dissolve in MSEs, decreasing the utilization of sulfur, especially under conditions of low electrolyte/sulfur (E/S) ratios. Improvement in the E/S ratio, otherwise, induces severe shuttling of polysulfides.[225]

5.2. Weak solvating electrolytes in LSBs

Due to the solvent dependence of the dissolution of polysulfides, manipulating the solvating ability of the solvents in electrolytes is pivotal to ameliorate the notorious shuttling effect of lithium polysulfides. Designing WSEs for LSBs not only suppresses the shuttle effect of lithium polysulfides and regulates the redox mechanism, but also effectively tames the lithium platting/stripping behavior, as discussed in LMBs. Benefiting from these above advantages in WSEs, various types of electrolytes, such as HCEs, LHCEs, fluorinated solvents with low polarity, and other WSEs have been widely investigated.

5.2.1. HCEs and LHCEs in LSBs. In HCEs, most of the solvents are coordinated with Li^+ due to the high salt/solvent ratio, leaving few free solvents to dissolve polysulfides. Consequently, compared with MSEs, less lithium polysulfides shuttle between cathodes and anodes during the discharge–charge process.[228] In 2004, Mikhaylik *et al.* investigated the effects of concentration of lithium salts (0.5, 1.85, and 2.5 M LiTFSI in DOL/DME) on the performance of LSBs and found that highly concentrated electrolytes exhibited lower rates of both Li corrosion and shuttle constant.[229] In 2013, Lee *et al.* further increased the concentration of lithium salt (LiTFSI) to 3 M and 5 M in DOL/DME and found that these HCEs could achieve almost an average CE of ~100%, implying their excellent ability to inhibit the polysulfide shuttle in LSBs (Fig. 17a), which was also proven by Shin *et al.* in the same year.[230,231] The concentration of LiTFSI was increased to as high as 7 M in the work reported by Suo *et al.* in 2003. They systemically investigated the effect of salt concentration on both the bulk properties of the electrolytes and suppression of polysulfide dissolution, as shown in Fig. 17b and c.[27]

Ionic liquids (ILs) are usually defined as molten salts with melting points lower than 100 °C; thus in this work we treated the IL-based electrolytes as HCEs because they are composed of molten salts and lithium salts.[234] Because of weak Lewis acidic cations and weak Lewis basic anions, ILs have been considered as one of the ideal solvents to reduce the dissolubility of polysulfides in LSBs. In 2006, Yuan *et al.* synthesized a novel IL, *N*-methyl-*N*-butyl-piperidinium bis(trifluoromethanesulfonyl) imide (PP14-TFSI), which was adopted as the solvent for electrolytes in LSBs (1 M LiTFSI in PP14-TFSI). They found that the IL-based electrolytes, compared with organic or polymer electrolytes,

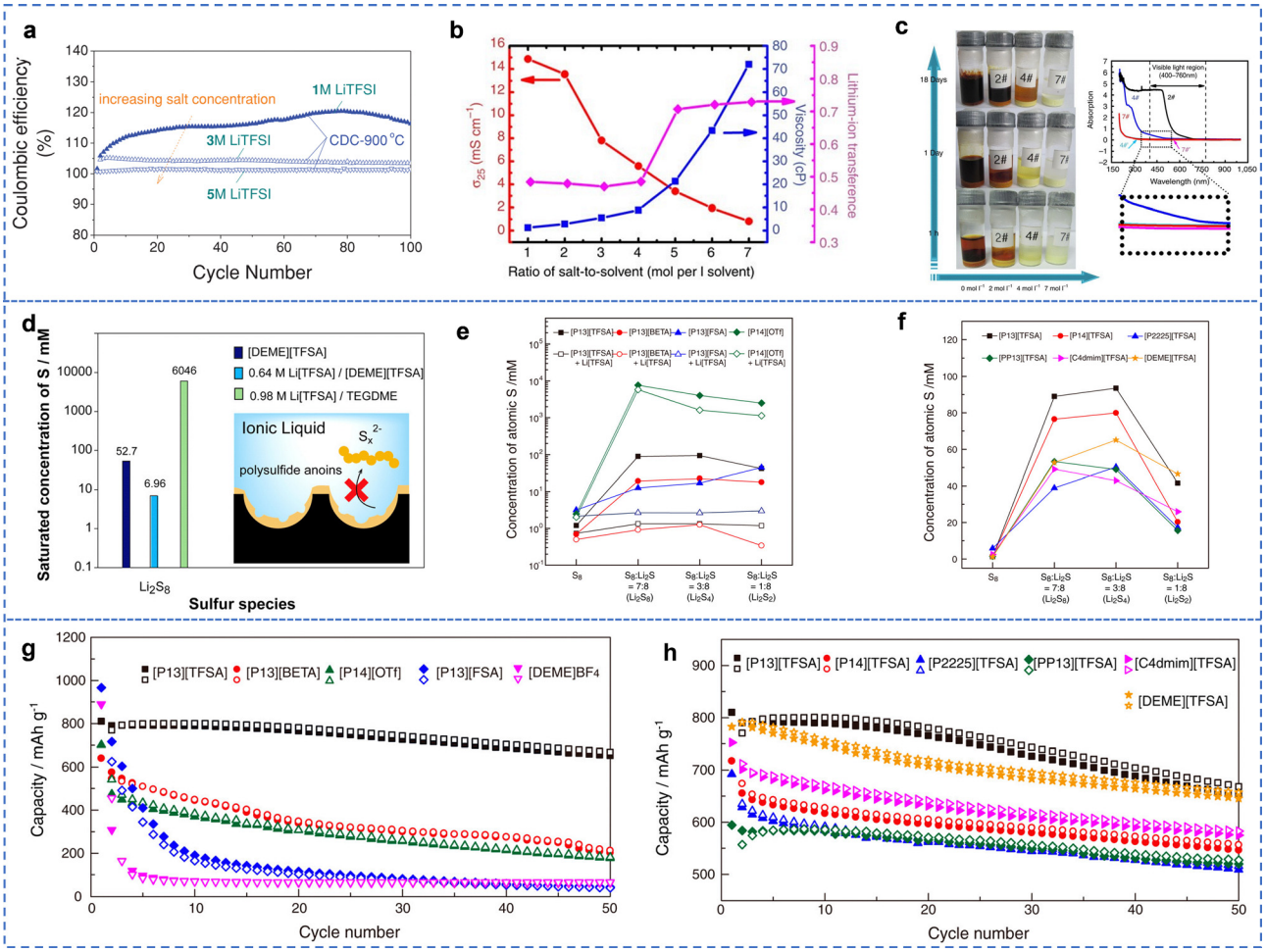

Fig. 17 (a) CEs of LSBs using electrolytes of different salt concentrations. Reproduced with permission.[230] Copyright 2013 WILEY. (b) Changes in viscosity, ionic conductivity, and the Li^+ transference number of electrolytes with the increase in salt concentration. (c) Dissolution of lithium polysulfides in electrolytes of different salt concentrations. Reproduced with permission.[27] Copyright 2013 Nature Publishing Group. (d) Solubility of Li_2S_8 in [DEME][TFSA], 0.64 M Li[TFSA]/[DEME][TFSA], and 0.98 M Li[TFSA]/TEGDME, and the redox mechanism in IL-based electrolytes. Reproduced with permission.[232] Copyright 2013 American Chemical Society. Saturation concentrations of sulfur species in ILs with (e) different anions and (f) different cations. Cycling performance of LSBs in IL-based electrolytes with (g) different anions and (h) different cations. Reproduced with permission.[233] Copyright 2013 American Chemical Society.

could greatly improve the specific capacities and cycling stability.[235] Glyme-Li salt molten complex electrolytes (LiTFSI-G4, 1 : 1 by mol) were also introduced as WSEs for LSBs and exhibited good reversibility with a capacity retention of 73.7% and a high CE > 97% after 50 cycles.[236] The Watanabe group thoroughly explored the effect of solvents, anions, and cations in IL-based electrolytes on the electrochemical reactions in LSBs.[232,233,237] Compared with LiTFSI-TEGDME, LiTFSI-DEME-TFSI could significantly improve the cycling stability and CE of LSBs due to its strong ability to inhibit the dissolution of polysulfides, as shown in Fig. 17d.[232] Moreover, they also found that the cations and anions in ILs had great influence on the solubility of lithium polysulfides in electrolytes, thus affecting the corresponding electrochemical performances (Fig. 17e–h). For example, P13-TFSI based electrolytes delivered superior electrochemical performances compared to P13–FSI, DEME–TFSI, and DEME–BF_4^- based electrolytes, which was attributed to their ability to dissolve sulfur species.[233] In 2018, Wang *et al.* adopted an ultrahigh concentrated electrolyte (12 M LiFSI in DME) to alleviate the issues in LSBs. They found that the ultrahigh concentration electrolyte significantly improved the compatibility with both the lithium metal anode and sulfur cathode, leading to a reversible specific capacity of 786 mA h g^{-1} after 300 cycles with CE > 99.7%.[238] In 2020, 6.5 M LiTFSI in FEC was adopted by Cui *et al.* as an electrolyte for LSBs. Due to its unique solvation structure, the flame-retardant HCE endowed LSBs with an ultra-stable cycling performance in a wide temperature range from −10 to 90 °C.[171]

Although the suppression of the shuttle effect of polysulfides and the corresponding cycling stability are significantly enhanced in HCEs, the poor ionic conductivity induced by high viscosity and the electrochemical kinetics are severely compromised.[230] Watanabe *et al.* found that the addition of HFE into Li(G4)TFSI not only improved the ionic conductivity, but also reduced the saturated concentration of sulfur species,

and thus substantially enhanced the cycling stability and rate performances of LSBs.[92] In 2014, Nazar *et al.* introduced HFE into the $(ACN)_2$–TFSI complex to further suppress the dissolution of polysulfides. As expected, $(ACN)_2$–TFSI–HFE exhibited similar viscosity with conventional ethers and showed enhanced compatibility with the lithium anode. Intriguingly, an uncharacteristic sloping voltage profile was observed, and the mechanism was further investigated by S K-edge XANES. LSBs using $(ACN)_2$–TFSI–HFE showed negligible capacity fading under optimized test protocols.[239] Besides HFE,[240–243] BTFE,[244] TTE,[245–247] TFEE,[248] 1,1,2,2-tetrafluoro-3-(1,1,2,2-tetrafluoroethoxy)propane (F-EPE),[249] hexa-fuoroisopropyl methyl ether (HFME),[250] OTE, ETE,[251] OFE,[252] fluorobenzene (FB),[105,253] 1,1,2,2-tetrafluoroethyl-2,2,3,3-tetrafluoropropyl ether (TFTFE),[254] and other partially fluorinated solvent,[255–258] have been also adopted as non-polar co-solvents in LSBs.

5.2.2. Other weak solvating electrolytes in LSBs. Other WSEs have also been explored in LSBs by regulating the Li^+–solvent or Li^+–anion interactions.[259,260] Amine *et al.* used IR-DOSY to investigate the solvating power of different solvents including DOL, DME, THF, MeTHF, and MtBE, with an order of DME > THF > MeTHF > DME > MtBE. As a result, the electrolyte comprising 1 M LiTFSI in DOL: MtBE exhibited the highest CE, resulting from the poor solvating ability of MtBE.[46] Liu *et al.* adopted DEE as a weak solvating solvent as the substitute of DOL/DME, obtaining the single-solvent electrolyte (1 M LiFSI in DEE). Due to the weak affinity between Li^+ and DEE, this electrolyte not only resuted in an anion-derived SEI, avoiding the corrosion of lithium metal, but also largely reduced the dissolution of polysulfides. As a result, LSBs using 1 M LiFSI/DEE delivered a high reversible specific capacity at a temperature as low as −60 °C (Fig. 18a).[124] Recently, Zhang *et al.* proposed an encapsulating lithium polysulfide electrolyte (DIPS–EPSE) using di-isopropyl sulfide (DIPS) as a cosolvent in 1 M LiTFSI–DME/DOL for LSBs. As shown in Fig. 18b, the downfield shift observed in ^{7}Li NMR of DIPS–EPSE resulted from the weak electron cloud around Li^+, implying the weak solvating power of DIPS. The results from MD also demonstrated the poor affinity between Li^+ and DIPS, leading to its exclusion from the inner solvation sheath of Li^+ (Fig. 18c). As a result, the lithium polysulfides tightly coordinated with DOL/DME, are encapsulated by DIPS as the outer sheath, preventing the lithium corrosion induced by polysulfides or DOL/DME. Consequently, DIPS–EPSE significantly enhanced the cycling stability of LSBs under practical conditions (Fig. 18d).[261] Nazar *et al.* first reported a sulfonamide (*N*,*N*-dimethyl triflimide, NMT)-based electrolyte with low ion-pairing salt ($Li[Al(Ohfip)_4]$). Due to the low solvating ability of NMT, this sulfonamide-based electrolyte exhibited as a non-polar solution for lithium polysulfides at ambient temperature, showing a solid–solid redox mechanism instead of a solid–liquid–solid electrochemical process (Fig. 18e and f). Increasing the operating temperature improved the solubility of polysulfides in the electrolyte, while effectively suppressed the shuttle effect, leading to superior electrochemical performance in LSBs at 50 °C with CEs approaching 99.7%.[262]

5.3. Strong solvating electrolytes in LSBs

Although WSEs could effectively improve the cycling stability of LSBs, the electrochemical kinetics and sulfur utilization were

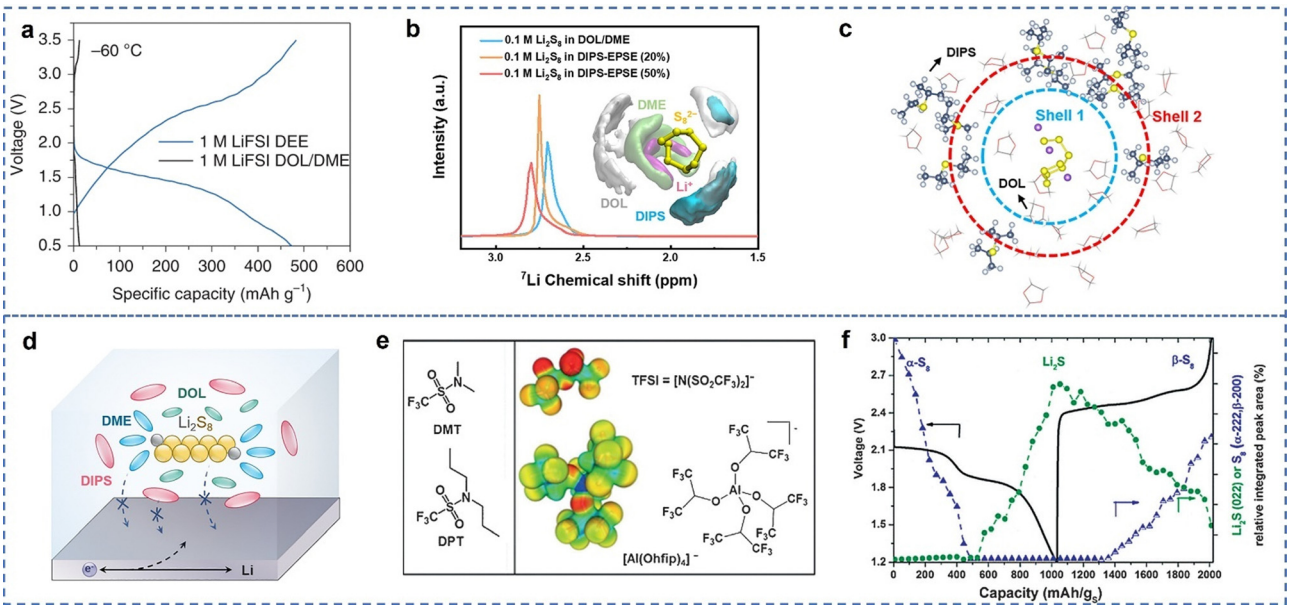

Fig. 18 (a) Discharge–charge curves of LSBs in different electrolytes at −60 °C. (b) ^{7}Li-NMR spectra of Li_2S_8 in different solvents; the inset shows the schematic distribution in the Li_2S_8–DOL/DME/DIPS complex. (c) Snapshots of the molecular distributions in the Li_2S_8–DOL/DME/DIPS complex, and (d) schematic illustration of the working mechanism. Reproduced with permission.[261] Copyright 2022 Elsevier. (e) Molecular structures of DMT, DPT, and $[Al(Ohfip)_4]^-$; electrostatic potentials of $[Al(Ohfip)_4]^-$ and $TFSI^-$. (f) *Operando* X-ray diffraction (XRD) of LSBs with 0.2 M $Li[Al(Ohfip)_4]$-DMT during the discharge–charge process. Reproduced with permission.[262] Copyright 2017 Wiley.

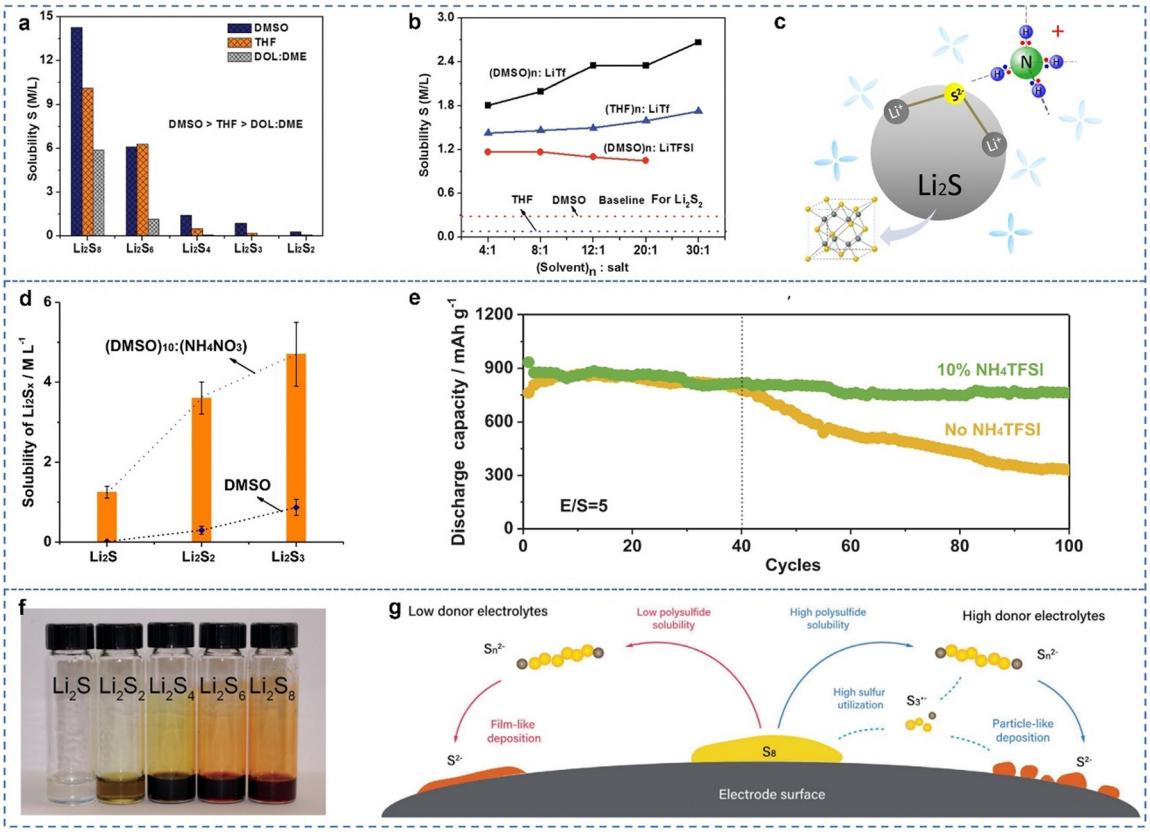

Fig. 19 (a) The solubility of Li_2S_x in pure solvents/mixed solvents. (b) The solubility of Li_2S_2 in DMSO or THF solvents with the addition of LiTFSI and LITf. Reproduced with permission.[264] Copyright 2015 Wiley. (c) Schematic illustration of the interaction between Li_2S and ammonium ion with N–H groups. (d) Increase in solubility in DMSO solvent with the NH_4NO_3 additive. Reproduced with permission.[265] Copyright 2017 American Chemical Society. (e) Cyclic performance of LSBs with and without the NH_4TFSI additive in the electrolyte. Reproduced with permission.[266] Copyright 2018 Wiley. (f) Pictures of sulfur species in CPL/acetamide. Reproduced with permission.[267] Copyright 2019 Wiley. (g) Schematic illustration of the redox process using low and high donor electrolytes in LSBs. Reproduced with permission.[268] Copyright 2020 Wiley.

severely compromised due to the sluggish kinetics induced by the quasi-solid–solid redox chemistry, especially under lean electrolytes. In order to upgrade the redox kinetics and sulfur utilization, SSEs have been widely investigated.

One of the effective strategies is improving the solubility of Li_2S_x ($1 \leq x \leq 8$) in solvents with a high DN or DC, promoting the liquid–liquid conversion or prompting the liquid–solid transformation. For example, at the end of discharge, the insulating solid Li_2S covered the electrodes, which severely limited the sulfur utilization, aggregated polarization, and weakened cycling stability. Therefore, the increase in the solubility of sulfur species in electrolytes has a pivotal role in improving the performance, especially under lean electrolytes. Liu *et al.* investigated the effects of solvents with different polarity properties on the solubility of polysulfides and the corresponding electrochemical performances. As shown in Fig. 19a, DMSO with the highest polarity properties, compared to THF and DOL/DME, exhibited the highest solubility of polysulfides, and the solubility of Li_2S_8 in DMSO was as high as 13 M L^{-1}. The solubility decreased with the decreasing chain length of polysulfides in all three systems. Moreover, the addition of LiTFSI and LiTf could enhance the solubility of Li_2S_2 in the solvents; however the solubility decreased with the increase in the salt concentration, as shown in Fig. 19b.[263] The introduction of a SSE (3 M LiTFSI in DMSO) resulted in high performance LSBs with a reversible specific capacity of 1200 mA h g^{-1} after 65 cycles.[264] Ammonium salt (NH_3NO_3) has been used as a strong coordinating additive to further dissolve Li_2S in DMSO by the same group. Owing to the strong hydrogen bond between ammonium and S^{2-}, the introduction of ammonium salt significantly improved the solubility of Li_2S in DMSO to 1.25 M (Fig. 19c and d), which was beneficial to the sulfur utilization and redox kinetics.[265] In 2018, they also used another ammonium salt (NH_3TFSI) as a strong solvating additive to improve the dissociation of Li_2S and reduce the formation of insoluble particles on the cathode, promoting sulfur utilization and the reversibility of redox chemistry under lean electrolyte. As a result, the addition of NH_3TFSI endowed LSBs with better cycling performance with higher CE (Fig. 19e).[266] In 2019, Yang *et al.* designed a safe eutectic solvent (ε-caprolactam (CPL)/acetamide) to dissolve the whole lithium sulfide family from Li_2S_8 to Li_2S, as shown in Fig. 19f. The superior dissolubility of the eutectic solvents can be attributed to the strong interaction between Li^+ and anions in sulfur species, and the interaction between the

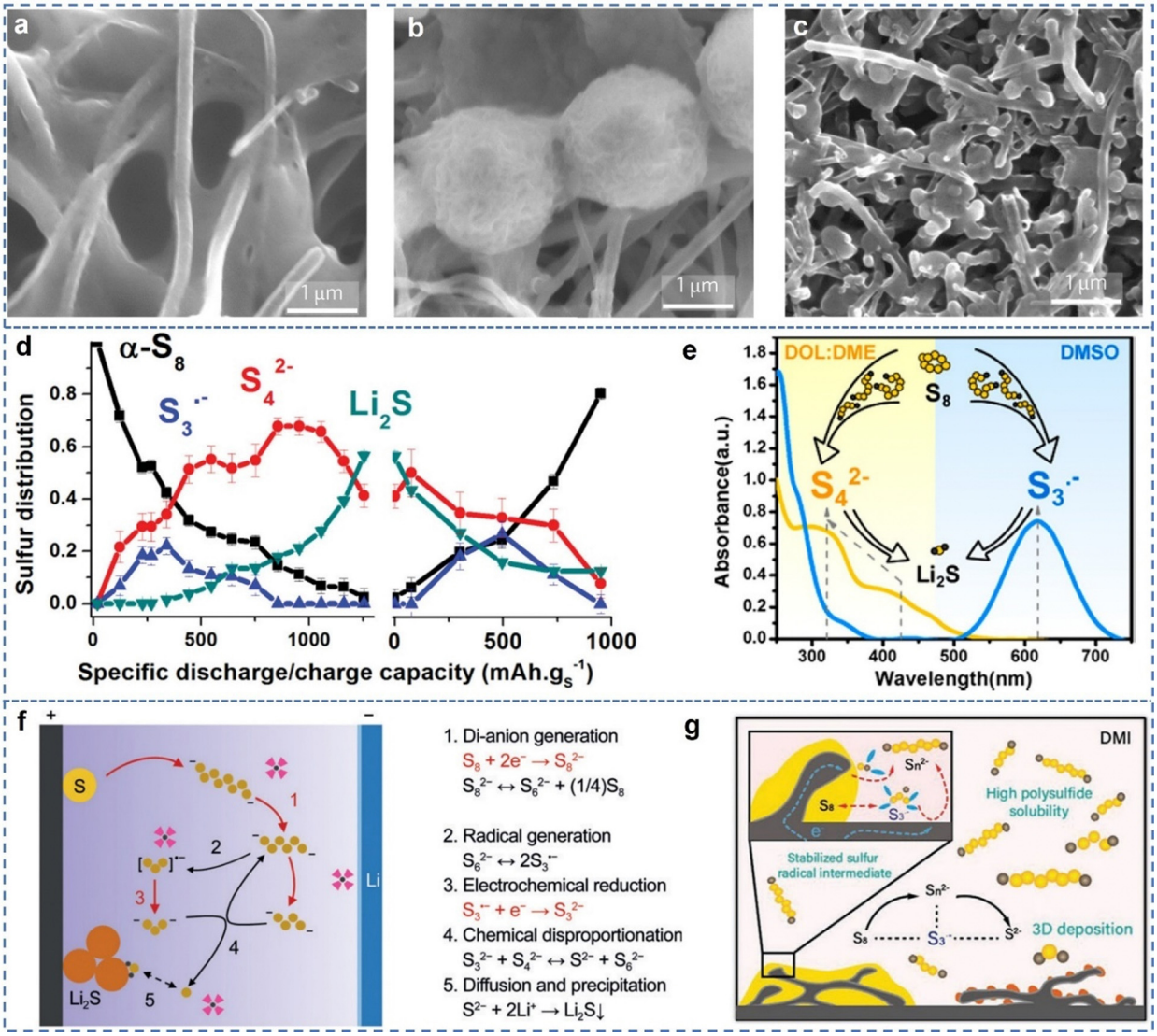

Fig. 20 SEM images of the deposited Li_2S morphology in (a) TMS, (b) DOL/DME, (c) DMSO. Reproduced with permission. (d) Distribution of sulfur species upon cycling derived from XANES spectra. Reproduced with permission.[269] Copyright 2015 Wiley. (e) UV-vis absorption spectra of polysulfide in different solvents and schematic illustration of the redox mechanism. Reproduced with permission.[270] Copyright 2016 American Chemical Society. (f) Schematic illustration of the radical pathway for LSBs in TMU-based electrolyte, and the corresponding reaction equations. Reproduced with permission.[30] Copyright 2018 Wiley. (g) Schematic illustration of the redox mechanisms in a DMI-based electrolyte. Reproduced with permission.[271] Copyright 2020 Wiley.

carbonyl oxygen atom and amide hydrogen. As a result, the LSBs demonstrated capacity retention of 90.3% and 94.5% after 40 cycles at 0.3 and 0.5C, respectively.[267]

The strong polar solvents not only influence the dissolubility of sulfur species during the redox process in LSBs, but also determine the deposited morphology of discharging products and the redox mechanism (Fig. 19g).[3,30,260,263,268–279] In 2017, Liu *et al.* investigated the morphology of deposited Li_2S as fully discharged products in solvents with different DN numbers. As shown in Fig. 20a–c, 2D Li_2S films were observed in tetramethylene sulfone (TMS) with a low DN (14.8 kcal mol^{-1}), while 3D Li_2S particles with sizes of >1 μm and 3D Li_2S particle with reduced sizes formed in intermediate-DN DME/DOL ($\sim$20) and high-DN DMSO solvents, respectively. They proposed that solvents with a low DN induced the formation of 2D films from polysulfides in solution, while high-DN solvents facilitated the formation of 3D particles directly from solutions due to the strong affinity between high-DN solvents and Li_2S_x, and improving the DN in solvents would increase the nucleation barriers, resulting in the formation of small particles.[3] Lu *et al.* systemically investigated the Li_2S deposition behavior in 8 solvents with different donicity, polarity and viscosity. They further proposed Li_2S growth models as guides to solvent selection, in which they revealed that 2D instantaneous nucleation with lateral lattice incorporation growth was fitted for Li_2S in solvents with low donicity, and Li_2S deposition in solvents with high donicity followed the 3D nucleation and growth model.[275] Anions with a high DN as additives are also used to

Table 6 Summary of the cycling performance in LSBs using different electrolytes

No.	Electrolytes	Cycling performance			Ref.
		Current density (C)	Initial capacities (mA h g^{-1})	Capacity retention/cycles	
1	5 M LiTFSI in DOL:DME + 0.2 M $LiNO_3$	0.2	~1350	70%/100	230
2	7 M LiTFSI in DOL:DME	0.2	1041	74%/100	27
3	1 M LiTFSI in PP14-TFSI	(50 mA g^{-1})	1055	71%/10	235
4	Li(G4)TFSI	(139 mA g^{-1})	1085	73.7%/50	236
5	12 M LiFSI in DME	(1000 mA g^{-1})	—	(644 mA g^{-1})/300	238
6	6.5 M LiTFSI in FEC	0.2	839.1	93%/100	171
7	3 M LiTFSI in AMImTFSI	0.1	—	92%/100	281
8	G2 : LiTFSI (0.8 : 1 by mol)	0.2	—	83%/100	210
9	1 M LiTFSI in DOL:D2	(230 mA g^{-1})	1195	~70%/100	282
10	1 M LiTFSI + 0.1M $LiNO_3$ in F-EPE:DME	0.1	~1100	78%/100	249
11	LiFSI-DME-1.8 HFME	0.2	~1225	79.3%/200	250
12	1 M LiFSI in DME/HFE	(100 mA g^{-1})	1449	53.4%/50	238
13	1.1 M LiFSI in TEP/TTE	0.5	813.6	92.4%/100	283
14	1 M LiFSI in OFE/DME	(100 mA g^{-1})	—	(775 mA g^{-1})/100	252
15	1 M LiFSI in DME/FB	0.5	—	70%/400	105
16	0.66 M LiFSI + 0.33 M LiTFSI + 0.2 DOL + 1 DME + 3 FB	1	—	97.6%/500	253
17	0.2 M $Li[Al(Ohfip)_4]$ in DMT	2	1500	—	262
18	3 M LiTFSI in DMSO	0.2	~1379	87%/65	264
19	1.2 M LiTFSI + 0.1 M $LiNO_3$ in CPL/acetamide	0.3	953	90.3%/40	267
20	0.4 M TFSI + 0.6 M $LiNO_3$ in DOL/DME	0.1	1200	88.7%/100	277

regulate the behavior of Li_2S deposition and the corresponding electrochemical process.[263] Liu *et al.* found that Br^- and NO_3^- with a high DN improved the solubility of Li_2S in electrolytes, facilitating the formation of 3D Li_2S and the complete utilization of sulfur.[276] Similar phenomenon was also observed by Kim *et al.*, resulting in LSBs with high sulfur utilization and excellent cycling stability (88.7% after 100 cycles at 0.1C).[277]

The redox chemistry is also highly related with the polarity of the solvents. Nazar *et al.* first used XANES to explore the redox mechanism in different solvents. They found that sulfur radical species $S_3^{\bullet-}$ were not stabilized in glyme-based electrolytes, but widely existed in solvents (DMSO and DMA) with a high DN, which prompted the full utilization of both sulfur and Li_2S (Fig. 20d).[269] Lu *et al.* revealed that $S_3^{\bullet-}$ was the most stable reaction intermediate in DMSO with a high DN, while S_4^{2-} was dominated in DOL/DME with a relatively low DN by UV-vis spectroscopy. These stable intermediates played an important role in determining the reaction pathways, and therefore, affected the corresponding electrochemical performances (Fig. 20e).[270] Zhang *et al.* investigated the effect of TMU with high dielectric constant because it had strong solvating power and excellent compatibility with lithium metal, which differed from other polar solvents such as DMSO. Moreover, active $S_3^{\bullet-}$ radicals still existed in the solvents, enabling enhanced sulfur utilization and excellent cycling stability. The sulfur redox mechanism was also proposed, as shown in Fig. 20f.[30] The $S_3^{\bullet-}$ radicals involved in redox chemistry have also been observed in other polar solvents such as dimethylacetamide (DMA), 1-methylimidazole (MeIm), NMP (Fig. 20g), *etc.*[271,274,279] The redox chemistry in SSEs usually includes the following equations:

$$S_8 + 2e^- \rightarrow S_8^{2-} \quad (1)$$

$$S_8^{2-} \rightarrow S_6^{2-} + 1/4S_8 \quad (2)$$

$$S_6^{2-} \rightarrow 2S_3^{\bullet-} \quad (3)$$

$$S_3^{\bullet-} + e^- \rightarrow S_3^{2-} \quad (4)$$

$$2S_3^{\bullet-} + 2S_3^{2-} \rightarrow 2S_4^{2-} \quad (5)$$

$$S_8^{2-} + 2e^- \rightarrow 2S_4^{2-} \quad (6)$$

As discussed above, the SSEs could improve the dissolution of Li_2S_x, facilitating the full utilization of active materials and fast redox conversion. However, the increase in Li_2S_x solubility, in turn, aggravates the notorious shuttle effect of polysulfide, resulting in severe Li corrosion and rapid capacity fading. This trade-off in SSEs urges scientists to design both novel electrolytes and sophisticated electrodes which could suppress the shuttling of polysulfides and facilitate the fast conversion at the same time, especially under practical conditions (Table 6).[219,280]

In LSBs, the trickiest issue is the trade-off between the dissolubility of polysulfides and their shuttle effect in the electrolytes: improving the dissolubility of polysulfides using SSEs aggravates their shuttle effect, leading to low CE and poor cycling stability, while suppressing the shuttle effect of polysulfides using WSEs decreases their solubility, resulting in low utilization of active materials and inferior kinetics. Thus, other strategies are also necessary for high-performance LSBs: in SSEs, multifunctional hosts or separators play a key role in alleviating the shuttle of polysulfide while maintaining high utilization of sulfur and excellent kinetics; in WSEs, redox mediators or catalytic hosts facilitate the redox process, significantly improving the electrochemical kinetics.[284]

For practical application, high sulfur loading, lean electrolyte, and limited excess lithium are imperative in LSBs. For example, in the case of a 500 W h kg^{-1} Li–S battery, a high sulfur loading $\geq$10 mg cm^{-2}, an N/P ratio $\leq$2.4, and an electrolyte/sulfur ratio $\leq$2.4 μl mg^{-1} are highly recommended.[5] Under such harsh circumstances, the above WSEs, MSEs, and

SSEs cannot address the challenge alone. Moreover, the soluble polysulfides inevitably react with highly reactive Li metal, leading to severe corrosion of Li metal and depletion of active materials. This is the reason why excessive lithium metal (500 μm) is widely adopted in LSBs for extended cycling life. Thus, here we propose that a comprehensive strategy should be adopted for practical LSBs with high energy density: SSEs with redox mediators are used as the electrolyte to improve the utilization of sulfur; functional separators or interlayers are used to suppress the shuttle of polysulfides; artificial SEIs or other lithium-based anodes are implemented to protect lithium metal; and multi-functional cathodes are used to enhance sulfur loading and trap and facilitate the conversion of lithium polysulfides.

6. Strategies of regulating solvation chemistry in LOBs

Lithium oxygen batteries (LOBs), using lithium metal and air or oxygen as the anode and cathode, respectively, have attracted significant attention due to their ultrahigh specific energy density ($\sim$3500 W h kg^{-1}).[285] Although aqueous electrolyte-based metal air batteries were proposed as early as the 1990s, the redox chemistry of LOBs in nonaqueous electrolytes was serendipitously discovered by Abraham *et al.* in 1996.[286]

The typical configuration of nonaqueous LOBs is composed of lithium metal as the anode, soluble air/O_2 as the active material of the cathode, Li^+ conducting nonaqueous solutions as the electrolyte, and usually porous materials as the substrates enabling direct contact with O_2 and Li^+. The redox reaction in nonaqueous LOBs with an ideal discharge product Li_2O_2, is proposed as follows:

$$O_2 + 2e^- + 2Li^+ \leftrightarrow Li_2O_2 \quad (7)$$

During the discharge process, lithium superoxide (LiO_2) is formed due to the reduction of O_2 *via* one electron transfer. Then, lithium peroxide (Li_2O_2) as the main discharge product is obtained *via* either disproportionation or further reduction of LiO_2, namely, the oxygen reduction reaction (ORR). In the charging process, Li_2O_2 was finally oxidized to O_2, namely, the oxygen evolution reaction (OER).[287–289] Based on the experimental and calculation results, two different redox mechanisms, namely, a solution-mediated mechanism and surface-mediated mechanism are proposed (Fig. 21a).[290,291]

The solution-mediated mechanism is as follows:

$$O_{2(sol)} + e^- + Li_{(sol)}^+ \rightarrow Li_{(sol)}^+ + O_{2(sol)}^- \quad (8)$$

$$2Li_{(sol)}^+ + 2\ O_{2(sol)}^- \rightarrow Li_2O_2 + O_2 \quad (9)$$

$$2Li_{(sol)}^+ + O_{2(sol)}^- \rightarrow Li_2O_2 \quad (10)$$

The surface-mediated mechanism is as follows:

$$O_{2(sol)} + e^- + Li_{(sol)}^+ \rightarrow LiO_2* \quad (11)$$

$$2LiO_2* \rightarrow Li_2O_{2*} + O_2 \quad (12)$$

$$LiO_2* + e^- + Li_{(sol)}^+ \rightarrow Li_2O_{2*} \quad (13)$$

Similar to LSBs, electrochemical chemistry in LOBs involves multi-phase transformation, Li corrosion, cross-talk of intermediates, and passivation of the cathode surface with insulting discharge products. Different from LSBs, gas–liquid–solid redox and severe decomposition of electrolytes and composite cathodes induced by highly active oxygen species also exist in nonaqueous LOBs. As the media directly contact with both the cathode and anode, electrolytes have significant effects on the redox mechanism, cycling stability, and electrochemical kinetics of LOBs.[292–294] Various solvents including ILs, solvated ILs, carbonates, ethers, sulfoxide, acetonitrile, and amide, have been extensively investigated; thus, a comprehensive review of the solvation chemistry in LOBs is highly demanded.

6.1. Moderate solvating chemistry in LOBs

Because of the wide application of moderate solvating carbonate-based electrolytes and ether-based electrolytes in LIBs and LSBs, respectively, they were also explored in LOBs. In 2002, Read first investigated the effects of cell components, especially the electrolytes on discharge capacity, rate performance and rechargeability of the LOBs using static/dynamic gas consumption measurements and SEM. The solvents included PC, EC, DME, DEC, DMC, GBL, THF, and TFP. It was shown that, compared with other configurations in LOBs, electrolyte formulation had the largest effect on the electrochemical performance and the nature of discharge products.[295,296] Peter *et al.* demonstrated that O_2 was the charging product by *in situ* differential electrochemical mass spectrometry (DEMS) and revealed, for the first time, that the LOBs could be cycled for 50 cycles at different current densities in $LiPF_6$/PC electrolyte.[297] However, as shown in Fig. 21b, they further investigated the decomposition of alkyl carbonate electrolytes in LOBs and found that different decomposition mechanisms existed in discharge and charge processes, leading to the passivation of both cathodes and anodes, which was the main reason for capacity fading and cell failures.[298] McCloskey *et al.* also revealed the decomposition of carbonate in LOBs using isotopic labelling techniques and DEMS. It was shown that carbonate decomposition dominated the discharge process, forming Li_2CO_3, Li alkyl carbonates, and a small amount of Li_2O_2 as the discharge product. In addition, CO_2 instead of O_2 was the main charge product in carbonate-based electrolyte (Fig. 21c).[292,299]

The inferior electrochemical performance of carbonate-based MSEs has prompted researchers to explore the ether-based MSEs for high-performance LOBs. McCloskey *et al.* demonstrated that, compared with carbonate, ether was more suitable for LOBs, since Li_2O_2 and O_2 were the predominate discharge and charge products, respectively, implying the improved reversibility of LOBs.[292] Aurbach *et al.* found that the cycling stability of LOBs with electrolytes composed of LiTFSI in DME, diglyme, triglyme and tetraglyme followed the order diglyme > DME > triglyme and tetraglyme.[301] However, solid evidence has also demonstrated that ether-based MSEs are severely decomposed due to the active oxygen species during the electrochemical process in LOBs, implying that

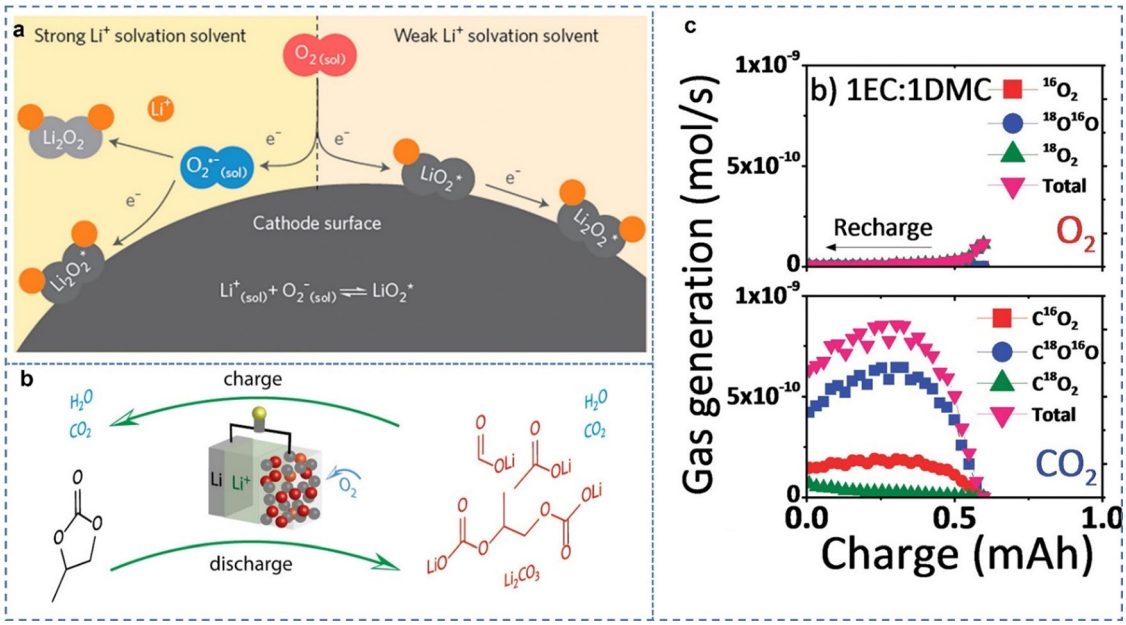

Fig. 21 (a) Schematic illustration of different redox mechanisms in LOBs with different solvents. Reproduced with permission.[300] Copyright 2020 American Chemical Society. (b) Decomposition mechanism of carbonate in LOBs. Reproduced with permission.[298] Copyright 2011 American Chemical Society. (c) Evolution of isotopically labelled CO_2 and O_2 during charging in EC/DMC electrolytes. Reproduced with permission.[292] Copyright 2011 American Chemical Society.

ethers in MSEs are also not ideal solvents in LOBs.[292,296,301–303] Therefore, some modified anti-oxidation molecules such as 2,4-dimethoxy-2,4-dimethylpentan-3-one (DMDMP), 2,2-dimethyl-3,6,9,12 tetroxa-2-silatridecane (1NM3), and 2,3-dimethyl-2,3-dimethyoxybutane (DMDMB) are employed as the novel solvents for LOBs.[304–306]

The moderate solvating ability in MSEs is not sufficient to dissolve LiO_2, inducing the following coating of insulting Li_2O_2 films on the porous substrate, resulting in fast capacity fading and poor electrochemical kinetics. Moreover, inferior compatibility of MSEs with lithium metal anodes and poor stability against high voltage also deteriorate their performance in LOBs. Therefore, novel electrolytes are urgently needed to address the challenges in MSEs.

6.2. Weak solvating chemistry in LOBs

The prerequisite for ideal electrolytes fin LOBs is the chemical stability with both the anode and cathodes. Molten salts or room temperature ionic liquids, due to their excellent chemical stability, have been widely investigated. In 2004, Katayama explored the redox behavior of oxygen in RTILs which consisted of $TFSI^-$ anions with aliphatic and alicyclic organic cations (trimethyl-*n*-hexylammonium, $TMHA^+$; 1-butyl-1methylpyrrolidinium, BMP^+) and aromatic cations (1-ethyl-3-methylimidazolium, EMI^+; 1,2-dimethyl-3-propylimidazolium, $DMPI^+$). The results unveiled that oxygen dissolved in these RTILs was reduced to LiO_2 and further to Li_2O_2 in aliphatic and alicyclic cations, while only LiO_2 was obtained in aromatic cations due to the nucleophilic attack of RTILs on imidazolium cations.[307] In 2005, Kuboki *et al.* revealed that hydrophobic ILs consisting of 1-ethyl-3-methylimidazolium bis(trifluoromethylsulfonyl)amide could work for 56 days in air and exhibited a high discharge capacity of 5360 mA h g^{-1}.[308] Other ILs such as 1-butyl-1-methylpyrrolidinium bis(trifluoromethylsulfonyl)imide (Pyr14TFSI),[309–311] [DEME][TFSI][312,313] have also been widely investigated in LOBs.

In 2018, a landmark work on molten salts ($LiNO_3/KNO_3$) in LOBs was reported by Nazar *et al.* They found that, as shown in Fig. 22a, at an elevated temperature, a highly reversible formation of LiO_2 *via* four-electron redox chemistry was first discovered in LOBs. The concentration of LiO_2 in the discharge products is highly associated with the operating temperatures and current densities (Fig. 22b and c). Combined with a bifunctional catalyst, the LOBs exhibited a significantly stable cycling performance of 150 cycles with an almost theoretical CE (Fig. 22d).[314] Addison *et al.* also investigated the $LiNO_3$–KNO_3 eutectic molten electrolytes in LOBs. They found that the molten salt electrolyte, compared with carbonate electrolytes, improved the cycling reversibility and rate capability due to the stability and moderate solubility of lithium peroxide in the molten salt electrolyte. Using state-of-the-art electrochemical and analytical techniques, they proved the excellent reversibility of formation and decomposition of Li_2O_2 with overpotentials as low as 50 mV (Fig. 22e).[315] The difference in the redox chemistry between these two reports may result from the function of the bifunctional catalysts used in the previous work.

The concentration of lithium salts is also investigated to improve the electrochemical performance of LOBs.[318,319] A series of aprotic electrolytes consisting of LiTFSI-$(Gx)_n$ (n = 1, 3, 5, 7; x = 3 or 4) were adopted for LOBs and it was found that the electrochemical performance was highly influenced by the concentration of lithium salts due to the competition of affinity of superoxide radicals with solvent Li^+ and solvents. As shown

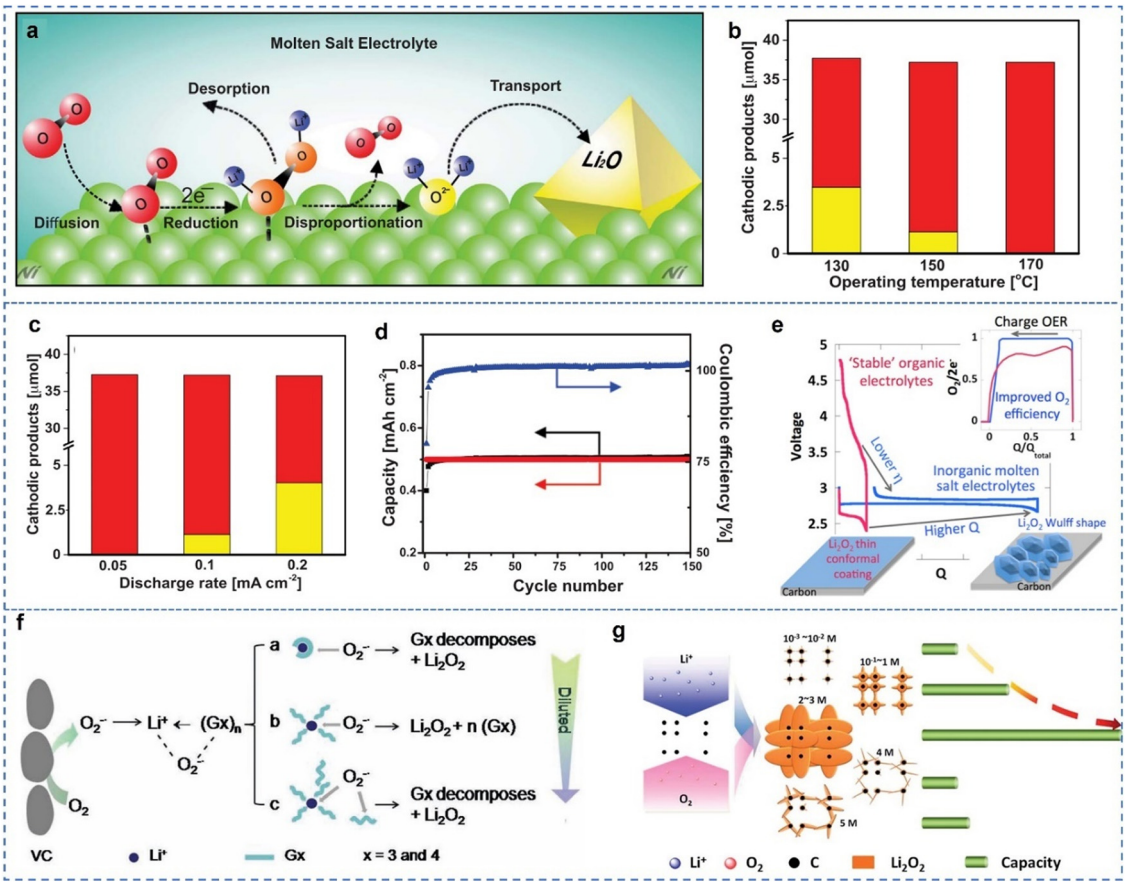

Fig. 22 (a) Schematic illustration of the pathway of four-electron redox chemistry in LOBs. The ratio of lithium superoxide and lithium peroxide at different (b) operating temperatures and (c) current densities. (d) Cycling performance of LOBs. Reproduced with permission.[314] Copyright 2018 AAAS. (e) Schematic illustration of different redox processes in LOBs with different electrolytes. Reproduced with permission.[315] Copyright 2016 American Chemical Society. (f) Schematic illustration of the reduction process in electrolytes with different concentrations of lithium salts. Reproduced with permission.[316] Copyright 2013 Wiley. (g) Schematic illustration of the capacities and morphologies during the discharge process with different concentrations of lithium salts. Reproduced with permission.[317] Copyright 2014 Royal Society of Chemistry.

in Fig. 22f, in dilute electrolytes or electrolytes with ultrahigh concentration of lithium salts, the decomposition of solvent was inevitable, while LiTFSI-$(Gx)_n$ with n = 5 showed less decomposition of solvents. As a result, LiTFSI-$(Gx)_5$ exhibited superior cycling performance at different current densities.[316] The morphologies of deposited discharge products were also investigated in electrolytes with lithium concentrations from 10^{-3} to 5 M by Liu *et al.* in 2014. As shown in Fig. 22g, when the concentration was about 2–3 M, LOBs exhibited the highly improved discharge capacities; however increasing or decreasing the concentration of lithium salts led to inferior discharge capacities, which was ascribed to the different growth model of Li_2O_2 induced by the different Li^+ solvation structures in the above electrolytes.[317] 3 M LiTFSI in DME significantly enhanced the cycling stability during the discharge-charge process of 2–4.5 V *vs.* Li^+/Li due to the excellent compatibility with both the cathode and anode. DFT results shown that the Li–DME complex in highly concentrated electrolytes had higher activation energy barriers for the decomposition of DME induced by superoxide radical anions, leading to an improved electrochemical reversibility.[320] A similar phenomenon was also observed in DMSO-based HCE (LiTFSI-3DMSO). LiTFSI-3DMSO (1 : 3 by mol) contained no free solvents but only Li^+–($TFSI^-$)–$(DMSO)_3$ complexes. The Gibbs activation energy barrier of these complexes for C–H bond scission in DMSO was higher than that in neat DMSO and dilute electrolytes, thus enhancing the stability of the electrolytes in superoxide radical anions. As a result, the LOBs using LiTFSI–3DMSO exhibited excellent cycling stability for more than 90 cycles.[321] Liu *et al.* adopted LHCEs (1.7 M LiTFSI in G4/TTE) to mitigate the side reactions in LOBs. Addition of a non-polar solvent could alter the Li^+ solvation structure, improving the ionic conductivity and electrochemical stability with both the anode and cathode, thus achieving better electrochemical performance of LOBs.[322] Recently, Zhang *et al.* investigated the LHCE (LiTFSI in G4/OTE) in LOBs. Compared with HCEs, LHCE provided high anodic and cathodic stability to active oxygen intermediates and lithium metal anodes, high oxygen solubility, low viscosity, and good wetting, thus remarkably improved the cycling stability of LOBs.[323] In 2021, Chen *et al.* used IL-based LHCEs (LiTFSI-[DEME][TFSI]-OTE) for high-performance LOBs.[313]

In 2011, Peter *et al.* investigated AN with a low DN of 14 kcal mol^{-1}, as a solvent for electrolytes in LOBs. They demonstrated that the final discharge product was Li_2O_2 which was derived from the disproportionation of LiO_2 during discharge and directly evolved into O_2 by a one-step process. However, there was not additional information about the electrochemical stability of AN or electrochemical performance of this WSE.[327] By substituting vulnerable groups in solvents with more stable electron-drawing functional groups, novel solvents such as 1NM3, DMDMB, and DMDMB were obtained. Their decomposition induced by oxidative oxygen intermediates during electrochemical process could be mitigated due to their low polarity.[305] Recently, Huang *et al.* designed a methylate cyclic ether 2,2,4,4,5,5-hexamethyl-1,3 dioxolane (HMD) as a stable solvent for electrolytes in LOBs. There are no hydrogen atoms on the alpha-carbon in HMD, avoiding the decomposition induced by hydrogen abstract reactions. As a result, LOBs using an HMD-based electrolyte delivered excellent cycling stability for 157 cycles, which was four times more than that achieved using DOL or DME-based electrolytes.[328] Yang *et al.* proposed sulfamide- and sulfonamide-based small molecules with DN $\leq$ 16.9 kcal mol^{-1} as the anti-oxidation solvents for electrolytes in LOBs. Since these solvents lack acidic protons and weak C–H bonds, their anti-oxidation was highly enhanced, making them suitable as solvents in LOBs. As a result, *N*,*N*-dimethyl-trifluoromethane sulfonamide ($DMCF_3SA$)-based electrolytes exhibited stable cycling for >90 cycles in LOBs at $\leq$4.2 V.[329]

6.3. Strong solvating chemistry in LOBs

Ideal electrolytes for high-performance LOBs should satisfy the following requirements: high O_2 solubility, excellent chemical and electrochemical stability toward other components in LOBs and oxidative intermediates, high coordination ability to dissolve enough discharge products including lithium peroxide and lithium superoxide, a wide liquid temperature range, high ionic conductivity and low viscosity.[330] Among these merits, the solubility of lithium peroxide or lithium superoxide is critical due to its significant influence on the redox chemistry of LOBs. Therefore, tremendous efforts have been devoted to design strong solvating molecules or ions with high DN or AN.[330–332] These strong solvating molecules or ions could be classified into three categories: polar solvent, anions, and mediators. It is worth noting that, in many cases, these three components work synergistically to enhance the electrochemical performance in LOBs.

In 2010, Abraham *et al.* investigated the effect of different cations and solvents in the electrolytes on discharge products and reversibility of LOBs. The cations included tetrabutylammonium ion (TBA^+) or Li^+, and solvents were composed of DMSO, DME, TEGDME, or AN with different DNs. It was clearly shown that only reversible one-electron redox process involving the O_2/O_2^- couple existed in electrolytes containing TBA^+ due to the formation of the stable TBA^+–O_2^- complex, while a stepwise redox process during discharge, forming O_2^-, O_2^{2-}, and O_2^-, existed in electrolytes containing Li^+. In electrolytes containing Li^+, the redox process was irreversible or quasi-reversible with different discharge products in different solvents.[293] High reversibility of formation/decomposition of Li_2O_2 is critical for constructing rechargeable LOBs, although in some electrolytes such as carbonate or ether-based electrolyte, the reversibility comes from the successive decomposition of electrolytes, instead of Li_2O_2, which leads to cell failure when the cycling process is extended. Peter *et al.* discovered the remarkable reversible Li_2O_2–O_2 couples in DMSO-based electrolytes (0.1 M $LiClO_4$ in DMSO) for 100 cycles. As shown in Fig. 23a–c, during the initial discharge process, reduction products were mainly composed of Li_2O_2 with little Li_2CO_3 or HCO_2Li, the signals of which disappeared during the following charge process. Intriguingly, the reversibility remained for 100 cycles, resulting into superior cycling stability with a capacity retention of 95% after 100 cycles and formation of Li_2O_2 with 99% purity at the 100th cycle.[324] They further investigated the function of DMSO with a high DN in improving the reversibility of LOBs by comparison of redox chemistry in solvents with different DNs. The effects of solvents including AN, DME, DMSO, and MeIm on the solubility of LiO_2 were investigated. Different from previously reported two deposition pathways of Li_2O_2, that is, solution-mediated and surface mediated mechanism as shown in equations 8–10 and 11–13, respectively, which were proposed and widely adopted in LOBs using solvents with different polarity, they instead proposed a unified mechanism based on the free energy (ΔG) of the reaction $LiO_{2*} \rightleftharpoons$ Li(sol) + O_2^-(sol) + ion pairs + higher aggregates (clusters). They discovered that when $\Delta G \ll 0$ (low DN), the surface-medicated mechanism dominated in Li_2O_2 deposition, while the solution-mediated mechanism was prevalent when $\Delta G \gg 0$ (high DN) (Fig. 23d). Thus, design stable and high DN electrolytes is essential for high-performance LOBs.[291] Although DMSO could facilitate the reversible discharge–charge process, decomposition of DMSO is inevitable.[326,332–334] Therefore, additional solvents or protection strategies are needed for the successful application of DMSO-based electrolytes in LOBs.[333,335] Besides, strong polar solvents such as MeIm, DMF, DMA, and hexamethylphosphoramide (HMPA) are also investigated in LOBs.[336–340] Similar to DMSO, they are vulnerable under the attack of oxidative oxygen species in LOBs. However, Khetan *et al.* developed a thermodynamic model and demonstrated an anticorrelation between the stability of solvents and their dissolution ability, proving that it was possible to design stable solvents with high polarity (Fig. 23f).[326] Moreover, Luntz *et al.* proposed the important function of a trace amount of water as additives to regulate the redox pathways in LOBs. As shown in Fig. 23e, water could dissolve LiO_2, thus enhancing the formation of Li_2O_2 toroids and leading to significant enhancement of capacity in LOBs. This work demonstrated that manipulating the solvating ability of additives was an effective and facile strategy to prompt a solution-based mechanism and improve the electrochemical performance in LOBs.[325]

Dudney *et al.* explored the influence of lithium salts ($LiPF_6$, $LiBF_4$, $LiClO_4$, and LiTFSI) on the discharge chemistry of LOBs and found that all the lithium salts underwent similar

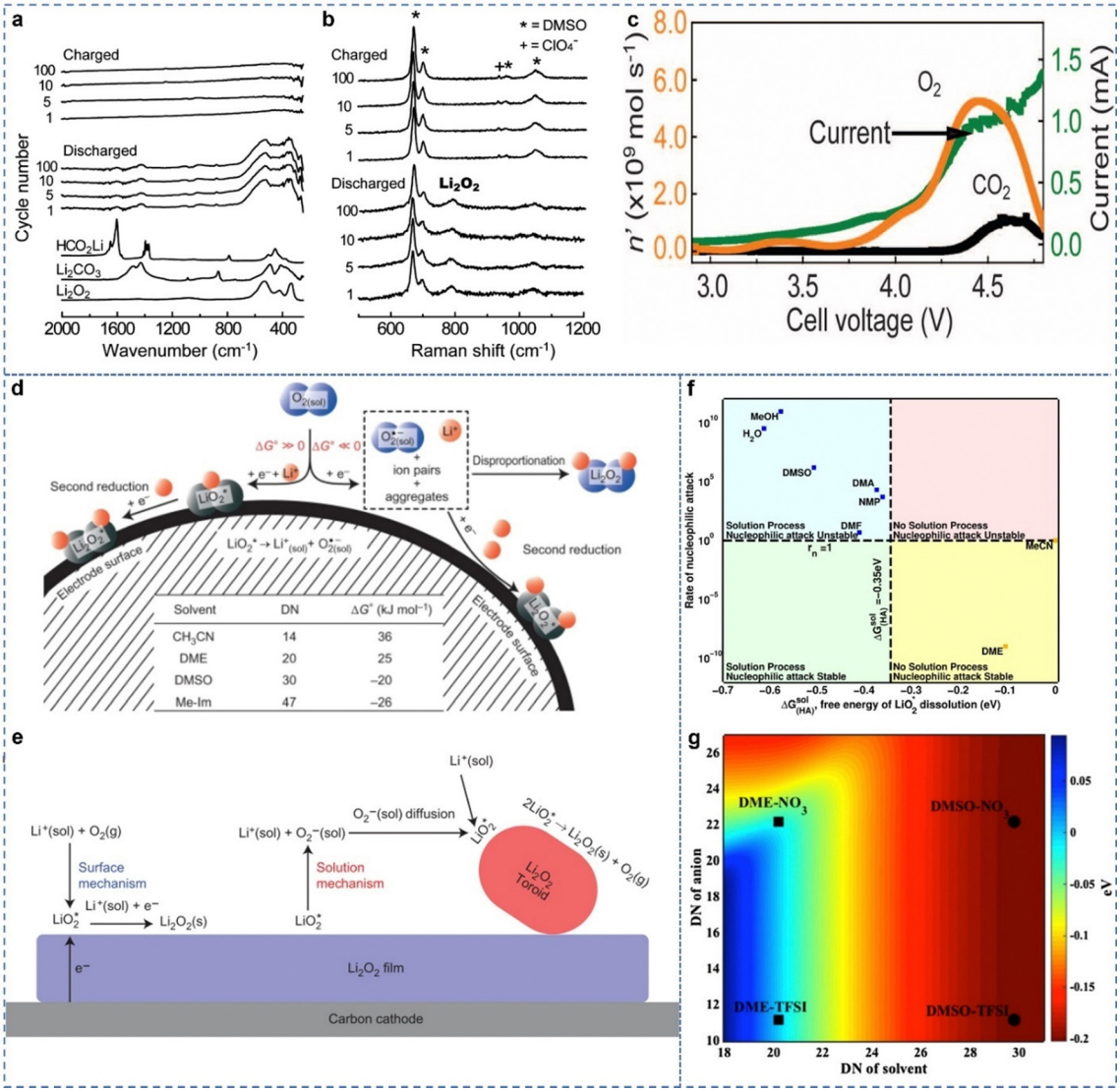

Fig. 23 (a) FTIR spectra and (b) Raman spectra of the electrochemical products in LOBs using DMSO-based electrolyte. (c) DEMS of LOBs using DMSO-based electrolytes. Reproduced with permission.[324] Copyright 2012 AAAS. (d) Schematic of the Li_2O_2 deposition mechanism depends on the free energy of Li_2O solution. Reproduced with permission.[291] Copyright 2014 Nature Publishing Group. (e) Schematic illustration of the surface-mediated and solution-mediated mechanisms of Li_2O_2 with or without high-DN additives. Reproduced with permission.[325] Copyright 2014 Nature Publishing Group. (f) Regions of the rate of nucleophilic attack and free energy of LiO_2 dissolution in different solvents. Reproduced with permission.[326] Copyright 2015 American Chemical Society. (g) Plot of free energy of Li^+ in electrolytes consisting of solvents and anions with different DNs.

decomposition, but $LiClO_4$ was the least reactive one.[341] Due to the different DNs of different anions, lithium salts exhibited an essential influence on the intermediate solvation, therefore determining the electrochemical performance in LOBs. Adopting $LiNO_3$ and LiTFSI as two typical lithium salts because of the difference in DNs between NO_3^- and $TFSI^-$, McCloskey *et al.* investigated the redox process of LOBs in DME-based electrolytes (1 M $LiNO_3$-LiTFSI in DME). Compared with $TFSI^-$, NO_3^- possessed strong solvating ability, indicated by its higher DN, forming stable Li^+–NO_3^- ion pairs, enhancing the Li^+ stability in electrolyte and improving intermediates' solubility. As a result, with the increasing ratio of $LiNO_3$, the capacity of LOBs increased significantly by more than fourfold. Moreover, addition of high-DN anions in solvents with a low DN is much more effective in boosting the electrochemical performance, while having a little influence in solvents with high DNs, as shown in Fig. 23g.[342]

Soluble redox mediators have also been widely adopted in LOBs because they effectively reduce the redox overpotentials and improve discharge capacities. One of the most impressive works on redox mediators was performed by Peter *et al.* in 2016. 2,5-Di-*tert*-butyl-1,4-benzoquinone (DBBQ), as the redox mediator, was introduced into 1 M LiTFSI in TEGDME. As shown in Fig. 24a and b, the reduction product of DBBQ, LiDBBQ, combined with oxygen in solution, forming $LiDBBQO_2$, which was further reduced to Li_2O_2 with a lower reaction barrier energy. Moreover, DBBQ could improve the solubility of LiO_2, resulting into the solution-mediated mechanism of Li_2O_2

deposition (Fig. 24c and d), enhancing the discharge capacity and redox reversibility. As a result, LOBs using DBBQ exhibited capacities 80–100 times higher than those achieved without DBBQ (Fig. 24e and f).[343] Other effective redox mediators including LiI,[344–346] LiBr,[347] TEMPO,[348,349] tetrathiafulvalene (TTF),[350,351] ethyl viologen ditriflate,[352,353] benzoquinone,[354] iron phthalocyanine,[355] tris[4-(diethylamino)phenyl]amine,[356] tris(pentafluorophenyl)borane (TPFPB),[357] *etc.* have also been adopted as redox mediators. Although these redox mediators exhibited high polarity with a high DN or AN, the effect of these mediators on the solubility of redox intermediates had not been provided, which was not beneficial to illustrating their roles in the improvement of electrochemical performance in LOBs.[343] The application of redox mediators makes the usage of moderate or weak solvating solvents in LOBs possible, since compared with strong solvating solvents, these solvents are less vulnerable from the nucleophilic attack or proton abstraction by oxygen radicals.

In all, although great progress has been achieved in electrolytes of LOBs, development of LOBs is still in its infancy. Tremendous efforts are needed not only in designing electrolytes, but also in the development of high-performance cathodes, anodes, *etc.*[358]

Since the redox processes in both LOBs and LSBs involve multiphase conversion reactions, design of electrolytes in LOBs faces similar issues in LSBs. Strong solvating electrolytes improve the discharge capacity and reduce the charge overpotential; however, they also lead to severe corrosion of lithium metal. Redox mediators in MSEs or WSEs are widely adopted to improve the overall performance of LOBs. Recent research demonstrated that the redox mediator shuttles between the cathode and anode, similar to the polysulfides in LSB, leading to the corrosion and dendrite formation in lithium metal anodes, and the consumption of the electrocatalytic redox mediator, leads to inferior electrochemical performance. For practical application, some other strategies such as functional separators, artificial SEI, electrolyte additives, and lithium composites anodes should be adopted to suppress the shuttle of the redox mediator and protect the lithium metal anode.[359]

For practical application, one also considers the E/C ratio in LOBs. Since the cathode in LOBs is oxygen, the weight ratio of electrolyte in LOBs is larger than those in other Li-based rechargeable batteries, implying that the amount used in LOBs has a huge effect on the overall energy density. The lithium–air battery system (LAB), which directly uses the oxygen present in air as an open system, is a more attractive version of LOBs. However, the effects of extra moisture and carbon dioxide in LABs on the lithium metal, catalysts, electrolytes, and the corresponding electrochemical performance should be effectively eliminated before massive application of LABs.[360]

7. Strategies of regulating solvation chemistry in aqueous LIBs

Due to the high polarity, low viscosity, low cost, and nonflammability of water, aqueous electrolytes using water as the solvent endow aqueous batteries with intrinsic safety, excellent rate performance, and high power density, which is the reason why aqueous electrolytes have been indispensable for all the batteries including lead-acid, zinc-manganese dioxide, nickel-cadmium, and nickel metal hydride batteries since the

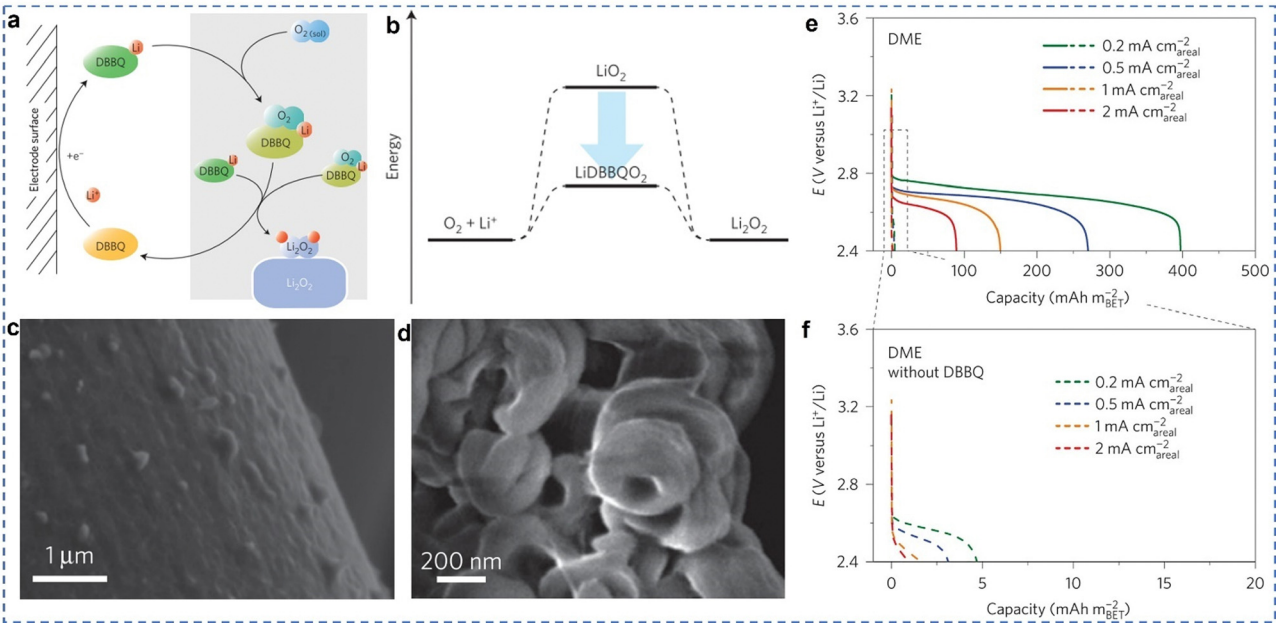

Fig. 24 (a) Schematic illustration of the reaction mechanism of DBBQ in LOBs, and (b) the corresponding energy barrier. (c) SEM of deposited Li_2O_2 (c) without or (d) with DBBQ in electrolytes. (e and f) Discharge profiles of LOBs with or without DBBQ in electrolytes. Reproduced with permission.[343] Copyright 2016 Nature Publishing Group.

discovery of Volta pile in 1799.[42,361–363] Some of these aqueous batteries, although with low energy density, are still popular in specific applications with high demand of safety and power density. Since the 1990s, nonaqueous LIBs using organic electrolytes, owing to their high energy density and excellent rechargeability, have dominated the market of energy storage and are omnipresent in the daily life. But safety issues in LIBs using organic electrolytes have drawn increasing attention due to their wide application in daily life. Thus, tremendous efforts have been made to design ALIBs to meet the demands of high energy density and excellent safety.

One of the most effective strategies to boost the energy density of ALIBs is improving the working potential windows.[364] In neutral solutions, the limitation of cathodic stable potential is about 2.626 V *vs.* Li^+/Li, below which water begins to decompose, leading to the formation of H_2 and OH^- (HER); while the limitation of anodic stable potential is about 3.856 V *vs.* Li^+/Li, above which the formation of O_2 and H^+ occurs (OER). The cut-off potentials of the HER and OER determine the narrow ESPW of water (1.23 V).[365] Although the potential limits of the OER and HER varies with pH, the ESPW does not change accordingly, and the narrow ESPW severely deteriorates the performance of ALIBs.[362,363,366] Recently, various anodes (VO_2, LiV_3O_8, $H_2V_3O_8$, $LiTi_2(PO_4)_3$, TiO_2, graphite, Mo_6S_8, and $Li_4Ti_5O_{12}$) and cathodes material ($LiMn_2O_4$, LCO, LFP, LNMO, and $Li_{1.05}Cr_{0.1}Mn_{1.85}O_4$) have been designed, and the fundamental mechanism is further investigated to boost the performance of ALIBs.[361,366–372] Moreover, broadening the ESPW of aqueous electrolytes by regulating the solvation chemistry is a more facile way to boost the energy density. In this section, only MSEs and WSEs are discussed since there are few SSEs because of the strong polarity of water.

7.1. Moderate solvating electrolytes ALIBs

Since water is one of the most polar solvents, we define electrolytes consisting of lithium salts ($\leq$2 M) and water as the typical moderate solvating electrolytes in ALIBs. In 2008, Sauvage *et al.* demonstrated the feasibility of 1 M $LiNO_3$/water with $LiFePO_4$ cathodes, and, compared with organic electrolytes, the aqueous electrolyte resulted in lower resistance and considerable improvement in the discharge capacity.[368] MSEs consisting of 1 M $LiNO_3$/water or 2 M Li_2SO_4/water were also adopted to investigate the electrochemical performance of $LiMn_2O_4$ in a three-electrode glass cell with active carbon and a saturated calomel electrode as counter and reference electrodes, respectively. These two MSEs provided the cells with long-term cycling but with inferior cycling stability compared to concentrated electrolyte (5 M $LiNO_3$ in water).[367] 1–2 M Li_2SO_4 aqueous solution was also used in $Li_{1.2}V_3O_8/LiMn_2O_4$, $LiTi_2(PO_4)_3/LixMn_2O_4$, and $LiTi_2(PO_4)_3/LiFePO_4$ cells (Table 7).[373–375] However, the low working voltage significantly decreased the energy density, while broadening

Table 7 Summary of the performance in ALIBs

No.	Electrolytes	Anode/cathode	ESPW (V)	Energy density (W h kg^{-1})	Cycling performance: Current density	Cycling performance: Capacity retention/cycles	Ref.
1	1 M Li_2SO_4 in water	$Li_{1.2}V_3O_8/LiMn_2O_4$	—	—	0.1C	36%/100	373
2	2 M Li_2SO_4 in water	$LiTi_2(PO_4)_3/Li_xMn_2O_4$	—	—	0.2C	89%/100	374
3	1 M Li_2SO_4 + 0.1 M LiOH in water	$LiTi_2(PO_4)_3$/LFP	—	—	6C	90%/1000	375
4	5 M $LiNO_3$ + 0.001 M LiOH in water	VO_2/LMO	—	—	1 mA	—	379
5	21 M LiTFSI in water	Mo_6O_8/LMO	3	100	0.15C	78%/100	10
6	21 M LiTFSI + 7 M LiOTf in water	C-TiO_2/LMO	~3.1	100	0.5C	78%/100	382
7	$Li(TFSI)_{0.7}(BETI)_{0.3}$ $2H_2O$	LTO/LCO	2.3–3.1	130	10C	75%/200	383
8	21 M LiTFSI + 7 M LiOTf in water + 10% wt PVA	S/LMO	2.24	195	0.2C	91%/100	228
9	32 M KOAc – 8 M LiOAc in water	C-TiO_2/LMO	2.7	—	0.5C	—	386
10	20 M (LiPTFSI + LiOTf) in water	LMO half cell	2.95	—	—	—	400
11	MSM : $LiClO_4$: H_2O are 1.8 : 1 : 1	LTO/LMO	~3.5 V	>160	4.5C	72.2%/1000	395
12	$Li(PTFSI)_{0.6}(TFSI)_{0.4}{\cdot}H_2O$	LTO/LCO	4.85	—	0.2C	77%/100	401
13	42 M LiTFSI + 21 M Me_3EtN-TFSI in water	LTO/LMO	3.25	145	1C	88%/100	387
14	15.3 M LiTFSI in AN-water	LTO/LMO	4.5	—	1C	98%/300	394
15	$LiClO_4$–H_2O–urea (1 : 3 : 2)	Mo_6O_8/LMO	3	100	10C	86%/2000	365
16	2 M LiTFSI – 94% PEG – 6% H_2O	L-LTO/LMO	3.2	110	1C	68.2%/300	40
17	21 M LiTFSI in water + 5% wt PAM	L-TiO_2/LMO	3.1	—	1C	86%/100	389
18	12.5 M $LiNO_3$ in water-PD + 6% wt TEGDA	Mo_6O_8/LMO	3.0	—	1C	98.5%/250	402
19	Li–H_2O–$MU_{0.27}$	NbO_2/LMO	4.5		3.5 C	Almost 100%/1500	41
20	21 M LiTFSI in water + 0.1 wt% TMSB	Mo_6O_8/LCO	—	120	2.5 C	87%/1000	371
21	21 M LiTFSI in water + 0.1% HTFSI (volume)	Mo_6O_8/LNMO	3	126	5C	70%/400	372
22	(21 M LiTFSI in water) : (9.25 M LiTFSI in DMC) (1 : 1 by weight)	LTO/LNMO	4.1	165	6C	76%/1000	393
23	15 M LiTFSI in TEGDME-H_2O	LTO/LMO	4.2	120	10C	55%/300	396
24	Li–0.9H_2O–1.3SL	LTO/LMO	4.1	128	1C	77.7%/200	397
25	10 M LiTFSI in DOL : H_2O (1 : 1)	LTO/LMO	4.7	—	1C	99%/100	398
26	4.5 M LiTFSI in KOH–$CO(NH_2)_2$–H_2O	LTO/LMO	3.3	103	1C	92%/470	399
27	21 M LiTFSI + 7 M LiOTf in water + 10 wt% PVA	Graphite/$(LiBr)_{0.5}(LiCl)_{0.5}$–graphite	—	460	0.2C	74%/150	391
28	LiTFSI $(TMS)_{0.5}$ water	LTO/LNMO	5.4	136	—	—	403
29	LiTFSI in sulfone : water (1 : 1 by mol)	LTO/LMO	3.4	141	1C	70%/300	404

the working potential window either led to rapid capacity fading or the failure of cells which were induced by side reactions. Therefore, design of alternative stable electrolytes with a wide working voltage window is, although challenging, urgently needed.

7.2. Weak solvating electrolytes in ALIBs

Decreasing the content of water or construction of robust electrode–electrolyte interphases, which are highly associated with solvation chemistry, are effective strategies to broaden the ESPW and mitigate side reactions.[372,376,377] WSEs including HCEs, LHCEs, and electrolytes with weak solvating solvents or additives, are crucial for achieving high-voltage ALIBs with improved electrochemical performances.[378]

7.2.1. HCEs and LHCEs in ALIBs. In 1994, Dahn *et al.* first proposed the ALIBs using HCEs (5 M $LiNO_3$ +0.001 M LiOH in water) as the electrolyte. The cells constructed with $LiMn_2O_4$ and VO_2 as the cathode and anode, respectively, exhibited an average voltage of 1.5 V with an energy density of 75 W h kg^{-1}.[379–381]

In 2013, Nowak *et al.* investigated the feasibility of LiTFSI in water and found that LiTFSI exhibited excellent solubility and stability even at elevated temperatures or under extreme pH conditions, paving the way for its wide application in ALIBs.[384] Later in 2015, a ground-breaking ''water in salt'' electrolyte consisting of 21 M LiTFSI in water, was explored by Suo *et al.* They found that increasing the salt concentration weakened the overall Li^+–water interaction, resulting in the introduction of $TFSI^-$ anions into the first solvation sheath of Li^+ and a decrease in water in the solvation sheath (Fig. 25a). Compared to free $TFSI^-$, Li^+–$TFSI^-$ complexes exhibited higher reduction potential, leading to a robust anion-derived SEI (Fig. 25b). As a result, this ''salt in water'' electrolytes exhibited a significantly enhanced ESPW of 3 V (Fig. 25c). Then, 2.3 V-class Mo_6O_8/$LiMn_2O_4$ (LMO) cells using ''salt in water'' electrolytes were constructed, and they delivered excellent cycling stability with a capacity retention of 68% after 1000 cycles and a high energy density of 100 W h kg^{-1}.[10,385] In 2016, they further increased the salt concentration to 28 M by an additional introduction of 7 M LiOTf (21 M LiTFSI + 7 M LiOTf in water). Consequently, the coordinated water in the Li^+ solvation sheath further decreased to 1.84; meanwhile, 0.53 OTf^- anion per Li^+ was introduced into the solvation sheath of Li^+ (Fig. 25d). According to the DTF results, the reduction potential of the Li_2OTf complex was about 2.77 V, higher than the onset potential of the HER (2.63 V), resulting in the prior decomposition of OTf anions, forming a robust LiF-rich SEI. The robust SEI could effectively suppress the HER even on TiO_2, which was proven to be a good catalyst for the HER. As a result, the ESPW of this electrolyte was further increased to 3.1 V, endowing C-TiO_2||$LiMn_2O_4$ cells with excellent cycling stability and a high energy density of 100 W h kg^{-1} (Fig. 25e).[382] Combined with electrochemical, spectroscopic, and computational techniques, the formation mechanism of the SEI in aqueous concentrated electrolyte was explored by Wang *et al.* It was revealed that competitive decomposition of water, salt anion, and dissolved gases synergistically led to the formation of dense electrode–electrolyte interphases in HCEs.[385] Yamada *et al.* investigated a hydrate-melt electrolyte $(Li(TFSI)_{0.7}(BETI)_{0.3}\ 2H_2O)$ in the ALIBs. They found that the formation of anion-derived SEI depended on not only the solvation sheath of Li^+ but also the electrodes themselves. As shown in Fig. 29f, different onset potentials for the HER and OER were obtained with different electrodes (Al, Zn, SUS, Pt, *etc.*). When stable Al was chosen as the current collector, the cells using the hydrate-melt electrolyte delivered a ESPW of ~2.3–3.1 V according to the materials of the cathode. As a result, $Li_4Ti_5O_{12}$ (LTO)||LCO cells delivered an ultrahigh energy density of 130 W h kg^{-1} (Fig. 25f and g).[383]

In 2018, Bao *et al.* designed a highly concentrated aqueous electrolyte consisting of 32 M potassium acetate (KOAc) and 8 M lithium acetate (LiOAc) in water for high-performance LTO||LMO ALIBs.[386] Recently, A 63 M super-concentrated aqueous electrolyte consisting of 42 M LiTFSI and 21 M asymmetric ammonium salt (Me_3EtN-TFSI) in water has been proposed. The introduction of Me_3EtN–TFSI significantly increased the solubility of LiTFSI in water, leading to an unprecedented salt/water molar ratio of 1.13. As a result, the super-concentrated electrolyte widely broadened the ESPW (3.25 V) and delivered a high energy density of 145 W h kg^{-1}.[387]

7.2.2. Other weak solvating electrolytes in ALIBs. Besides directly increasing the salt concentration, introduction of other additives is another effective way to weaken the Li^+–water affinity, thus widening the ESPW and suppressing the side reaction induced by water decomposition. Poly(ethylene glycol) (PEG), as a water-miscible polymer was adopted to alter the hydrogen-bonding structure *via* a molecular crowding effect, significantly suppressing the water activity in aqueous electrolyte. As a result, a wide ESPW of 3.2 V was achieved in the electrolyte (2 M LiTFSI – 94% PEG – 6% H_2O) containing only 2 M lithium salt. LTO||LMO full cells using this electrolyte showed a high energy density of 110 W h kg^{-1} and long-term cycling stability with a capacity retention of 68.2% after 300 cycles (Fig. 26a and b).[40] They further demonstrated that in this LiTSI-based molecular crowding electrolyte, an insoluble LiF-rich SEI was successfully constructed, which was crucial in suppressing the HER in ALIBs.[388] Polyacrylamide (PAM) was introduced into a highly concentrated electrolyte (21 M LiTFSI in water) by Li *et al.* to boost the electrochemical performance of ALIBs. The appearance of PAM in the primary solvation sheath of Li^+ not only reduced free water near the interface, but also promoted the formation of the anion-derived SEI, significantly boosting the cycling stability of LTO/LMO full cells with 86% retention after 100 cycles.[389] Other polymer additives such as PEO, sugar, and PVA are also explored in aqueous electrolytes, which could significantly broaden the ESPWs and improve the energy density.[228,376,386,390–392]

Organic solvents are also investigated as the cosolvents in aqueous electrolytes.[393–399] Wang *et al.* first introduced DMC into the aqueous electrolytes by directly mixing 21 M LiTFSI–water and 9.25 M LiTFSI–DMC solutions. The addition of DMC significantly altered the components at the inner-Helmholtz interface, forming a LIF and Li_2CO_3-rich interphase, expanding

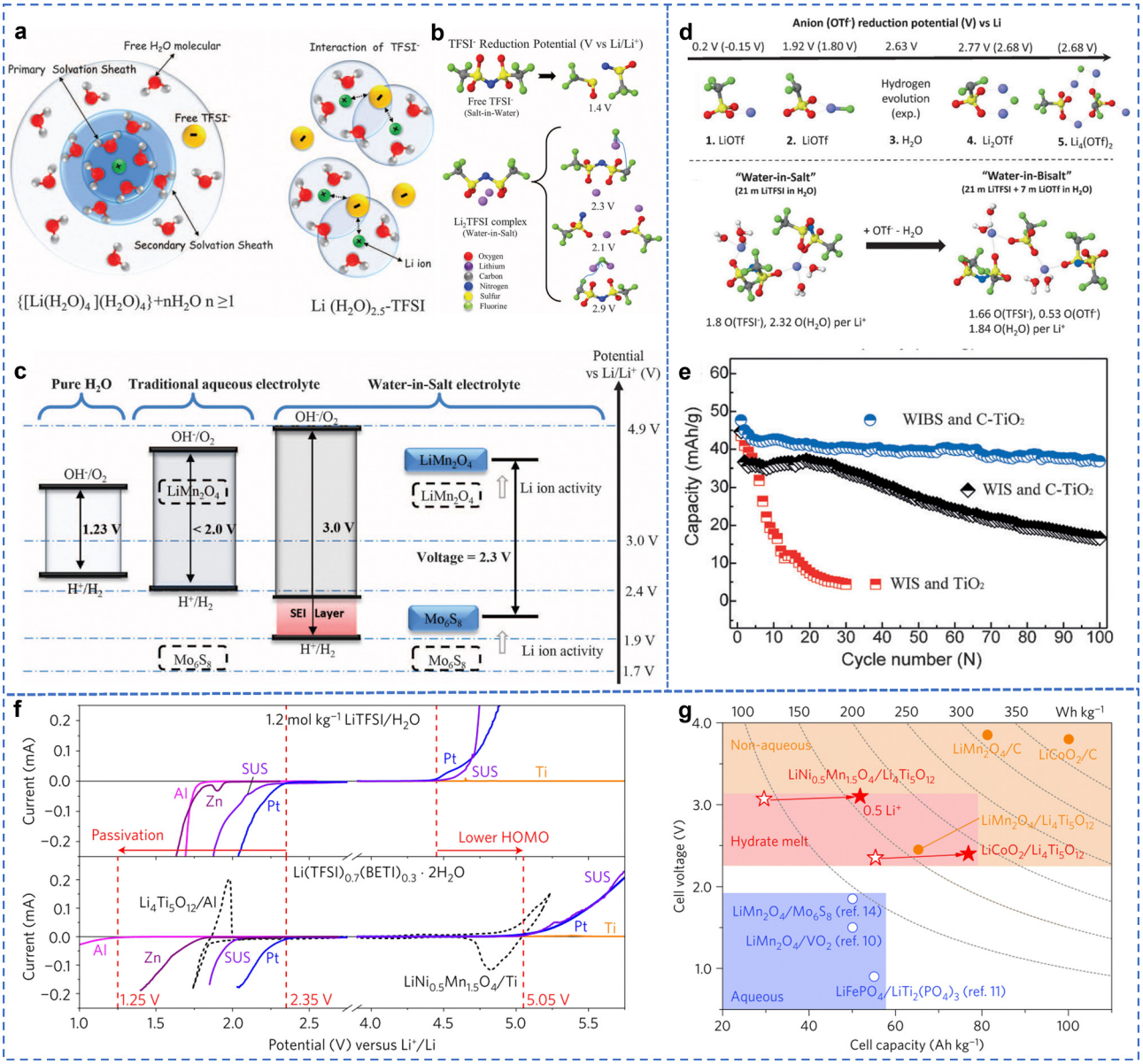

Fig. 25 (a) Schematic illustration of the Li^+ solvation sheath in dilute and "water in salt" electrolytes. (b) Reduced potential of free TFSI anion and its complexes calculated from DFT. (c) Change in the ESPW in the "water in salt" electrolytes. Reproduced with permission.[10] Copyright 2015 AAAS. (d) Reduced potential of the LiOTf complex, and the influence of the addition of LiOTf in the solvation sheath of Li^+. (e) Cycling performance of C-TiO_2/$LiMn_2O_4$ with different electrolytes at a current density of 0.5 C. Reproduced with permission.[382] Copyright 2016 Wiley. (f) LSV profiles of different electrolytes on different substrates. (g) Theoretical (filled circles and stars) and actual (open circles and stars) energy densities in different rechargeable batteries. Reproduced with permission.[383] Copyright 2016 Nature Publishing group.

the ESPW to 4.1 V. As a result, LTO||LNMO cells delivered a high energy density of 165 W h kg^{-1} after 1000 cycles.[393] Addition of AN also minimized the free water at the interface and induced a thin and robust organicinorganic interphase, largely expanding the ESPW to 4.5 V, thus significantly improving the electrochemical performance of LTO||LMO cells.[394] Chen *et al.* investigated TEGDME as the cosolvent and found that the addition of TEGDME changed the solvation structure of Li^+, leading to unique electrode–electrolyte interphases on both the cathode and anode. These interphases kinetically expanded the ESPW to 4.2 V and significantly improved the cycling stability of ALIBs with a high energy density of 120 W h kg^{-1}.[396] Other organic molecules such as DOL,[398] urea,[365] SL,[397] *etc.*, have also been explored in ALIBs (Table 7). Recently, Wang *et al.* investigated the asymmetric donor–acceptor molecule, methylurea (MU), in aqueous electrolyte. Due to the acceptor and donor functional groups in MU, a unique core–shell like cluster solvation structure was formed in the aqueous electrolyte, constructing localized super-concentrated domain in electrolytes. As a result, a wide ESPW of 4.5 V was achieved and excellent cycling stability of NbO_2||LMO full cells with a high energy density of 175 W h kg^{-1} was realized (Fig. 26c–e).[41]

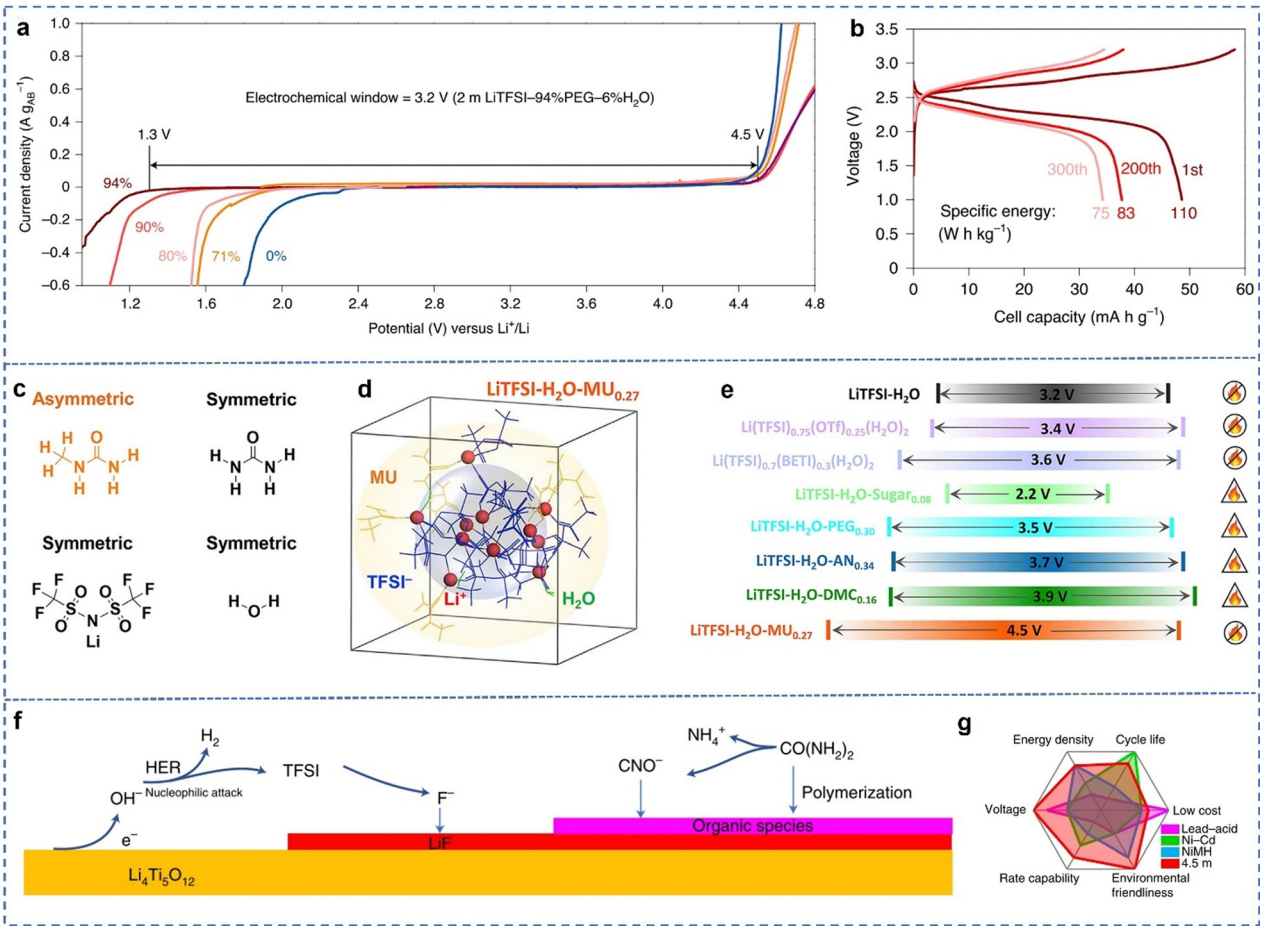

Fig. 26 (a) Electrochemical stable potential widows of different electrolytes. (b) Discharge–charge curves of LTO/LMO cells in 2 M LiTFSI – 94% PEG – 6% H_2O. Reproduced with permission.[40] Copyright 2020 Nature Publishing group. (c) Molecular structures of MU, urea, anions, and water. (d) Core–shell cluster of solvation structure of Li^+ in Li–H_2O–$MU_{0.27}$ electrolyte, derived from MD simulation. (e) The ESPWs of different aqueous electrolytes. Reproduced with permission.[41] Copyright 2022 Elsevier. (f) Schematic illustration of the reactions on the surface of the anode using 4.5 M LiTFSI in KOH–$CO(NH_2)_2$–H_2O electrolyte. (g) Comparison of ALIBs using 4.5 M LiTFSI in KOH–$CO(NH_2)_2$–H_2O electrolyte with other types of aqueous batteries in different aspects.

In 2022, an intriguing aqueous electrolyte composed of 4.5 M LiTFSI in KOH–$CO(NH_2)_2$–H_2O was reported by Wang *et al.* The strong affinity between $CO(NH_2)_2$ and water significantly reduced the water in the primary solvation sheath of Li^+, leading to a robust SEI composed of a LiF-rich inner layer and an organic outer layer, suppressing the HER near the anodes. Compared to 21 M LiTFSI in water, this electrolyte exhibited a wider ESPW of 3.2 V with a lower salt concentration. Thus, LMO||LTO full cells showed excellent cycling stability with a capacity retention of 92% after 470 cycles, outperforming the overall performances of commercial Ni-Cd, NIMH, and lead-acid batteries (Fig. 26f and g).[399] For convenience, typical electrochemical performances of ALIBs are listed in Table 7.

Although remarkable progress has been made in aqueous electrolytes for ALIBs, huge challenges including unsatisfying electrochemical performance and ambiguous mechanism regarding ESPW, SEI formation and its function still exist and more efforts are needed to overcome them.[405–414]

First, what plays a more important role in extending the ESPW in ALIBs, the concentration of lithium salts, or the less solvating organic solvents and polymer additives? There is no doubt that high salt concentration can significantly expand the ESPW. However, only an ESPW of 3.25 V was obtained even in electrolyte with a salt concentration as high as 63 M.[387] In another electrolyte only with a salt concentration of 4.5 M but consisting other organic solvents (4.5 M LiTFSI in KOH–$CO(NH_2)_2$–H_2O), an ESPW of 3.3 V was achieved.[399] Moreover, 10 M LiTFSI in DOL : H_2O (1 : 1) could further enhance the ESPW to 4.4 V. For now, the largest ESPW (5.4 V) was achieved in LiTFSI $(TMS)_{0.5}$ water.[403] From the conclusion above, it is difficult to distinguish the roles of salt concentration and other weak solvating components in the ESPW, and elaborately designed experiments are needed since clear understanding the roles of salt concentration and organic solvents is enlightening for further electrolyte design.

Second, the mechanism of SEI formation and its effects on the ESPW. There are two ways to expand the ESPW of ALIBs:

minizine the water content in the electrolytes or design a stable SEI to avoid a direct reaction between water and the electrode. Since reducing the water contents can compromise the safety and power density of ALIBs, designing a stable SEI seems a more effective strategy to widen the ESPW of ALIBs. However, previous reports only provide limited information of components of SEI, but the mechanism is lacking. For instance, Yamada *et al.* found that the formation of SEIs is related with both the solvation structure of Li^+ and electrodes, but the root cause was not given in the reports.[383] Understanding the mechanism of SEI and its effect needs *in situ*/*operando* or real-time characterization studies, which will be discussed in the next section.

For the electrolytes in practical ALIBs, two other aspects should be taken into consideration: the E/C ratio and self-discharge induced by electrolyte decomposition. Because of the high weight ratio of electrolyte in ALIBs, the E/C ratio has an important influence on the overall energy density. For example, Wang *et al.* found that when the E/C ratio decreased from 3 g A h^{-1} to 2 g A h^{-1}, the energy density increased from 117 W h kg^{-1} to 132 W h kg^{-1},[415] implying that lean electrolyte with low density (dilute, instead of high concentrated electrolytes) has advantages in improving the energy density of ALIBs. Second, the high ionic conductivity of aqueous electrolytes aggravates the reaction between electrolytes and electrodes, especially in high-voltage ALIBs, leading to the decomposition of electrolyte and self-discharge, which severely hinder the massive application of ALIBs.[415]

8. Summary and outlook

8.1. Summary

In summary, since the discovery of Voltaic pile in 1799, especially the commercialization of LIBs, batteries have emerged as the most important devices for energy storage, in which electrolytes are indispensable. In order to address the issues, such as unsatisfying energy density, inferior safety, high cost, *etc.*, novel rechargeable batteries including LMBs, LSBs, LOBs, and ALIBs have attracted tremendous attention recently. As the media come in directly contact with electrodes, electrolytes paly crucial roles in not only ion transportation, but also regulating the redox mechanism, expanding the ESPW, suppressing side reactions, and improving kinetics, which are all highly associated with the solvation chemistry in the electrolytes. According to the relative intensity of the affinity between Li^+–solvent and Li^+–anions, electrolytes are classified into three categories: moderate solvating electrolytes, weak solvating electrolytes, and strong solvating electrolytes depending on the polarity of solvents or anions, which is identified using parameters like the dielectric constant, donor number or relative solvating power. It is worth noting that these categories are not precisely defined and vary from system to system, and the roles these three types of electrolytes play are also different in different types of rechargeable lithium-based batteries.

In this review, five representative battery systems were chosen, since some of them share similar issues, while in other battery systems, the redox mechanism and the corresponding main challenges are totally different. Thus, a comprehensive review of the solvation chemistry in different battery systems not only sheds lights on designing novel electrolytes based on battery systems with similar issues, but also provides a whole picture of the function of solvation chemistry in different battery systems. In LMBs, MSEs and SSEs usually cannot suppress the formation of lithium dendrites, leading to the premature failure or safety issues in LMBs. In WSEs, anions participate in the solvation of Li^+, while part of solvent is expelled from, the primary solvation sheath of Li^+ due to the relative stronger affinity of Li^+–anion than that of Li^+–solvent, leading to anion-derived, robust electrode–electrolyte interphases, effectively suppressing the lithium dendrites, significantly expanding the ESPW, and significantly improving the long-term cycling stability. Those anion-derived, robust EEIs are also helpful in suppressing the co-intercalation of solvents, expanding ESPW, and improving long-term cycling stability in LIBs, while all three types of electrolytes exhibit advantages in nonaqueous LIBs for different applications. In LSBs or LOBs, the complex two-phase (solid–liquid–solid) or three-phase (gas–liquid–solid) redox pathways, combined with the poor conductivity of discharge products severely affect the utilization of active materials and the cycling life, which are the major challenges in these two systems. The strong solvating solvents in SSEs could improve the solubility of redox intermediates or discharge products, significantly altering the redox pathways, resulting into boosted electrochemical performance, especially high specific capacity, and excellent kinetics. In ALIBs, increasing the energy density *via* expanding the ESPW is of overwhelming importance due to the narrow ESPW of water. Thus, WSEs that significantly minimize free water and/or construct robust electrode–electrolyte interphases significantly broaden the ESPW, implying their potential in high-performance ALIBs. It is worth noting that we mainly focused on the regulation of cation–solvent interactions in this review. Anions with different conformers or structures in lithium salts may also have a great influence on the solvation chemistry, which deserves systematic investigation in future. Design novel lithium salts with different anions or anions with different conformers is also an effective strategy to design novel electrolytes. Moreover, what we discussed above is the effect of electrolytes on addressing the most challenging issues in rechargeable batteries, and electrolytes are, although important, not omnipotent. Thus, deliberate design of electrodes, separators, binders, and other components as a whole, is pivotal to achieve satisfying batteries.

Although great progress has been made in this filed, there are still huge challenges which remain unresolved: (1) how to efficiently design electrolyte with desired solvation structures? Most of the designed electrolytes were based on previous experiences and/or the ''trial and error'' mode, and facile strategies to design electrolytes to meet specific requirements for different electrochemical systems are still lacking. (2) How

to clarify the multiscale structural–property relationship between molecule structures in electrolytes, solvation structure, electrode–electrolyte interfaces, kinetics, redox mechanism, and electrochemical performances, especially under extreme conditions? Unveiling the multiscale structural–property relationship is the prerequisite to understand the mechanism of solvation chemistry and design desired electrolyte; however, further advanced characterization techniques or theoretical calculation/simulation methods are highly needed. (3) Commercial application of electrolyte.

8.2. Outlook

Although great progress has been achieved recently, designing high-performance electrolytes and understanding the fundamental solvation chemistry still face great challenges. For better understanding and further precisely manipulating the solvation chemistry, the proposed issues and strategies need to be addressed and adopted, respectively.[416]

8.2.1. Advanced theoretical calculation and simulation techniques. Up to now, most of the research on electrolyte design is based on the empirical ''trial and error'' method, which severely slows down the development of electrolyte and is not beneficial for understanding the redox mechanism of solvation chemistry. Although theoretical calculation or simulation such as DFT and MD have been widely used in electrolyte design, the simplified model or approximate algorithm cannot precisely describe the properties of different electrolytes. For instance, vacuum or a given environment (in one specific solvent) is adopted to calculate the HOMO/LUMO of the components of electrolytes consisting of lithium salts and various solvents or additives in DFT calculation; when simulating the solvation structure of Li^+ in electrolytes using MD, usually not more than 1000 molecules are adopted. Especially under multi-physical fields, using conventional models, it is difficult to bridge the time-and-length scale to obtain macroscale properties. Moreover, high-throughput calculations make computational cost a huge financial burden.[417] Therefore, two strategies have been proposed in this section:

8.2.1.1. Material knowledge informed machine learning. Traditional material computing is centred on solving mathematical models, and there are unsolved challenges such as the limited size of computable systems, and difficulty in modelling complex scenes. Machine learning methods establish an approximate model for the relationship between input and output through a non-explicit way, which can avoid the numerical solving of the theoretical model, thereby alleviating the huge computational requirement bottlenecks. However, the application of classical machine learning algorithms in the field of materials science[418] suffers from poor interpretability and insufficient high-quality samples.

We propose the adoption of material knowledge informed machine learning (MIML) to enhance the capabilities of the current material computing approaches. MIML is a combination of machine learning techniques with explicit prior material knowledge. In fact, many of the success stories in materials science belong to a specific form of MIML, such as deep density functions,[419] chemical syntheses planning,[420] *ab initio* solution of many-electron systems with deep neural networks,[421,422] *etc.* Using MIML-based algorithms, the computational workflows become partially interpretable, and due to the introduction of prior knowledge or mathematical models, the demand for training data is greatly reduced, and even zero-data training could be achieved. From a multiscale simulation perspective for material design, we aim to build MIML-based general partial differential equation (PDE) solvers for macroscopic to mesoscopic simulation and propose neural network surrogate models for *ab initio* solutions with built-in physical constraints of the Schrödinger equation in the future. In conclusion, MIML-enabled materials computing platforms have the potential to scale up multiscale simulations to much larger systems with high accuracy.

8.2.1.2. Integrated platform based on ''AI + big data''. Benefiting from their high efficiency, artificial intelligence (AI) (the core of which is machine learning (ML), high-throughput simulation and experiment) and big-data techniques have attracted increasing attention in molecule design, material development, property prediction, mechanism analysis, relationship mining, *etc.*[423–428]

Therefore, we propose an integrated ''AI + big data'' driven platform. According to the demands, high-throughput calculation and simulation based on ML are first adopted to screen potential molecules, followed by high-throughput experiments conducted by mobile robotic technicians for synthesis and characterization. All the results obtained from the above process are stored in a database, which provides enough data for machine learning to optimize the material design and performance prediction. Finally, ideal materials with satisfying performance are obtained efficiently. Moreover, the integrated platform is a highly effective tool to understand the nanoscale mechanism or reaction, such as the solvation chemistry in electrolytes, which is still difficult because of the inadequate experimental techniques.

8.2.1. Advanced *in situ*/*operando* characterization techniques. Atoms and stereo structures of the solvent molecules determine their solvating ability, which in turn affects the solvation structure of cations and their desolvation process. Li^+ solvation structures in electrolytes decide the properties of electrode–electrolytes interphases, which, combined with the de-solvation behavior, are highly associated with the final electrochemical performance of rechargeable batteries, that is, by molecule design, integrated multiscale regulation of solvent molecules, Li^+ solvation structures and behavior, redox pathways, electrode–electrolyte interphases, and the electrochemical performance can be achieved. But the fundamental details of the multiscale regulation strategies (how the solvent molecules affect the solvation chemistry, and how the solvation chemistry influence the electrochemical performance?) are hardly obtained directly with *ex situ* characterization techniques, such as *ex situ* TEM, XPS, SEM, XRD, Raman, FTIR, *etc.*

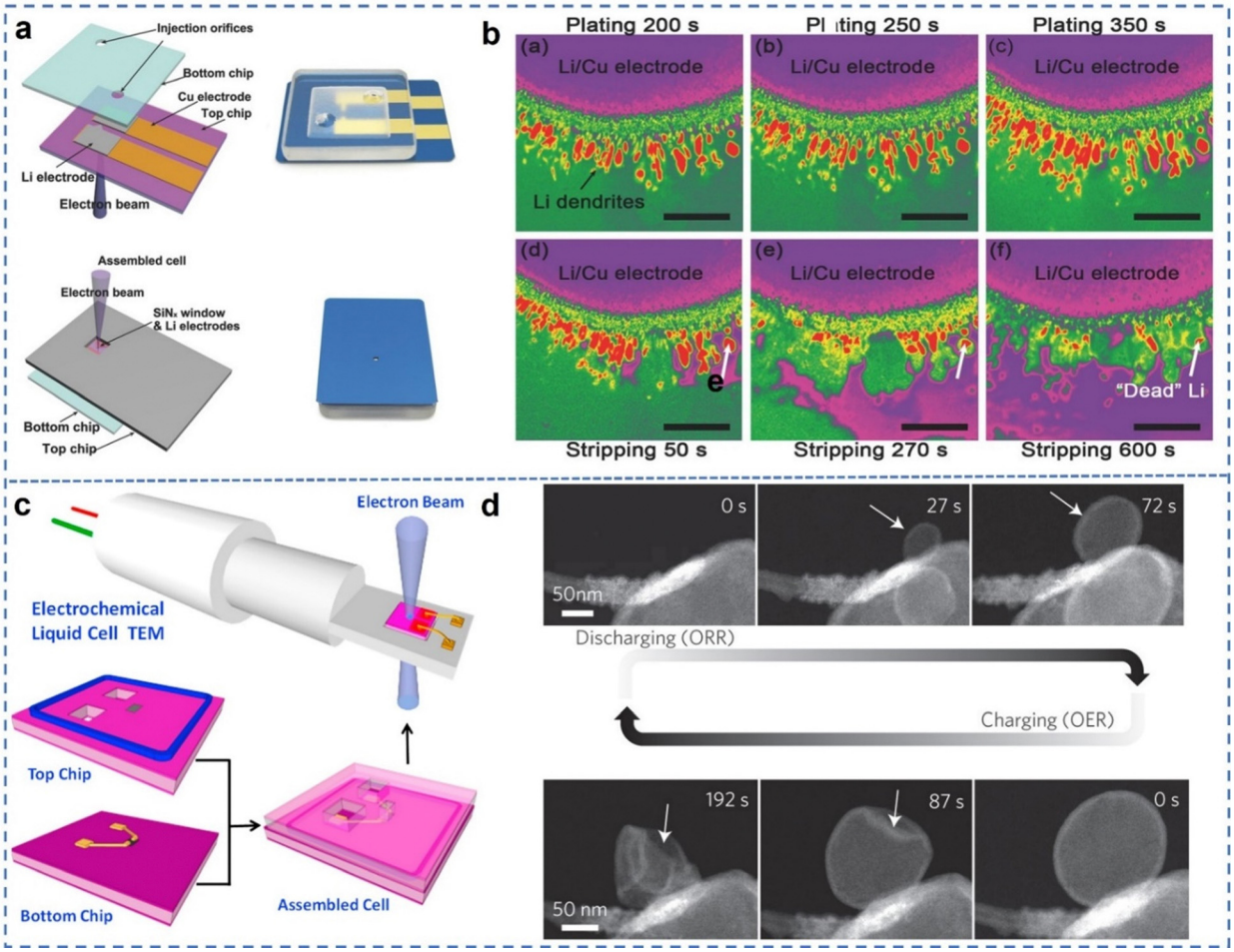

Fig. 27 (a) Schematic illustration and photographs of an *in situ* SEM liquid cell from bottom and top views. (b) SEM images during the lithium plating/stripping process. Reproduced with permission.[429] Copyright 2017 Wiley. (c) Schematic illustration of *in situ* TEM using an electrochemical liquid cell. Reproduced with permission.[430] Copyright 2015 Elsevier. (d) *In situ* TEM images of LOBs during the discharge–charge process. Reproduced with permission.[431] Copyright 2017 Nature publishing group.

To fully understand the mechanism of integrated multiscale regulation, several challenges related to characterization techniques need to be addressed. The first challenge is the temporal scale and operating environment. Although *ex situ* characterization studies provide value information at a relatively low cost, their drawbacks hinder their application: on the one hand, the detailed information about the evolution of electrode structures, electrode–electrolyte interphases, lithium dendrite growth, redox process, degradation mechanism are missing; on the other hand, due to the sensitivity of lithium-based batteries to air, moisture, or radiation, results from *ex situ* characterization may not precisely or fully imply what truly happens in these batteries. Thus, *in situ*/*operando* characterization techniques are imperative for an in-depth understanding of the functions of solvation chemistry in various rechargeable batteries (Fig. 27). Rong *et al.* developed an *in situ* electrochemical scanning electronic microscopy technique, which was adopted to investigate lithium dendrites, lithium dissolution and the formation of ''dead Li'' in the lithium plating/stripping process using 1 M LiTFSI–DOL–DME with the addition of $LiNO_3$ and Li_2S_8, as shown in Fig. 27a and b. Combined with DFT results, they concluded that the addition of $LiNO_3$ and Li_2S_8 can effectively suppress the formation of Li dendrites.[429] *In situ* TEM with a liquid cell (Fig. 27c) was also developed.[430] As shown in Fig. 27d, using environmental *in situ* TEM, Luo *et al.* found that the release of O_2 in LOBs produce a hollow discharging product with an outer Li_2O shell and an inner Li_2O_2 shell. Moreover, the release of O_2 is closely associated with Li^+ diffusion and electron-transport at spatial and temporal scales, which in turn control the morphology and products.[431]

In-situ/*operando* characterization techniques applied in energy storage and conversion can be divided into six categories according to their working mechanism: (i) the first category is based on X-rays, including *in situ*/*operando* X-ray diffraction (XRD), X-ray pair distribution function (XPDF), X-ray absorption (XAS), transmission X-ray microscopy (TXM), and coherent X-ray diffraction imaging (CXDI); (ii) the second is about electron related techniques, including *in situ*/*operando* SEM and TEM; (iii) the third is about neutron related

Table 8 Summary of the characteristics of typical *in situ*/*operando* characterization techniques

	Functions	Limitation	Accessibility/ cost	Combined techniques	Ref.
Optical microscope	• Observe dendrite in LMBs • Observe side reaction in LOBs or ALIBs	• Limited resolution	Easy/low	Raman, FTIR, DEMS	436, 437 and 440
XRD	• Co-intercalation of solvents in LIBs • Evolution of electrode	• Limited resolution • Only for crystalline component	Medium/low	DEMS, EQCM	436, 437 and 440
X-Ray absorption spectroscopy (XAS)	• Interfacial reaction during SEI formation • Evolution of electrode	• Destructive	Medium/ medium	—	436, 437 and 440
SEM	• Interfacial reaction during SEI formation • Lithium dendrites in LMBs	• Site-specific • Vacuum Environment • Destructive	Difficult/high	EQCM	432, 434 and 436
TEM	• Interfacial reaction during SEI formation • Redox of electrodes • Lithium dendrites in LMBs • Reaction mechanism in LSBs and LOBs	• Site-specific • Vacuum environment • Destructive	Difficult/high	—	442 and 448
Atomic force microscope (AFM)	• Interfacial reaction during SEI formation	• Site-specific • Environment Sensitivity • Destructive	Difficult/high	EQCM	432,434,436
Cryo-electron microscopy	• Interfacial reaction during SEI formation • Formation of lithium dendrites • Evolution of electrodes	• Site-specific	Difficult/high	—	16 and 441
Electrochemical quartz crystal microbalance (EQCM)	• Interfacial reaction during SEI formation • Lithium dendrites in LMBs • Desolvation of Li^+ • Co-intercalation of solvents in LIBs • Adsorption of polysulfides in LSBs • Redox mechanism	• Limited resolution	• Medium/ medium	AFM, SEM, Raman, XRD, FTIR	435, 449 and 450
Scanning electrochemical microscopy (SECM)	• Interfacial reaction during SEI formation	• Site-specific • Environment sensitivity Destructive	Medium/ medium	—	451 and 452
Differential electrochemical mass spectroscopy (DEMS)	• Interfacial reaction during SEI formation • Redox mechanisms in LOBs • Electrolyte decomposition • Degradation mechanism of electrodes	• Limited resolution	Medium/ medium	Raman, FTIR, EQCM	7 and 438
Raman or surface-enhanced Raman scattering	• Redox Mechanism in LSBs and LOBs • Interfacial reaction during SEI formation	• Limited resolution	Medium/ medium	DEMS, EQCM	445
Fourier transform infrared spectroscopy (FTIR)	• Redox Mechanism in LSBs and LOBs • Interfacial reaction during SEI formation	Limited resolution	Medium/ medium	DEMS, EQCM	433 and 453
NMR	• Solvation structure	• Limited resolution	Medium/ medium	EQCM	440

techniques, including neutron depth profiling (NDP), neutron imaging (NI), and neutron reflectometry (NR); (IV) the fourth is about optical techniques, including *in situ*/*operando* Raman, Fourier transform infrared spectroscopy(FTIR), and optical microscopy (OM); (V) the fifth is about scanning probe microscopy, including *in situ*/*operando* atomic force microscopy (AFM) and scanning electrochemical microscopy (SECM); and (VI) the sixth is about other characterization techniques, including *in situ*/*operando* electrochemical quartz crystal microbalance (EQCM), differential electrochemical mass spectroscopy (DEMS), and nuclear magnetic resonance (NMR). The working mechanism and applications of *in situ*/*operando* characterization techniques have been summarized in some excellent reviews.[429,430,432–447] In this review, we provide an overview of the advantages and disadvantages of typical *in situ*/*operando* characterization techniques applied in batteries (Table 8). It is worth noting that some *in situ* characterization techniques (*in situ* TEM or SEM) are adopted using simplified cells to simulate the practical batteries under operating conditions, which also cannot reflect the true reactions

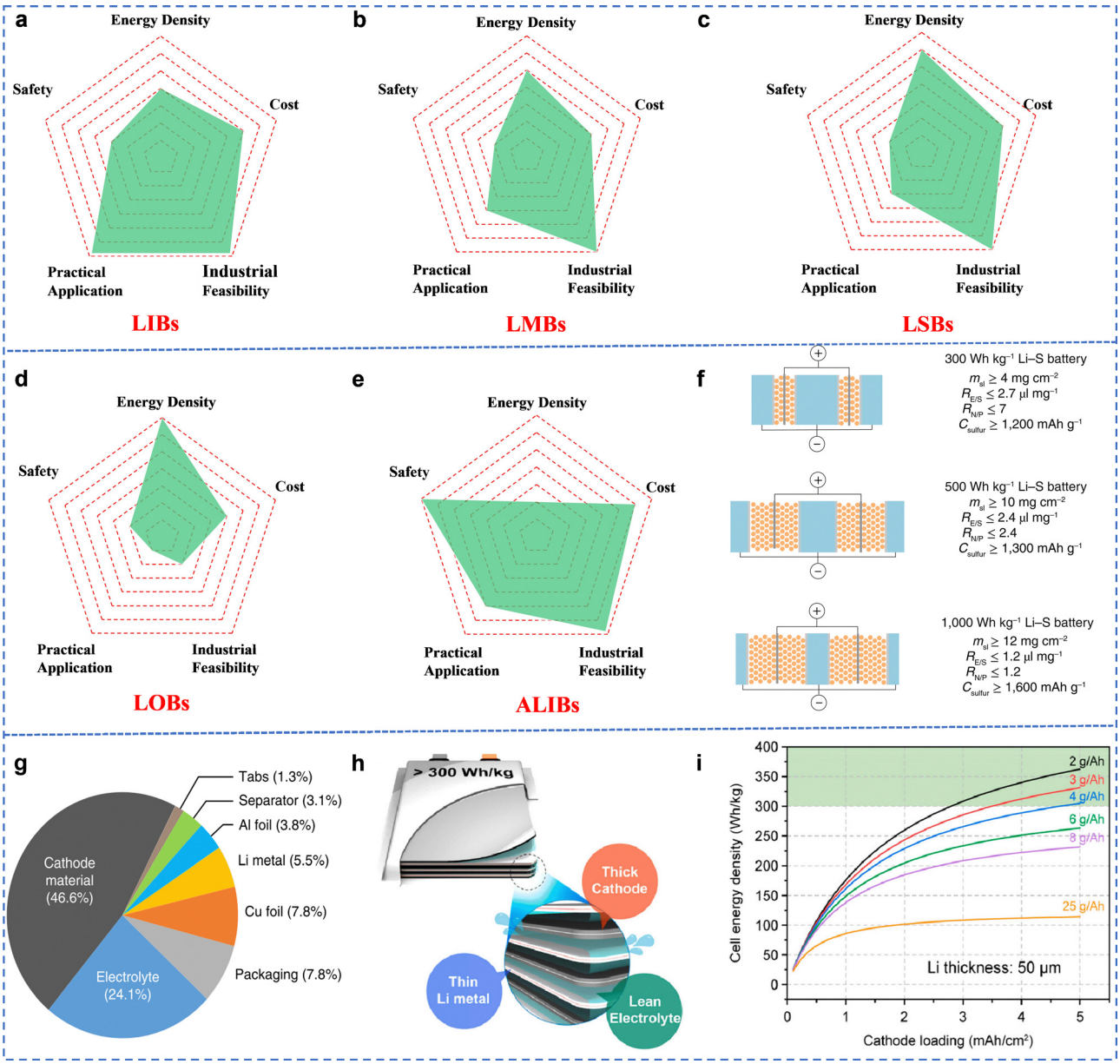

Fig. 28 Radia plots of (a) LIB, (b) LMBs, (c) LSBs, (d) LOBs, and (e) ALIBs in various aspects. (f) Recommended key parameters for LSBs with different energy densities. Reproduced with permission.[5] Copyright 2022 Nature Publishing Group. (g) Weight distributions of all cell components in LMBs with an energy density of 300 W h kg^{-1} at a level of 1 Ah (N/P ratio of 2.6 and an E/C ratio of 3 g A h^{-1}). Reproduced with permission.[454] Copyright 2019 Nature Publishing Group. (h) Schematic illustration of LMB pouch cells with high energy density. Reproduced with permission.[455] Copyright 2019 Elsevier. (i) Calculated energy density of LMBs with various cathode loading and electrolyte contents. Reproduced with permission.[456] Copyright 2020 American Chemical Society.

occurring during the cycling process. *In operando* characterization techniques, although expensive and hard to access, provide real-time and precise information.

The second challenge is the spatial scale of characterization techniques. A spatial scale ranging from nanometre to millimetre is highly demanded to comprehensively investigate the effects of solvation chemistry on various rechargeable batteries. Characterization techniques with a large spatial scale provide an overview of electrochemical processes or precise identification of failure locations, while those with a small spatial scale provide details about reaction mechanisms. For instance, in the context of Li dendrites in LMBs, the distribution of lithium dendrites and growth process can be easily characterized using OM or X-ray diffraction topography (XRT) with a large spatial scale, while TEM with a small spatial scale provides evidence about the SEI and evolution of single or several lithium dendrites at specific locations. Although great progress has been made in this field, such as *in situ* Raman, *in situ* FTIR, *etc.*, advanced techniques which can provide multiscale and direct details during the whole process form electrolyte design to

operation of batteries, are urgently needed to further understand the solvation chemistry in liquid electrolytes.[440] A combination of different characterization techniques with different spatial scales is an effective way to address the spatial multiscale issues in individual techniques (Table 8). For instance, EQCM can be widely combined with other *in situ* characterization techniques such as AFM, XRD, FTIR, Raman, DEMS, and EC-STM.[435]

8.2.3. Practical consideration for electrolytes in rechargeable batteries. Regarding electrolytes in various rechargeable batteries, one must not only pay attention to their effects on the improvement of electrochemical and the corresponding mechanisms, but also consider their practical issues such as the effect of weight content of electrolyte on the overall energy density of the whole cell, additional cost of novel electrolytes, the industrial feasibility, and their effects on the environment and safety.

The practical potential of novel electrolytes is highly associated with battery systems. The characteristics of different rechargeable batteries have been given in Fig. 28. Because of the excellent overall performance, LIBs have been widely used recently; the commercial application further reduces the cost of manufacturing and materials. For instance, the price of the conventional electrolyte (1.2 M $LiPF_6$ in EC:EMC) decreased from \$21.6 in 2010 to \$15.0 in 2018, making it (lithium salts and solvents) suitable for massive application.[457] Compared with $LiPF_6$ used in conventional electrolytes, the LiFSI or TFSI used in moderate solvating electrolytes in LSBs and LOBs, or HCEs or LHCEs in LMBs is very expensive because of the limited practical application.[458] For now, although the overall performance of LIBs is better than that of other four battery systems, they still have their own advantages: LMBs, LSBs and LOBs possess higher specific energy density, and ALIBs are intrinsically safe. Overcoming these challenging issues is crucial for meeting the overwhelming demands for rechargeable batteries with ultra-high energy density and intrinsic safety, which will definitely prompt the boom of LMBs, LSBs, LOBs, and ALIBs and further address the disadvantages faced by battery technologies nowadays (Fig. 28a–e).

Another important parameter in various rechargeable batteries related to electrolyte is the E/C ratio (the weight of electrolyte in batteries), which directly influences the energy density of the cells. As shown in Fig. 28f, the ratio of electrolyte to sulfur (volume : weight) in LSBs decreases from 2.7 μL mg^{-1} to 1.2 μL mg^{-1} in order to increase the energy density from 300 W h kg^{-1} to 1000 W h kg^{-1}.[5] In the LMBs with an energy density of 300 W h kg^{-1}, the weight ratio of electrolyte is about 24.1% at a E/C ratio as low as 3 g A h^{-1}, demonstrating the huge influence of electrolytes on the energy density of batteries (Fig. 28g and h). Decreasing the E/C ratio from 25 g A h^{-1} to 2 g A h^{-1} could triple the energy density of LMBs with the same composition of the anode and cathode, as shown in Fig. 28i.[454] In the CR2032 coin cells, usually more than 75 μL of electrolytes is added to maintain a long cycling life, the E/C ratio of which is more than 20 times than that typically used in pouch cells, leaving a huge gap between the coin cell and practical pouch cell.[455,458,459] It is also true in LOBs and ALIBs that a low E/C ratio leads to high energy density. However, the typical E/C ratios used in pouch cells of LIBs cannot meet the demands for long-term cycling life or satisfactory kinetics in LMBs, LSBs or LOBs. In LMBs, the constant reaction between highly reactive Li and electrolyte is inevitable, resulting in the depletion of the lean electrolyte during long-term cycling process. In LSBs or LOBs, more electrolytes are necessary to improve the specific capacity and ameliorate the kinetics induced by multiphase transformation. Therefore, the statement that ''under the condition of maintaining satisfying electrochemical performance, it is better to reduce the E/C ratio'' is more accurate.[460–462]

Moreover, the effects of electrolyte on the other components in rechargeable batteries should also be taken into consideration. One of the most notorious cases is the corrosion of the collector or stainless-steel shell induced by lithium salts such as LiTFSI or LiFSI at high cut-off voltages.[463–466] Other strategies such as protective coating of collectors or modification of electrolytes need to be adopted to address the corrosion issues, leading to additional cost. Besides, in fluorinated electrolytes, the environmental issues during the manufacture process and their effects on industrial equipment are also important factors for the practical application of electrolytes.[467]

Conflicts of interest

There are no conflicts to declare.

Acknowledgements

This work was supported by the Natural Science Foundation of Hunan Province (2023JJ40662), the National Defense Science and Technology Key Laboratory Supporting Project (WDZC20235250508), and the Seed Fund of National University of Defense Technology.

References

1 J. W. Choi and D. Aurbach, *Nat. Rev. Mater.*, 2016, **1**, 1.
2 B. Dunn, H. Kamath and J. M. Tarascon, *Science*, 2011, **334**, 928–935.
3 H. Pan, J. Chen, R. Cao, V. Murugesan, N. N. Rajput, K. S. Han, K. Persson, L. Estevez, M. H. Engelhard, J.-G. Zhang, K. T. Mueller, Y. Cui, Y. Shao and J. Liu, *Nat. Energy*, 2017, **2**, 813–820.
4 X. Ji, K. T. Lee and L. F. Nazar, *Nat. Mater.*, 2009, **8**, 500–506.
5 G. Zhou, H. Chen and Y. Cui, *Nat. Energy*, 2022, **7**, 312–319.
6 N. Wang, Y. Wang, Z. Bai, Z. Fang, X. Zhang, Z. Xu, Y. Ding, X. Xu, Y. Du, S. Dou and G. Yu, *Energy Environ. Sci.*, 2020, **13**, 562–570.
7 Z. Peng, S. A. Freunberger, Y. Chen and P. G. Bruce, *Science*, 2012, **337**, 563–566.
8 W. Sun, F. Wang, B. Zhang, M. Zhang, V. Kupers, X. Ji, C. Theile, P. Bieker, K. Xu, C. Wang and M. Winter, *Science*, 2021, **371**, 46–51.

9 D. H. S. Tan, Y. T. Chen, H. Yang, W. Bao, B. Sreenarayanan, J. M. Doux, W. Li, B. Lu, S. Y. Ham, B. Sayahpour, J. Scharf, E. A. Wu, G. Deysher, H. E. Han, H. J. Hah, H. Jeong, J. B. Lee, Z. Chen and Y. S. Meng, *Science*, 2021, **373**, 1494–1499.
10 L. Suo, O. Borodin, T. Gao, M. Olguin, J. Ho, X. Fan, C. Luo, C. Wang and K. Xu, *Science*, 2015, **350**, 938–943.
11 F. Bu, P. Xiao, J. Chen, M. F. Aly Aboud, I. Shakir and Y. Xu, *J. Mater. Chem. A*, 2018, **6**, 6414–6421.
12 P. Xiao, S. Li, C. Yu, Y. Wang and Y. Xu, *ACS Nano*, 2020, **14**, 10210–10218.
13 P. Wang, G. Zhang, X. Y. Wei, R. Liu, J. J. Gu and F. F. Cao, *J. Am. Chem. Soc.*, 2021, **143**, 3280–3283.
14 E. Peled, *J. Electrochem. Soc.*, 1979, **126**, 2047–2051.
15 Q. Zhao, S. Stalin and L. A. Archer, *Joule*, 2021, **5**, 1119–1142.
16 Y. Li, Y. Li, A. Pei, K. Yan, Y. Sun, C. L. Wu, L. M. Joubert, R. Chin, A. L. Koh, Y. Yu, J. Perrino, B. Butz, S. Chu and Y. Cui, *Science*, 2017, **358**, 506–510.
17 T. Abe, H. Fukuda, Y. Iriyama and Z. Ogumi, *J. Electrochem. Soc.*, 2004, **151**, A1120.
18 K. Xu, A. von Cresce and U. Lee, *Langmuir*, 2010, **26**, 11538–11543.
19 C. Yan, H. R. Li, X. Chen, X. Q. Zhang, X. B. Cheng, R. Xu, J. Q. Huang and Q. Zhang, *J. Am. Chem. Soc.*, 2019, **141**, 9422–9429.
20 X. B. Cheng, R. Zhang, C. Z. Zhao and Q. Zhang, *Chem. Rev.*, 2017, **117**, 10403–10473.
21 J. G. Zhang, W. Xu, J. Xiao, X. Cao and J. Liu, *Chem. Rev.*, 2020, **120**, 13312–13348.
22 Z. Wang, Z. Sun, J. Li, Y. Shi, C. Sun, B. An, H. M. Cheng and F. Li, *Chem. Soc. Rev.*, 2021, **50**, 3178–3210.
23 Y. Yamada, J. Wang, S. Ko, E. Watanabe and A. Yamada, *Nat. Energy*, 2019, **4**, 269–280.
24 Y. Yamada, K. Furukawa, K. Sodeyama, K. Kikuchi, M. Yaegashi, Y. Tateyama and A. Yamada, *J. Am. Chem. Soc.*, 2014, **136**, 5039–5046.
25 X. Chen and Q. Zhang, *Acc. Chem. Res.*, 2020, **53**, 1992–2002.
26 X. Shen, P. Li, X. Liu, S. Chen, X. Ai, H. Yang and Y. Cao, *Chem. Sci.*, 2021, **12**, 9037–9041.
27 L. Suo, Y. S. Hu, H. Li, M. Armand and L. Chen, *Nat. Commun.*, 2013, **4**, 1481.
28 X. Fan, X. Ji, L. Chen, J. Chen, T. Deng, F. Han, J. Yue, N. Piao, R. Wang, X. Zhou, X. Xiao, L. Chen and C. Wang, *Nat. Energy*, 2019, **4**, 882–890.
29 J. Hao, L. Yuan, C. Ye, D. Chao, K. Davey, Z. Guo and S. Qiao, *Angew. Chem., Int. Ed.*, 2021, **60**, 7366–7375.
30 G. Zhang, H. J. Peng, C. Z. Zhao, X. Chen, L. D. Zhao, P. Li, J. Q. Huang and Q. Zhang, *Angew. Chem., Int. Ed.*, 2018, **57**, 16732–16736.
31 N. V. Plechkova and K. R. Seddon, *Chem. Soc. Rev.*, 2008, **37**, 123–150.
32 K. Xu, *Chem. Rev.*, 2014, **114**, 11503–11618.
33 K. Xu, *Chem. Rev.*, 2004, **104**, 4303–4417.
34 C. Ye, H. Jin, J. Shan, Y. Jiao, H. Li, Q. Gu, K. Davey, H. Wang and S. Z. Qiao, *Nat. Commun.*, 2021, **12**, 7195.
35 S. Wei, S. Xu, A. Agrawral, S. Choudhury, Y. Lu, Z. Tu, L. Ma and L. A. Archer, *Nat. Commun.*, 2016, **7**, 11722.
36 C. Ye, J. Shan, D. Chao, P. Liang, Y. Jiao, J. Hao, Q. Gu, K. Davey, H. Wang and S. Z. Qiao, *J. Am. Chem. Soc.*, 2021, **143**, 16902–16907.
37 L. Xue, H. Gao, W. Zhou, S. Xin, K. Park, Y. Li and J. B. Goodenough, *Adv. Mater.*, 2016, **28**, 9608–9612.
38 H. Wang, D. Yu, X. Wang, Z. Niu, M. Chen, L. Cheng, W. Zhou and L. Guo, *Angew. Chem., Int. Ed.*, 2019, **58**, 16451–16455.
39 Y. Gu, W. W. Wang, Y. J. Li, Q. H. Wu, S. Tang, J. W. Yan, M. S. Zheng, D. Y. Wu, C. H. Fan, W. Q. Hu, Z. B. Chen, Y. Fang, Q. H. Zhang, Q. F. Dong and B. W. Mao, *Nat. Commun.*, 2018, **9**, 1339.
40 J. Xie, Z. Liang and Y. C. Lu, *Nat. Mater.*, 2020, **19**, 1006–1011.
41 R. Lin, C. Ke, J. Chen, S. Liu and J. Wang, *Joule*, 2022, **6**, 399–417.
42 H. Zhang, X. Liu, H. Li, I. Hasa and S. Passerini, *Angew. Chem., Int. Ed.*, 2021, **60**, 598–616.
43 C. Franco, *Eur. Chem. Bull.*, 2015, **4**, 92–97.
44 S. Chae, W.-J. Kwak, K. S. Han, S. Li, M. H. Engelhard, J. Hu, C. Wang, X. Li and J.-G. Zhang, *ACS Energy Lett.*, 2021, **6**, 387–394.
45 C.-C. Su, M. He, R. Amine, T. Rojas, L. Cheng, A. T. Ngo and K. Amine, *Energy Environ. Sci.*, 2019, **12**, 1249–1254.
46 C. C. Su, M. He, R. Amine, Z. Chen and K. Amine, *Angew. Chem., Int. Ed.*, 2018, **57**, 12033–12036.
47 C. C. Su, M. He, J. Shi, R. Amine, J. Zhang and K. Amine, *Angew. Chem., Int. Ed.*, 2020, **59**, 18229–18233.
48 J. Xu, J. Zhang, T. P. Pollard, Q. Li, S. Tan, S. Hou, H. Wan, F. Chen, H. He, E. Hu, K. Xu, X. Q. Yang, O. Borodin and C. Wang, *Nature*, 2023, **614**, 694–700.
49 Z. Wu, R. Li, S. Zhang, L. lv, T. Deng, H. Zhang, R. Zhang, J. Liu, S. Ding, L. Fan, L. Chen and X. Fan, *Chem*, 2022, **9**, 650–664.
50 H. Zhang, R. Li, L. Chen, Y. Fan, H. Zhang, R. Zhang, L. Zheng, J. Zhang, S. Ding, Y. Wu, B. Ma, S. Zhang, T. Deng, L. Chen, Y. Shen and X. Fan, *Angew. Chem., Int. Ed.*, 2023, **62**, e202218970.
51 B. D. Adams, J. M. Zheng, X. D. Ren, W. Xu and J. G. Zhang, *Adv. Energy Mater.*, 2018, **8**, 1702097.
52 M. D. Tikekar, S. Choudhury, Z. Tu and L. A. Archer, *Nat. Energy*, 2016, **1**, 1–7.
53 C. Zhu, C. Sun, R. Li, S. Weng, L. Fan, X. Wang, L. Chen, M. Noked and X. Fan, *ACS Energy Lett.*, 2022, **7**, 1338–1347.
54 Y. S. Cohen, Y. Cohen and D. Aurbach, *J. Phys. Chem. B*, 2000, **104**, 12282–12291.
55 E. Peled and S. Menkin, *J. Electrochem. Soc.*, 2017, **164**, A1703–A1719.
56 A. Gupta and A. Manthiram, *Adv. Energy Mater.*, 2020, **10**, 2001972.
57 J. Hou, M. Yang, D. Wang and J. Zhang, *Adv. Energy Mater.*, 2020, **10**, 1904152.
58 C. K. Huang, J. S. Sakamoto, J. Wolfenstine and S. Surampudi, *J. Electrochem. Soc.*, 2000, **147**, 2893.
59 Q. Li, D. Lu, J. Zheng, S. Jiao, L. Luo, C. M. Wang, K. Xu, J. G. Zhang and W. Xu, *ACS Appl. Mater. Interfaces*, 2017, **9**, 42761–42768.

60 N. Zhang, T. Deng, S. Zhang, C. Wang, L. Chen, C. Wang and X. Fan, *Adv. Mater.*, 2021, **34**, e2107899.
61 X. Fan and C. Wang, *Chem. Soc. Rev.*, 2021, **50**, 10486–10566.
62 L. Dong, Y. Liu, D. Chen, Y. Han, Y. Ji, J. Liu, B. Yuan, Y. Dong, Q. Li, S. Zhou, S. Zhong, Y. Liang, M. Yang, C. Yang and W. He, *Energy Storage Mater.*, 2022, **44**, 527–536.
63 S. Mao, Q. Wu, F. Ma, Y. Zhao, T. Wu and Y. Lu, *Chem. Commun.*, 2021, **57**, 840–858.
64 F. Wu, S. Fang, M. Kuenzel, A. Mullaliu, J.-K. Kim, X. Gao, T. Diemant, G.-T. Kim and S. Passerini, *Joule*, 2021, **5**, 2177–2194.
65 J. Yang, X. Liu, Y. Wang, X. Zhou, L. Weng, Y. Liu, Y. Ren, C. Zhao, M. Dahbi, J. Alami, D. A. Ei-Hady, G. L. Xu, K. Amine and M. Shao, *Adv. Energy Mater.*, 2021, **11**, 2101956.
66 M. J. Lee, J. Han, K. Lee, Y. J. Lee, B. G. Kim, K. N. Jung, B. J. Kim and S. W. Lee, *Nature*, 2022, **601**, 217–222.
67 K. Yoshida, M. Nakamura, Y. Kazue, N. Tachikawa, S. Tsuzuki, S. Seki, K. Dokko and M. Watanabe, *J. Am. Chem. Soc.*, 2011, **133**, 13121–13129.
68 J. Tan, J. Matz, P. Dong, J. Shen and M. Ye, *Adv. Energy Mater.*, 2021, **11**, 2100046.
69 Y. Li and Y. Qi, *Energy Environ. Sci.*, 2019, **12**, 1286–1295.
70 Z. Li, Y. Chen, X. Yun, P. Gao, C. Zheng and P. Xiao, *Adv. Funct. Mater.*, 2023, DOI: **10.1002/adfm.202300502**.
71 X. Fan, X. Ji, F. Han, J. Yue, J. Chen, L. Chen, T. Deng, J. Jiang and C. Wang, *Sci. Adv.*, 2018, **4**, eaau9245.
72 G. M. A. Girard, M. Hilder, D. Nucciarone, K. Whitbread, S. Zavorine, M. Moser, M. Forsyth, D. R. MacFarlane and P. C. Howlett, *J. Phys. Chem. C*, 2017, **121**, 21087–21095.
73 W. R. McKinnon and J. R. Dahn, *J. Electrochem. Soc.*, 1985, **132**, 364–366.
74 C. A. Angell, C. Liu and E. Sanchez, *Nature*, 1993, **362**, 137–139.
75 S. Wang, J. Qu, F. Wu, K. Yan and C. Zhang, *ACS Appl. Mater. Interfaces*, 2020, **12**, 8366–8375.
76 F. Qiu, X. Li, H. Deng, D. Wang, X. Mu, P. He and H. Zhou, *Adv. Energy Mater.*, 2018, **9**, 1803372.
77 S.-K. Jeong, H.-Y. Seo, D.-H. Kim, H.-K. Han, J.-G. Kim, Y. B. Lee, Y. Iriyama, T. Abe and Z. Ogumi, *Electrochem. Commun.*, 2008, **10**, 635–638.
78 J. Qian, W. A. Henderson, W. Xu, P. Bhattacharya, M. Engelhard, O. Borodin and J. G. Zhang, *Nat. Commun.*, 2015, **6**, 6362.
79 L. Xiao, Z. Zeng, X. Liu, Y. Fang, X. Jiang, Y. Shao, L. Zhuang, X. Ai, H. Yang, Y. Cao and J. Liu, *ACS Energy Lett.*, 2019, **4**, 483–488.
80 Z. Zeng, V. Murugesan, K. S. Han, X. Jiang, Y. Cao, L. Xiao, X. Ai, H. Yang, J.-G. Zhang, M. L. Sushko and J. Liu, *Nat. Energy*, 2018, **3**, 674–681.
81 Y. Maeyoshi, D. Ding, M. Kubota, H. Ueda, K. Abe, K. Kanamura and H. Abe, *ACS Appl. Mater. Interfaces*, 2019, **11**, 25833–25843.
82 X. Fan, L. Chen, X. Ji, T. Deng, S. Hou, J. Chen, J. Zheng, F. Wang, J. Jiang, K. Xu and C. Wang, *Chem*, 2018, **4**, 174–185.
83 T. Tamura, T. Hachida, K. Yoshida, N. Tachikawa, K. Dokko and M. Watanabe, *J. Power Sources*, 2010, **195**, 6095–6100.
84 L. Suo, W. Xue, M. Gobet, S. G. Greenbaum, C. Wang, Y. Chen, W. Yang, Y. Li and J. Li, *Proc. Natl. Acad. Sci. U. S. A.*, 2018, **115**, 1156–1161.
85 J. Wang, Y. Yamada, K. Sodeyama, C. H. Chiang, Y. Tateyama and A. Yamada, *Nat. Commun.*, 2016, **7**, 12032.
86 J. Alvarado, M. A. Schroeder, T. P. Pollard, X. Wang, J. Z. Lee, M. Zhang, T. Wynn, M. Ding, O. Borodin, Y. S. Meng and K. Xu, *Energy Environ. Sci.*, 2019, **12**, 780–794.
87 X. Ren, L. Zou, S. Jiao, D. Mei, M. H. Engelhard, Q. Li, H. Lee, C. Niu, B. D. Adams, C. Wang, J. Liu, J.-G. Zhang and W. Xu, *ACS Energy Lett.*, 2019, **4**, 896–902.
88 J. Fu, X. Ji, J. Chen, L. Chen, X. Fan, D. Mu and C. Wang, *Angew. Chem., Int. Ed.*, 2020, **59**, 22194–22201.
89 X. Cao, H. Jia, W. Xu and J.-G. Zhang, *J. Electrochem. Soc.*, 2021, **168**, 010522.
90 X. Dong, Y. Lin, P. Li, Y. Ma, J. Huang, D. Bin, Y. Wang, Y. Qi and Y. Xia, *Angew. Chem., Int. Ed.*, 2019, **58**, 5623–5627.
91 X. Ren, P. Gao, L. Zou, S. Jiao, X. Cao, X. Zhang, H. Jia, M. H. Engelhard, B. E. Matthews, H. Wu, H. Lee, C. Niu, C. Wang, B. W. Arey, J. Xiao, J. Liu, J. G. Zhang and W. Xu, *Proc. Natl. Acad. Sci. U. S. A.*, 2020, **117**, 28603–28613.
92 K. Dokko, N. Tachikawa, K. Yamauchi, M. Tsuchiya, A. Yamazaki, E. Takashima, J.-W. Park, K. Ueno, S. Seki, N. Serizawa and M. Watanabe, *J. Electrochem. Soc.*, 2013, **160**, A1304–A1310.
93 H. Moon, T. Mandai, R. Tatara, K. Ueno, A. Yamazaki, K. Yoshida, S. Seki, K. Dokko and M. Watanabe, *J. Phys. Chem. C*, 2015, **119**, 3957–3970.
94 K. Ueno, J. Murai, K. Ikeda, S. Tsuzuki, M. Tsuchiya, R. Tatara, T. Mandai, Y. Umebayashi, K. Dokko and M. Watanabe, *J. Phys. Chem. C*, 2015, **120**, 15792–15802.
95 S. Chen, J. Zheng, D. Mei, K. S. Han, M. H. Engelhard, W. Zhao, W. Xu, J. Liu and J. G. Zhang, *Adv. Mater.*, 2018, **30**, e1706102.
96 S. Chen, J. Zheng, L. Yu, X. Ren, M. H. Engelhard, C. Niu, H. Lee, W. Xu, J. Xiao, J. Liu and J.-G. Zhang, *Joule*, 2018, **2**, 1548–1558.
97 X. Ren, S. Chen, H. Lee, D. Mei, M. H. Engelhard, S. D. Burton, W. Zhao, J. Zheng, Q. Li, M. S. Ding, M. Schroeder, J. Alvarado, K. Xu, Y. S. Meng, J. Liu, J.-G. Zhang and W. Xu, *Chem*, 2018, **4**, 1877–1892.
98 L. Yu, S. Chen, H. Lee, L. Zhang, M. H. Engelhard, Q. Li, S. Jiao, J. Liu, W. Xu and J.-G. Zhang, *ACS Energy Lett.*, 2018, **3**, 2059–2067.
99 X. Cao, X. Ren, L. Zou, M. H. Engelhard, W. Huang, H. Wang, B. E. Matthews, H. Lee, C. Niu, B. W. Arey, Y. Cui, C. Wang, J. Xiao, J. Liu, W. Xu and J.-G. Zhang, *Nat. Energy*, 2019, **4**, 796–805.
100 X. Cao, L. Zou, B. E. Matthews, L. Zhang, X. He, X. Ren, M. H. Engelhard, S. D. Burton, P. Z. El-Khoury, H.-S. Lim, C. Niu, H. Lee, C. Wang, B. W. Arey, C. Wang, J. Xiao, J. Liu,

W. Xu and J.-G. Zhang, *Energy Storage Mater.*, 2021, **34**, 76–84.
101 X. Ren, L. Zou, X. Cao, M. H. Engelhard, W. Liu, S. D. Burton, H. Lee, C. Niu, B. E. Matthews, Z. Zhu, C. Wang, B. W. Arey, J. Xiao, J. Liu, J.-G. Zhang and W. Xu, *Joule*, 2019, **3**, 1662–1676.
102 X. Fan, L. Chen, O. Borodin, X. Ji, J. Chen, S. Hou, T. Deng, J. Zheng, C. Yang, S. C. Liou, K. Amine, K. Xu and C. Wang, *Nat. Nanotechnol.*, 2018, **13**, 715–722.
103 X. Cao, P. Gao, X. Ren, L. Zou, M. H. Engelhard, B. E. Matthews, J. Hu, C. Niu, D. Liu, B. W. Arey, C. Wang, J. Xiao, J. Liu, W. Xu and J. G. Zhang, *Proc. Natl. Acad. Sci. U. S. A.*, 2021, **118**, e2020357118.
104 T. Doi, Y. Shimizu, M. Hashinokuchi and M. Inaba, *J. Electrochem. Soc.*, 2017, **164**, A6412–A6416.
105 Z. Jiang, Z. Zeng, X. Liang, L. Yang, W. Hu, C. Zhang, Z. Han, J. Feng and J. Xie, *Adv. Funct. Mater.*, 2020, **31**, 2005991.
106 S. Li, Q. Liu, W. Zhang, L. Fan, X. Wang, X. Wang, Z. Shen, X. Zang, Y. Zhao, F. Ma and Y. Lu, *Adv. Sci.*, 2021, **8**, 2003240.
107 Z. Wang, F. Zhang, Y. Sun, L. Zheng, Y. Shen, D. Fu, W. Li, A. Pan, L. Wang, J. Xu, J. Hu and X. Wu, *Adv. Energy Mater.*, 2021, **11**, 2003752.
108 T. Li, X. Q. Zhang, N. Yao, Y. X. Yao, L. P. Hou, X. Chen, M. Y. Zhou, J. Q. Huang and Q. Zhang, *Angew. Chem., Int. Ed.*, 2021, **60**, 22683–22687.
109 J. Holoubek, K. Kim, Y. Yin, Z. Wu, H. Liu, M. Li, A. Chen, H. Gao, G. Cai, T. A. Pascal, P. Liu and Z. Chen, *Energy Environ. Sci.*, 2022, **15**, 1647–1658.
110 Z. Chang, Y. Qiao, H. Yang, H. Deng, X. Zhu, P. He and H. Zhou, *Energy Environ. Sci.*, 2020, **13**, 4122–4131.
111 J. Wang, J. Yang, Q. Xiao, J. Zhang, T. Li, L. Jia, Z. Wang, S. Cheng, L. Li, M. Liu, H. Liu, H. Lin and Y. Zhang, *Adv. Funct. Mater.*, 2020, **31**, 2007434.
112 Z. Chang, Y. Qiao, H. Deng, H. Yang, P. He and H. Zhou, *Joule*, 2020, **4**, 1776–1789.
113 Y. Jin, P. M. L. Le, P. Gao, Y. Xu, B. Xiao, M. H. Engelhard, X. Cao, T. D. Vo, J. Hu, L. Zhong, B. E. Matthews, R. Yi, C. Wang, X. Li, J. Liu and J.-G. Zhang, *Nat. Energy*, 2022, **7**, 718–725.
114 Y. Yin, Y. Yang, D. Cheng, M. Mayer, J. Holoubek, W. Li, G. Raghavendran, A. Liu, B. Lu, D. M. Davies, Z. Chen, O. Borodin and Y. S. Meng, *Nat. Energy*, 2022, **7**, 548–559.
115 C. S. Rustomji, Y. Yang, T. K. Kim, J. Mac, Y. J. Kim, E. Caldwell, H. Chung and Y. S. Meng, *Science*, 2017, **356**, eaal4263.
116 Y. Yang, D. M. Davies, Y. Yin, O. Borodin, J. Z. Lee, C. Fang, M. Olguin, Y. Zhang, E. S. Sablina, X. Wang, C. S. Rustomji and Y. S. Meng, *Joule*, 2019, **3**, 1986–2000.
117 Y. Yang, Y. Yin, D. M. Davies, M. Zhang, M. Mayer, Y. Zhang, E. S. Sablina, S. Wang, J. Z. Lee, O. Borodin, C. S. Rustomji and Y. S. Meng, *Energy Environ. Sci.*, 2020, **13**, 2209–2219.
118 W. Xue, Z. Shi, M. Huang, S. Feng, C. Wang, F. Wang, J. Lopez, B. Qiao, G. Xu, W. Zhang, Y. Dong, R. Gao, Y. Shao-Horn, J. A. Johnson and J. Li, *Energy Environ. Sci.*, 2020, **13**, 212–220.
119 W. Xue, M. Huang, Y. Li, Y. G. Zhu, R. Gao, X. Xiao, W. Zhang, S. Li, G. Xu, Y. Yu, P. Li, J. Lopez, D. Yu, Y. Dong, W. Fan, Z. Shi, R. Xiong, C.-J. Sun, I. Hwang, W.-K. Lee, Y. Shao-Horn, J. A. Johnson and J. Li, *Nat. Energy*, 2021, **6**, 495–505.
120 W. Xue, R. Gao, Z. Shi, X. Xiao, W. Zhang, Y. Zhang, Y. G. Zhu, I. Waluyo, Y. Li, M. R. Hill, Z. Zhu, S. Li, O. Kuznetsov, Y. Zhang, W.-K. Lee, A. Hunt, A. Harutyunyan, Y. Shao-Horn, J. A. Johnson and J. Li, *Energy Environ. Sci.*, 2021, **14**, 6030–6040.
121 H. Wang, Z. Yu, X. Kong, W. Huang, Z. Zhang, D. G. Mackanic, X. Huang, J. Qin, Z. Bao and Y. Cui, *Adv. Mater.*, 2021, **33**, e2008619.
122 Y. Chen, Z. Yu, P. Rudnicki, H. Gong, Z. Huang, S. C. Kim, J. C. Lai, X. Kong, J. Qin, Y. Cui and Z. Bao, *J. Am. Chem. Soc.*, 2021, **143**, 18703–18713.
123 T. Ma, Y. Ni, Q. Wang, W. Zhang, S. Jin, S. Zheng, X. Yang, Y. Hou, Z. Tao and J. Chen, *Angew. Chem., Int. Ed.*, 2022, **61**, e202207927.
124 J. Holoubek, H. Liu, Z. Wu, Y. Yin, X. Xing, G. Cai, S. Yu, H. Zhou, T. A. Pascal, Z. Chen and P. Liu, *Nat. Energy*, 2021, **6**, 303–313.
125 Z. Yu, H. Wang, X. Kong, W. Huang, Y. Tsao, D. G. Mackanic, K. Wang, X. Wang, W. Huang, S. Choudhury, Y. Zheng, C. V. Amanchukwu, S. T. Hung, Y. Ma, E. G. Lomeli, J. Qin, Y. Cui and Z. Bao, *Nat. Energy*, 2020, **5**, 526–533.
126 Z. Yu, P. E. Rudnicki, Z. Zhang, Z. Huang, H. Celik, S. T. Oyakhire, Y. Chen, X. Kong, S. C. Kim, X. Xiao, H. Wang, Y. Zheng, G. A. Kamat, M. S. Kim, S. F. Bent, J. Qin, Y. Cui and Z. Bao, *Nat. Energy*, 2022, **7**, 94–106.
127 T. Zhou, Y. Zhao, M. El Kazzi, J. W. Choi and A. Coskun, *Angew. Chem., Int. Ed.*, 2022, **61**, e202115884.
128 Y. Zhao, T. Zhou, T. Ashirov, M. E. Kazzi, C. Cancellieri, L. P. H. Jeurgens, J. W. Choi and A. Coskun, *Nat. Commun.*, 2022, **13**, 2575.
129 L. Tan, S. Chen, Y. Chen, J. Fan, D. Ruan, Q. Nian, L. Chen, S. Jiao and X. Ren, *Angew. Chem., Int. Ed.*, 2022, **61**, e202203693.
130 P. Xiao, Y. Zhao, Z. Piao, B. Li, G. Zhou and H.-M. Cheng, *Energy Environ. Sci.*, 2022, **15**, 2435–2444.
131 Z. Wang, Z. Sun, Y. Shi, F. Qi, X. Gao, H. Yang, H. M. Cheng and F. Li, *Adv. Energy Mater.*, 2021, **11**, 2100935.
132 J. Holoubek, M. Yu, S. Yu, M. Li, Z. Wu, D. Xia, P. Bhaladhare, M. S. Gonzalez, T. A. Pascal, P. Liu and Z. Chen, *ACS Energy Lett.*, 2020, **5**, 1438–1447.
133 Q. Zheng, Y. Yamada, R. Shang, S. Ko, Y.-Y. Lee, K. Kim, E. Nakamura and A. Yamada, *Nat. Energy*, 2020, **5**, 291–298.
134 S. H. Lee, J. Y. Hwang, J. Ming, Z. Cao, H. A. Nguyen, H. G. Jung, J. Kim and Y. K. Sun, *Adv. Energy Mater.*, 2020, **10**, 2000567.
135 W. Deng, W. Dai, X. Zhou, Q. Han, W. Fang, N. Dong, B. He and Z. Liu, *ACS Energy Lett.*, 2020, **6**, 115–123.

136 S. Jurng, Z. L. Brown, J. Kim and B. L. Lucht, *Energy Environ. Sci.*, 2018, **11**, 2600–2608.
137 B. Roy, P. Cherepanov, C. Nguyen, C. Forsyth, U. Pal, T. C. Mendes, P. Howlett, M. Forsyth, D. MacFarlane and M. Kar, *Adv. Energy Mater.*, 2021, **11**, 2101422.
138 H. Zheng, H. Xiang, F. Jiang, Y. Liu, Y. Sun, X. Liang, Y. Feng and Y. Yu, *Adv. Energy Mater.*, 2020, **10**, 2001440.
139 X.-Q. Zhang, X. Chen, L.-P. Hou, B.-Q. Li, X.-B. Cheng, J.-Q. Huang and Q. Zhang, *ACS Energy Lett.*, 2019, **4**, 411–416.
140 Z. Wang, F. Qi, L. Yin, Y. Shi, C. Sun, B. An, H. M. Cheng and F. Li, *Adv. Energy Mater.*, 2020, **10**, 1903843.
141 Z. Jiang, J. Mo, C. Li, H. W. Li, Q. Zhang, Z. Zeng, J. Xie and Y. Li, *Energy Environ. Mater.*, 2022, DOI: **10.1002/eem2.12440**.
142 T. Zheng, J. Xiong, B. Zhu, X. Shi, Y.-J. Cheng, H. Zhao and Y. Xia, *J. Mater. Chem. A*, 2021, **9**, 9307–9318.
143 P. Xiao, R. Luo, Z. Piao, C. Li, J. Wang, K. Yu, G. Zhou and H.-M. Cheng, *ACS Energy Lett.*, 2021, **6**, 3170–3179.
144 N. Piao, S. F. Liu, B. Zhang, X. Ji, X. L. Fan, L. Wang, P. F. Wang, T. Jin, S. C. Liou, H. C. Yang, J. J. Jiang, K. Xu, M. A. Schroeder, X. M. He and C. S. Wang, *ACS Energy Lett.*, 2021, **6**, 1839–1848.
145 S. Liu, X. Ji, N. Piao, J. Chen, N. Eidson, J. Xu, P. Wang, L. Chen, J. Zhang, T. Deng, S. Hou, T. Jin, H. Wan, J. Li, J. Tu and C. Wang, *Angew. Chem., Int. Ed.*, 2020, **60**, 3661–3671.
146 W. Zhang, Q. Wu, J. Huang, L. Fan, Z. Shen, Y. He, Q. Feng, G. Zhu and Y. Lu, *Adv. Mater.*, 2020, **32**, e2001740.
147 W. Zhang, Z. Shen, S. Li, L. Fan, X. Wang, F. Chen, X. Zang, T. Wu, F. Ma and Y. Lu, *Adv. Funct. Mater.*, 2020, **30**, 2003800.
148 R. Xu, X. Shen, X. X. Ma, C. Yan, X. Q. Zhang, X. Chen, J. F. Ding and J. Q. Huang, *Angew. Chem., Int. Ed.*, 2020, **60**, 4215–4220.
149 C.-Z. Zhao, X.-B. Cheng, R. Zhang, H.-J. Peng, J.-Q. Huang, R. Ran, Z.-H. Huang, F. Wei and Q. Zhang, *Energy Storage Mater.*, 2016, **3**, 77–84.
150 Q. Zhao, N. W. Utomo, A. L. Kocen, S. Jin, Y. Deng, V. X. Zhu, S. Moganty, G. W. Coates and L. A. Archer, *Angew. Chem., Int. Ed.*, 2021, **61**, e202116214.
151 C. Yan, X. B. Cheng, Y. X. Yao, X. Shen, B. Q. Li, W. J. Li, R. Zhang, J. Q. Huang, H. Li and Q. Zhang, *Adv. Mater.*, 2018, **30**, e1804461.
152 Y. Jie, X. Liu, Z. Lei, S. Wang, Y. Chen, F. Huang, R. Cao, G. Zhang and S. Jiao, *Angew. Chem., Int. Ed.*, 2020, **59**, 3505–3510.
153 D. Xiao, Q. Li, D. Luo, G. Li, H. Liu, L. Shui, S. Gourley, G. Zhou, X. Wang and Z. Chen, *Small*, 2020, **16**, e2004688.
154 H. Yang, X. Chen, N. Yao, N. Piao, Z. Wang, K. He, H.-M. Cheng and F. Li, *ACS Energy Lett.*, 2021, **6**, 1413–1421.
155 S. Gu, S. W. Zhang, J. Han, Y. Deng, C. Luo, G. Zhou, Y. He, G. Wei, F. Kang, W. Lv and Q. H. Yang, *Adv. Funct. Mater.*, 2021, **31**, 2102128.
156 L. P. Hou, X. Q. Zhang, B. Q. Li and Q. Zhang, *Angew. Chem., Int. Ed.*, 2020, **59**, 15109–15113.
157 Z. Piao, P. Xiao, R. Luo, J. Ma, R. Gao, C. Li, J. Tan, K. Yu, G. Zhou and H. M. Cheng, *Adv. Mater.*, 2022, **34**, e2108400.
158 S. Li, W. Zhang, Q. Wu, L. Fan, X. Wang, X. Wang, Z. Shen, Y. He and Y. Lu, *Angew. Chem., Int. Ed.*, 2020, **59**, 14935–14941.
159 H. Sun, G. Zhu, Y. Zhu, M. C. Lin, H. Chen, Y. Y. Li, W. H. Hung, B. Zhou, X. Wang, Y. Bai, M. Gu, C. L. Huang, H. C. Tai, X. Xu, M. Angell, J. J. Shyue and H. Dai, *Adv. Mater.*, 2020, **32**, e2001741.
160 S. Jiao, X. Ren, R. Cao, M. H. Engelhard, Y. Liu, D. Hu, D. Mei, J. Zheng, W. Zhao, Q. Li, N. Liu, B. D. Adams, C. Ma, J. Liu, J.-G. Zhang and W. Xu, *Nat. Energy*, 2018, **3**, 739–746.
161 R. Tatara, Y. Yu, P. Karayaylali, A. K. Chan, Y. Zhang, R. Jung, F. Maglia, L. Giordano and Y. Shao-Horn, *ACS Appl. Mater. Interfaces*, 2019, **11**, 34973–34988.
162 N. Piao, X. Ji, H. Xu, X. Fan, L. Chen, S. Liu, M. N. Garaga, S. G. Greenbaum, L. Wang, C. Wang and X. He, *Adv. Energy Mater.*, 2020, **10**, 1903568.
163 X. Zheng, L. Huang, W. Luo, H. Wang, Y. Dai, X. Liu, Z. Wang, H. Zheng and Y. Huang, *ACS Energy Lett.*, 2021, **6**, 2054–2063.
164 X. Ren, X. Zhang, Z. Shadike, L. Zou, H. Jia, X. Cao, M. H. Engelhard, B. E. Matthews, C. Wang, B. W. Arey, X. Q. Yang, J. Liu, J. G. Zhang and W. Xu, *Adv. Mater.*, 2020, **32**, e2004898.
165 Z. Jiang, Z. Zeng, H. Zhang, L. Yang, W. Hu, X. Liang, J. Feng, C. Yu, S. Cheng and J. Xie, *iScience*, 2022, **25**, 103490.
166 Q. K. Zhang, X. Q. Zhang, L. P. Hou, S. Y. Sun, Y. X. Zhan, J. L. Liang, F. S. Zhang, X. N. Feng, B. Q. Li and J. Q. Huang, *Adv. Energy Mater.*, 2022, **12**, 2200139.
167 L. Shen, H. B. Wu, F. Liu, J. Shen, R. Mo, G. Chen, G. Tan, J. Chen, X. Kong, X. Lu, Y. Peng, J. Zhu, G. Wang and Y. Lu, *Adv. Funct. Mater.*, 2020, **30**, 2003055.
168 T. Doi, R. J. Taccori, R. Fujii, T. Nagashima, T. Endo, Y. Kimura and M. Inaba, *ChemSusChem*, 2021, **14**, 2445–2451.
169 X. Zhang, L. Zou, Y. Xu, X. Cao, M. H. Engelhard, B. E. Matthews, L. Zhong, H. Wu, H. Jia, X. Ren, P. Gao, Z. Chen, Y. Qin, C. Kompella, B. W. Arey, J. Li, D. Wang, C. Wang, J. G. Zhang and W. Xu, *Adv. Energy Mater.*, 2020, **10**, 2000368.
170 J. Wang, Q. Zheng, M. Fang, S. Ko, Y. Yamada and A. Yamada, *Adv. Sci.*, 2021, **8**, e2101646.
171 Z. Yu, J. Zhang, C. Wang, R. Hu, X. Du, B. Tang, H. Qu, H. Wu, X. Liu, X. Zhou, X. Yang and G. Cui, *J. Energy Chem.*, 2020, **51**, 154–160.
172 T. Chen, Z. Jin, Y. Liu, X. Zhang, H. Wu, M. Li, W. Feng, Q. Zhang and C. Wang, *Angew. Chem., Int. Ed.*, 2022, **61**, e202207645.
173 G. Cai, J. Holoubek, M. Li, H. Gao, Y. Yin, S. Yu, H. Liu, T. A. Pascal, P. Liu and Z. Chen, *Proc. Natl. Acad. Sci. U. S. A.*, 2022, **119**, e2200392119.
174 C. Niu, D. Liu, J. A. Lochala, C. S. Anderson, X. Cao, M. E. Gross, W. Xu, J.-G. Zhang, M. S. Whittingham, J. Xiao and J. Liu, *Nat. Energy*, 2021, **6**, 723–732.
175 A. N. Dey and B. P. Sullivan, *J. Electrochem. Soc.*, 1970, **117**, 222.

176 R. Fong, U. von Sacken and J. R. Dahn, *J. Electrochem. Soc.*, 1990, **137**, 2009–2013.
177 T. Abe, N. Kawabata, Y. Mizutani, M. Inaba and Z. Ogumi, *J. Electrochem. Soc.*, 2003, **150**, A257.
178 J. Wang, Y. Yamada, K. Sodeyama, E. Watanabe, K. Takada, Y. Tateyama and A. Yamada, *Nat. Energy*, 2017, **3**, 22–29.
179 X. Li, X. Ou and Y. Tang, *Adv. Energy Mater.*, 2020, **10**, 2002567.
180 S.-K. Jeong, M. Inaba, Y. Iriyama, T. Abe and Z. Ogumi, *Electrochem. Solid-State Lett.*, 2003, **6**, A13.
181 Y. Yamada, Y. Takazawa, K. Miyazaki and T. Abe, *J. Phys. Chem. C*, 2010, **114**, 11680–11685.
182 Y. Yamada, K. Usui, C. H. Chiang, K. Kikuchi, K. Furukawa and A. Yamada, *ACS Appl. Mater. Interfaces*, 2014, **6**, 10892–10899.
183 J. Ming, Z. Cao, W. Wahyudi, M. Li, P. Kumar, Y. Wu, J.-Y. Hwang, M. N. Hedhili, L. Cavallo, Y.-K. Sun and L.-J. Li, *ACS Energy Lett.*, 2018, **3**, 335–340.
184 J. Alvarado, M. A. Schroeder, M. Zhang, O. Borodin, E. Gobrogge, M. Olguin, M. S. Ding, M. Gobet, S. Greenbaum, Y. S. Meng and K. Xu, *Mater. Today*, 2018, **21**, 341–353.
185 L. L. Jiang, C. Yan, Y. X. Yao, W. Cai, J. Q. Huang and Q. Zhang, *Angew. Chem., Int. Ed.*, 2021, **60**, 3402–3406.
186 Y. Yamada, M. Yaegashi, T. Abe and A. Yamada, *Chem. Commun.*, 2013, **49**, 11194–11196.
187 T. R. Jow, S. A. Delp, J. L. Allen, J.-P. Jones and M. C. Smart, *J. Electrochem. Soc.*, 2018, **165**, A361–A367.
188 J. Xu, X. Wang, N. Yuan, J. Ding, S. Qin, J. M. Razal, X. Wang, S. Ge and Y. Gogotsi, *Energy Storage Mater.*, 2019, **23**, 383–389.
189 J. Xu, X. Wang, N. Yuan, B. Hu, J. Ding and S. Ge, *J. Power Sources*, 2019, **430**, 74–79.
190 R. Petibon, C. P. Aiken, L. Ma, D. Xiong and J. R. Dahn, *Electrochim. Acta*, 2015, **154**, 287–293.
191 H. Jia, Y. Xu, X. Zhang, S. D. Burton, P. Gao, B. E. Matthews, M. H. Engelhard, K. S. Han, L. Zhong, C. Wang and W. Xu, *Angew. Chem., Int. Ed.*, 2021, **60**, 12999–13006.
192 H. Jia, L. Zou, P. Gao, X. Cao, W. Zhao, Y. He, M. H. Engelhard, S. D. Burton, H. Wang, X. Ren, Q. Li, R. Yi, X. Zhang, C. Wang, Z. Xu, X. Li, J. G. Zhang and W. Xu, *Adv. Energy Mater.*, 2019, **9**, 1900784.
193 J. Chen, X. Fan, Q. Li, H. Yang, M. R. Khoshi, Y. Xu, S. Hwang, L. Chen, X. Ji, C. Yang, H. He, C. Wang, E. Garfunkel, D. Su, O. Borodin and C. Wang, *Nat. Energy*, 2020, **5**, 386–397.
194 Z. Cao, X. Zheng, Q. Qu, Y. Huang and H. Zheng, *Adv. Mater.*, 2021, **33**, e2103178.
195 M. He, C.-C. Su, Z. Feng, L. Zeng, T. Wu, M. J. Bedzyk, P. Fenter, Y. Wang and Z. Zhang, *Adv. Energy Mater.*, 2017, **7**, 1700109.
196 X. Zheng, T. Huang, Y. Pan, W. Wang, G. Fang, K. Ding and M. Wu, *ACS Appl. Mater. Interfaces*, 2017, **9**, 18758–18765.
197 X. J. Wang, H. S. Lee, H. Li, X. Q. Yang and X. J. Huang, *Electrochem. Commun.*, 2010, **12**, 386–389.
198 J. Im, J. Lee, M.-H. Ryou, Y. M. Lee and K. Y. Cho, *J. Electrochem. Soc.*, 2017, **164**, A6381–A6385.
199 Y. X. Yao, X. Chen, C. Yan, X. Q. Zhang, W. L. Cai, J. Q. Huang and Q. Zhang, *Angew. Chem., Int. Ed.*, 2020, **60**, 4090–4097.
200 Y.-G. Cho, M. Li, J. Holoubek, W. Li, Y. Yin, Y. S. Meng and Z. Chen, *ACS Energy Lett.*, 2021, **6**, 2016–2023.
201 S. Klein, S. van Wickeren, S. Röser, P. Bärmann, K. Borzutzki, B. Heidrich, M. Börner, M. Winter, T. Placke and J. Kasnatscheew, *Adv. Energy Mater.*, 2021, **11**, 2003738.
202 Y. Wu, D. Ren, X. Liu, G. L. Xu, X. Feng, Y. Zheng, Y. Li, M. Yang, Y. Peng, X. Han, L. Wang, Z. Chen, Y. Ren, L. Lu, X. He, J. Chen, K. Amine and M. Ouyang, *Adv. Energy Mater.*, 2021, **11**, 2102299.
203 J. Ming, Z. Cao, Y. Wu, W. Wahyudi, W. Wang, X. Guo, L. Cavallo, J.-Y. Hwang, A. Shamim, L.-J. Li, Y.-K. Sun and H. N. Alshareef, *ACS Energy Lett.*, 2019, **4**, 2613–2622.
204 W. Wahyudi, V. Ladelta, L. Tsetseris, M. M. Alsabban, X. Guo, E. Yengel, H. Faber, B. Adilbekova, A. Seitkhan, A. H. Emwas, M. N. Hedhili, L. J. Li, V. Tung, N. Hadjichristidis, T. D. Anthopoulos and J. Ming, *Adv. Funct. Mater.*, 2021, **31**, 2101593.
205 A. O. Tezel, D. K. Streich, A. Guéguen, M. Hahlin, S. Sunde, K. Edström, P. Novák and A. M. Svensson, *J. Electrochem. Soc.*, 2020, **167**, 130504.
206 X. Liu, X. Shen, H. Li, P. Li, L. Luo, H. Fan, X. Feng, W. Chen, X. Ai, H. Yang and Y. Cao, *Adv. Energy Mater.*, 2021, **11**, 2003905.
207 Z. M. Hao-Ran Cheng, Ying-Jun Guo, Chun-Sheng Sun, Qian Li and Jun Ming, *J. Electrochem.*, 2022, **28**, 2219012.
208 P. Xiao, L. Sun, D. Liao, P. O. Agboola, I. Shakir and Y. Xu, *ACS Appl. Mater. Interfaces*, 2018, **10**, 33269–33275.
209 R. Steudel, *Chem. Rev.*, 2002, **102**, 3905–3945.
210 Q. Pang, A. Shyamsunder, B. Narayanan, C. Y. Kwok, L. A. Curtiss and L. F. Nazar, *Nat. Energy*, 2018, **3**, 783–791.
211 M. Barghamadi, A. S. Best, A. I. Bhatt, A. F. Hollenkamp, M. Musameh, R. J. Rees and T. Rüther, *Energy Environ. Sci.*, 2014, **7**, 3902–3920.
212 S. S. Zhang and J. Power, *Sources*, 2013, **231**, 153–162.
213 C. Barchasz, F. Molton, C. Duboc, J. C. Lepretre, S. Patoux and F. Alloin, *Anal. Chem.*, 2012, **84**, 3973–3980.
214 M. Cuisinier, P.-E. Cabelguen, S. Evers, G. He, M. Kolbeck, A. Garsuch, T. Bolin, M. Balasubramanian and L. F. Nazar, *J. Phys. Chem. Lett.*, 2013, **4**, 3227–3232.
215 L. Wang, Q. Li, H. Yang, J. Yang, Y. Nuli and J. Wang, *Chem. Commun.*, 2016, **52**, 14430–14433.
216 H. Yang, Q. Li, C. Guo, A. Naveed, J. Yang, Y. Nuli and J. Wang, *Chem. Commun.*, 2018, **54**, 4132–4135.
217 F. Liu, G. Sun, H. B. Wu, G. Chen, D. Xu, R. Mo, L. Shen, X. Li, S. Ma, R. Tao, X. Li, X. Tan, B. Xu, G. Wang, B. S. Dunn, P. Sautet and Y. Lu, *Nat. Commun.*, 2020, **11**, 5215.
218 S. Nanda, A. Bhargav and A. Manthiram, *Joule*, 2020, **4**, 1121–1135.
219 X. Yang, J. Luo and X. Sun, *Chem. Soc. Rev.*, 2020, **49**, 2140–2195.

220 J. Lian, W. Guo and Y. Fu, *J. Am. Chem. Soc.*, 2021, **143**, 11063–11071.
221 A. Hu, M. Zhou, T. Lei, Y. Hu, X. Du, C. Gong, C. Shu, J. Long, J. Zhu, W. Chen, X. Wang and J. Xiong, *Adv. Energy Mater.*, 2020, **10**, 2002180.
222 S. Li, W. Zhang, J. Zheng, M. Lv, H. Song and L. Du, *Adv. Energy Mater.*, 2020, **11**, 2000779.
223 J. Xie, S. Y. Sun, X. Chen, L. P. Hou, B. Q. Li, H. J. Peng, J. Q. Huang, X. Q. Zhang and Q. Zhang, *Angew. Chem., Int. Ed.*, 2022, **61**, e202204776.
224 D. Aurbach, E. Pollak, R. Elazari, G. Salitra, C. S. Kelley and J. Affinito, *J. Electrochem. Soc.*, 2009, **156**, A694.
225 H.-J. Peng, J.-Q. Huang, X.-B. Cheng and Q. Zhang, *Adv. Energy Mater.*, 2017, **7**, 1700260.
226 S. S. Zhang, *Electrochim. Acta*, 2012, **70**, 344–348.
227 R. D. Rauh, K. M. Abraham, G. F. Pearson, J. K. Surprenant and S. B. Brummer, *J. Electrochem. Soc.*, 1979, **126**, 523–527.
228 C. Yang, L. Suo, O. Borodin, F. Wang, W. Sun, T. Gao, X. Fan, S. Hou, Z. Ma, K. Amine, K. Xu and C. Wang, *Proc. Natl. Acad. Sci. U. S. A.*, 2017, **114**, 6197–6202.
229 Y. V. Mikhaylik and J. R. Akridge, *J. Electrochem. Soc.*, 2004, **151**, A1969.
230 J. T. Lee, Y. Zhao, S. Thieme, H. Kim, M. Oschatz, L. Borchardt, A. Magasinski, W. I. Cho, S. Kaskel and G. Yushin, *Adv. Mater.*, 2013, **25**, 4573–4579.
231 E. S. Shin, K. Kim, S. H. Oh and W. I. Cho, *Chem. Commun.*, 2013, **49**, 2004–2006.
232 J.-W. Park, K. Yamauchi, E. Takashima, N. Tachikawa, K. Ueno, K. Dokko and M. Watanabe, *J. Phys. Chem. C*, 2013, **117**, 4431–4440.
233 J.-W. Park, K. Ueno, N. Tachikawa, K. Dokko and M. Watanabe, *J. Phys. Chem. C*, 2013, **117**, 20531–20541.
234 M. Watanabe, M. L. Thomas, S. Zhang, K. Ueno, T. Yasuda and K. Dokko, *Chem. Rev.*, 2017, **117**, 7190–7239.
235 L. X. Yuan, J. K. Feng, X. P. Ai, Y. L. Cao, S. L. Chen and H. X. Yang, *Electrochem. Commun.*, 2006, **8**, 610–614.
236 N. Tachikawa, K. Yamauchi, E. Takashima, J. W. Park, K. Dokko and M. Watanabe, *Chem. Commun.*, 2011, **47**, 8157–8159.
237 K. Ueno, J.-W. Park, A. Yamazaki, T. Mandai, N. Tachikawa, K. Dokko and M. Watanabe, *J. Phys. Chem. C*, 2013, **117**, 20509–20516.
238 J. Zheng, X. Fan, G. Ji, H. Wang, S. Hou, K. C. DeMella, S. R. Raghavan, J. Wang, K. Xu and C. Wang, *Nano Energy*, 2018, **50**, 431–440.
239 M. Cuisinier, P. E. Cabelguen, B. D. Adams, A. Garsuch, M. Balasubramanian and L. F. Nazar, *Energy Environ. Sci.*, 2014, **7**, 2697–2705.
240 A. Nakanishi, K. Ueno, D. Watanabe, Y. Ugata, Y. Matsumae, J. Liu, M. L. Thomas, K. Dokko and M. Watanabe, *J. Phys. Chem. C*, 2019, **123**, 14229–14238.
241 T. Seita, Y. Matsumae, J. Liu, R. Tatara, K. Ueno, K. Dokko and M. Watanabe, *ACS Energy Lett.*, 2019, **5**, 1–7.
242 M. Yanagi, K. Ueno, A. Ando, S. Li, Y. Matsumae, J. Liu, K. Dokko and M. Watanabe, *J. Electrochem. Soc.*, 2020, **167**, 070531.
243 C. Zhao, A. Daali, I. Hwang, T. Li, X. Huang, D. Robertson, Z. Yang, S. Trask, W. Xu, C. J. Sun, G. L. Xu and K. Amine, *Angew. Chem., Int. Ed.*, 2022, **61**, e202203466.
244 M. L. Gordin, F. Dai, S. Chen, T. Xu, J. Song, D. Tang, N. Azimi, Z. Zhang and D. Wang, *ACS Appl. Mater. Interfaces*, 2014, **6**, 8006–8010.
245 N. Azimi, W. Weng, C. Takoudis and Z. Zhang, *Electrochem. Commun.*, 2013, **37**, 96–99.
246 K. A. See, H. L. Wu, K. C. Lau, M. Shin, L. Cheng, M. Balasubramanian, K. G. Gallagher, L. A. Curtiss and A. A. Gewirth, *ACS Appl. Mater. Interfaces*, 2016, **8**, 34360–34371.
247 C. Zhao, G. L. Xu, T. Zhao and K. Amine, *Angew. Chem., Int. Ed.*, 2020, **59**, 17634–17640.
248 S. Drvarič Talian, S. Jeschke, A. Vizintin, K. Pirnat, I. Arčon, G. Aquilanti, P. Johansson and R. Dominko, *Chem. Mater.*, 2017, **29**, 10037–10044.
249 Y. Chen, Z. Gong and Y. Yang, *J. Electrochem. Soc.*, 2018, **165**, A1915–A1919.
250 F. Huang, G. Ma, Z. Wen, J. Jin, S. Xu and J. Zhang, *J. Mater. Chem. A*, 2018, **6**, 1612–1620.
251 M. Shin, H. L. Wu, B. Narayanan, K. A. See, R. S. Assary, L. Zhu, R. T. Haasch, S. Zhang, Z. Zhang, L. A. Curtiss and A. A. Gewirth, *ACS Appl. Mater. Interfaces*, 2017, **9**, 39357–39370.
252 J. Zheng, G. Ji, X. Fan, J. Chen, Q. Li, H. Wang, Y. Yang, K. C. DeMella, S. R. Raghavan and C. Wang, *Adv. Energy Mater.*, 2019, **9**, 1803774.
253 Z. Han, S. Li, M. Sun, R. He, W. Zhong, C. Yu, S. Cheng and J. Xie, *J. Energy Chem.*, 2022, **68**, 752–761.
254 W. Shin, L. Zhu, H. Jiang, W. F. Stickle, C. Fang, C. Liu, J. Lu and X. Ji, *Mater. Today*, 2020, **40**, 63–71.
255 Z. Yue, H. Dunya, S. Aryal, C. U. Segre and B. Mandal, *J. Power Sources*, 2018, **401**, 271–277.
256 Q. J. Meisner, T. Rojas, N. L. Dietz Rago, J. Cao, J. Bareño, T. Glossmann, A. Hintennach, P. C. Redfern, D. Pahls, L. Zhang, I. D. Bloom, A. T. Ngo, L. A. Curtiss and Z. Zhang, *J. Power Sources*, 2019, **438**, 226939.
257 X. Wang, Y. Tan, G. Shen and S. Zhang, *J. Energy Chem.*, 2020, **41**, 149–170.
258 C. C. Su, M. He, R. Amine and K. Amine, *Angew. Chem., Int. Ed.*, 2019, **58**, 10591–10595.
259 D. Shanmukaraj, S. Lois, S. Fantini, F. Malbosc and M. Armand, *Chem. Mater.*, 2017, **30**, 246–251.
260 J. Chen, K. S. Han, W. A. Henderson, K. C. Lau, M. Vijayakumar, T. Dzwiniel, H. Pan, L. A. Curtiss, J. Xiao, K. T. Mueller, Y. Shao and J. Liu, *Adv. Energy Mater.*, 2016, **6**, 1600160.
261 L.-P. Hou, X.-Q. Zhang, N. Yao, X. Chen, B.-Q. Li, P. Shi, C.-B. Jin, J.-Q. Huang and Q. Zhang, *Chem*, 2022, **8**, 1083–1098.
262 A. Shyamsunder, W. Beichel, P. Klose, Q. Pang, H. Scherer, A. Hoffmann, G. K. Murphy, I. Krossing and L. F. Nazar, *Angew. Chem., Int. Ed.*, 2017, **56**, 6192–6197.
263 A. Gupta, A. Bhargav and A. Manthiram, *ACS Energy Lett.*, 2020, **6**, 224–231.

264 H. Pan, X. Wei, W. A. Henderson, Y. Shao, J. Chen, P. Bhattacharya, J. Xiao and J. Liu, *Adv. Energy Mater.*, 2015, **5**, 1500113.
265 H. Pan, K. S. Han, M. Vijayakumar, J. Xiao, R. Cao, J. Chen, J. Zhang, K. T. Mueller, Y. Shao and J. Liu, *ACS Appl. Mater. Interfaces*, 2017, **9**, 4290–4295.
266 H. Pan, K. S. Han, M. H. Engelhard, R. Cao, J. Chen, J.-G. Zhang, K. T. Mueller, Y. Shao and J. Liu, *Adv. Funct. Mater.*, 2018, **28**, 1707234.
267 Q. Cheng, W. Xu, S. Qin, S. Das, T. Jin, A. Li, A. C. Li, B. Qie, P. Yao, H. Zhai, C. Shi, X. Yong and Y. Yang, *Angew. Chem., Int. Ed.*, 2019, **58**, 5557–5561.
268 H. Shin, M. Baek, A. Gupta, K. Char, A. Manthiram and J. W. Choi, *Adv. Energy Mater.*, 2020, **10**, 2001456.
269 M. Cuisinier, C. Hart, M. Balasubramanian, A. Garsuch and L. F. Nazar, *Adv. Energy Mater.*, 2015, **5**, 1401801.
270 Q. Zou and Y. C. Lu, *J. Phys. Chem. Lett.*, 2016, **7**, 1518–1525.
271 M. Baek, H. Shin, K. Char and J. W. Choi, *Adv. Mater.*, 2020, **32**, e2005022.
272 Y.-C. Lu, Q. He and H. A. Gasteiger, *J. Phys. Chem. C*, 2014, **118**, 5733–5741.
273 H. Chu, H. Noh, Y. J. Kim, S. Yuk, J. H. Lee, J. Lee, H. Kwack, Y. Kim, D. K. Yang and H. T. Kim, *Nat. Commun.*, 2019, **10**, 188.
274 A. Gupta, A. Bhargav and A. Manthiram, *Adv. Energy Mater.*, 2019, **9**, 1803096.
275 Z. Li, Y. Zhou, Y. Wang and Y.-C. Lu, *Adv. Energy Mater.*, 2019, **9**, 1802207.
276 B. Yang, H. Jiang, Y. Zhou, Z. Liang, T. Zhao and Y. C. Lu, *ACS Appl. Mater. Interfaces*, 2019, **11**, 25940–25948.
277 H. Chu, J. Jung, H. Noh, S. Yuk, J. Lee, J. H. Lee, J. Baek, Y. Roh, H. Kwon, D. Choi, K. Sohn, Y. Kim and H. T. Kim, *Adv. Energy Mater.*, 2020, **10**, 2000493.
278 F. Wu, F. Chu, G. A. Ferrero, M. Sevilla, A. B. Fuertes, O. Borodin, Y. Yu and G. Yushin, *Nano Lett.*, 2020, **20**, 5391–5399.
279 N. Zhong, C. Lei, R. Meng, J. Li, X. He and X. Liang, *Small*, 2022, **18**, e2200046.
280 B. Chen, X. Zhong, G. Zhou, N. Zhao and H. M. Cheng, *Adv. Mater.*, 2022, **34**, e2105812.
281 Y. Peng, R. Badam, T. P. Jayakumar, W. Wannapakdee, C. Changtong and N. Matsumi, *J. Electrochem. Soc.*, 2022, **169**, 050515.
282 W. Weng, V. G. Pol and K. Amine, *Adv. Mater.*, 2013, **25**, 1608–1615.
283 H. Yang, C. Guo, J. Chen, A. Naveed, J. Yang, Y. Nuli and J. Wang, *Angew. Chem., Int. Ed.*, 2019, **58**, 791–795.
284 H. Hao, T. Hutter, B. L. Boyce, J. Watt, P. Liu and D. Mitlin, *Chem. Rev.*, 2022, **122**, 8053–8125.
285 T. Liu, J. P. Vivek, E. W. Zhao, J. Lei, N. Garcia-Araez and C. P. Grey, *Chem. Rev.*, 2020, **120**, 6558–6625.
286 K. M. Abraham and Z. Jiang, *J. Electrochem. Soc.*, 1996, **143**, 1–5.
287 L. N. Song, W. Zhang, Y. Wang, X. Ge, L. C. Zou, H. F. Wang, X. X. Wang, Q. C. Liu, F. Li and J. J. Xu, *Nat. Commun.*, 2020, **11**, 2191.
288 P. Wang, Y. Ren, R. Wang, P. Zhang, M. Ding, C. Li, D. Zhao, Z. Qian, Z. Zhang, L. Zhang and L. Yin, *Nat. Commun.*, 2020, **11**, 1576.
289 H. Wang, X. Wang, M. Li, L. Zheng, D. Guan, X. Huang, J. Xu and J. Yu, *Adv. Mater.*, 2020, **32**, e2002559.
290 J. Lai, Y. Xing, N. Chen, L. Li, F. Wu and R. Chen, *Angew. Chem., Int. Ed.*, 2020, **59**, 2974–2997.
291 L. Johnson, C. Li, Z. Liu, Y. Chen, S. A. Freunberger, P. C. Ashok, B. B. Praveen, K. Dholakia, J. M. Tarascon and P. G. Bruce, *Nat. Chem.*, 2014, **6**, 1091–1099.
292 B. D. McCloskey, D. S. Bethune, R. M. Shelby, G. Girishkumar and A. C. Luntz, *J. Phys. Chem. Lett.*, 2011, **2**, 1161–1166.
293 C. O. Laoire, S. Mukerjee, K. M. Abraham, E. J. Plichta and M. A. Hendrickson, *J. Phys. Chem. C*, 2010, **114**, 9178–9186.
294 X. Mu, H. Pan, P. He and H. Zhou, *Adv. Mater.*, 2020, **32**, e1903790.
295 J. Read, *J. Electrochem. Soc.*, 2002, **149**, A1190.
296 J. Read, *J. Electrochem. Soc.*, 2006, **153**, A96.
297 T. Ogasawara, A. Debart, M. Holzapfel, P. Novak and P. G. Bruce, *J. Am. Chem. Soc.*, 2006, **128**, 1390–1393.
298 S. A. Freunberger, Y. Chen, Z. Peng, J. M. Griffin, L. J. Hardwick, F. Barde, P. Novak and P. G. Bruce, *J. Am. Chem. Soc.*, 2011, **133**, 8040–8047.
299 W. Xu, K. Xu, V. V. Viswanathan, S. A. Towne, J. S. Hardy, J. Xiao, Z. Nie, D. Hu, D. Wang and J.-G. Zhang, *J. Power Sources*, 2011, **196**, 9631–9639.
300 W. J. Kwak, Rosy, D. Sharon, C. Xia, H. Kim, L. R. Johnson, P. G. Bruce, L. F. Nazar, Y. K. Sun, A. A. Frimer, M. Noked, S. A. Freunberger and D. Aurbach, *Chem. Rev.*, 2020, **120**, 6626–6683.
301 D. Sharon, D. Hirshberg, M. Afri, A. A. Frimer and D. Aurbach, *Chem. Commun.*, 2017, **53**, 3269–3272.
302 S. A. Freunberger, Y. Chen, N. E. Drewett, L. J. Hardwick, F. Barde and P. G. Bruce, *Angew. Chem., Int. Ed.*, 2011, **50**, 8609–8613.
303 Z. Huang, J. Meng, M. Xie, Y. Shen and Y. Huang, *J. Mater. Chem. A*, 2020, **8**, 14198–14204.
304 Z. Zhang, J. Lu, R. S. Assary, P. Du, H.-H. Wang, Y.-K. Sun, Y. Qin, K. C. Lau, J. Greeley, P. C. Redfern, H. Iddir, L. A. Curtiss and K. Amine, *J. Phys. Chem. C*, 2011, **115**, 25535–25542.
305 D. Sharon, P. Sharon, D. Hirshberg, M. Salama, M. Afri, L. J. W. Shimon, W. J. Kwak, Y. K. Sun, A. A. Frimer and D. Aurbach, *J. Am. Chem. Soc.*, 2017, **139**, 11690–11693.
306 B. D. Adams, R. Black, Z. Williams, R. Fernandes, M. Cuisinier, E. J. Berg, P. Novak, G. K. Murphy and L. F. Nazar, *Adv. Energy Mater.*, 2015, **5**, 1400867.
307 Y. Katayama, H. Onodera, M. Yamagata and T. Miura, *J. Electrochem. Soc.*, 2004, **151**, A59.
308 T. Kuboki, T. Okuyama, T. Ohsaki and N. Takami, *J. Power Sources*, 2005, **146**, 766–769.
309 J. Herranz, A. Garsuch and H. A. Gasteiger, *J. Phys. Chem. C*, 2012, **116**, 19084–19094.
310 M. Piana, J. Wandt, S. Meini, I. Buchberger, N. Tsiouvaras and H. A. Gasteiger, *J. Electrochem. Soc.*, 2014, **161**, A1992–A2001.

311 A. R. Neale, R. Sharpe, S. R. Yeandel, C. H. Yen, K. V. Luzyanin, P. Goddard, E. A. Petrucco and L. J. Hardwick, *Adv. Funct. Mater.*, 2021, **31**, 2010627.
312 U. Ulissi, G. A. Elia, S. Jeong, F. Mueller, J. Reiter, N. Tsiouvaras, Y. K. Sun, B. Scrosati, S. Passerini and J. Hassoun, *ChemSusChem*, 2018, **11**, 229–236.
313 Y. Cai, Q. Zhang, Y. Lu, Z. Hao, Y. Ni and J. Chen, *Angew. Chem., Int. Ed.*, 2021, **60**, 25973–25980.
314 C. Xia, C. Y. Kwok and L. F. Nazar, *Science*, 2018, **361**, 777–781.
315 V. Giordani, D. Tozier, H. Tan, C. M. Burke, B. M. Gallant, J. Uddin, J. R. Greer, B. D. McCloskey, G. V. Chase and D. Addison, *J. Am. Chem. Soc.*, 2016, **138**, 2656–2663.
316 F. Li, T. Zhang, Y. Yamada, A. Yamada and H. Zhou, *Adv. Energy Mater.*, 2013, **3**, 532–538.
317 Y. Liu, L. Suo, H. Lin, W. Yang, Y. Fang, X. Liu, D. Wang, Y.-S. Hu, W. Han and L. Chen, *J. Mater. Chem. A*, 2014, **2**, 9020–9024.
318 Q. Dong, X. Yao, Y. Zhao, M. Qi, X. Zhang, H. Sun, Y. He and D. Wang, *Chem*, 2018, **4**, 1345–1358.
319 X. Bi, M. Li, C. Liu, Y. Yuan, H. Wang, B. Key, R. Wang, R. Shahbazian-Yassar, L. A. Curtiss, J. Lu and K. Amine, *Angew. Chem., Int. Ed.*, 2020, **59**, 22978–22982.
320 B. Liu, W. Xu, P. Yan, X. Sun, M. E. Bowden, J. Read, J. Qian, D. Mei, C.-M. Wang and J.-G. Zhang, *Adv. Funct. Mater.*, 2016, **26**, 605–613.
321 B. Liu, W. Xu, P. Yan, S. T. Kim, M. H. Engelhard, X. Sun, D. Mei, J. Cho, C. M. Wang and J. G. Zhang, *Adv. Energy Mater.*, 2017, **7**, 1602605.
322 Q. Zhao, Y. Zhang, G. Sun, L. Cong, L. Sun, H. Xie and J. Liu, *ACS Appl. Mater. Interfaces*, 2018, **10**, 26312–26319.
323 W.-J. Kwak, S. Chae, R. Feng, P. Gao, J. Read, M. H. Engelhard, L. Zhong, W. Xu and J.-G. Zhang, *ACS Energy Lett.*, 2020, **5**, 2182–2190.
324 Z. Peng, S. A. Freunberger, Y. Chen and P. G. Bruce, *Science*, 2012, **337**, 563–566.
325 N. B. Aetukuri, B. D. McCloskey, J. M. Garcia, L. E. Krupp, V. Viswanathan and A. C. Luntz, *Nat. Chem.*, 2015, **7**, 50–56.
326 A. Khetan, A. Luntz and V. Viswanathan, *J. Phys. Chem. Lett.*, 2015, **6**, 1254–1259.
327 Z. Peng, S. A. Freunberger, L. J. Hardwick, Y. Chen, V. Giordani, F. Barde, P. Novak, D. Graham, J. M. Tarascon and P. G. Bruce, *Angew. Chem., Int. Ed.*, 2011, **50**, 6351–6355.
328 Z. Huang, H. Zeng, M. Xie, X. Lin, Z. Huang, Y. Shen and Y. Huang, *Angew. Chem., Int. Ed.*, 2019, **58**, 2345–2349.
329 S. Feng, M. Huang, J. R. Lamb, W. Zhang, R. Tatara, Y. Zhang, Y. G. Zhu, C. F. Perkinson, J. A. Johnson and Y. Shao-Horn, *Chem*, 2019, **5**, 2630–2641.
330 B. Xie, H. S. Lee, H. Li, X. Q. Yang, J. McBreen and L. Q. Chen, *Electrochem. Commun.*, 2008, **10**, 1195–1197.
331 D. Shanmukaraj, S. Grugeon, G. Gachot, S. Laruelle, D. Mathiron, J. M. Tarascon and M. Armand, *J. Am. Chem. Soc.*, 2010, **132**, 3055–3062.
332 M. J. Trahan, S. Mukerjee, E. J. Plichta, M. A. Hendrickson and K. M. Abraham, *J. Electrochem. Soc.*, 2012, **160**, A259–A267.
333 M. Roberts, R. Younesi, W. Richardson, J. Liu, J. Zhu, K. Edstrom and T. Gustafsson, *ECS Electrochem. Lett.*, 2014, **3**, A62–A65.
334 R. Younesi, P. Norby and T. Vegge, *ECS Electrochem. Lett.*, 2014, **3**, A15–A18.
335 E. Knipping, C. Aucher, G. Guirado and L. Aubouy, *Batteries Supercaps*, 2018, **2**, 200–204.
336 Y. Chen, S. A. Freunberger, Z. Peng, F. Barde and P. G. Bruce, *J. Am. Chem. Soc.*, 2012, **134**, 7952–7957.
337 W. Walker, V. Giordani, J. Uddin, V. S. Bryantsev, G. V. Chase and D. Addison, *J. Am. Chem. Soc.*, 2013, **135**, 2076–2079.
338 B. Zhou, L. Guo, Y. Zhang, J. Wang, L. Ma, W. H. Zhang, Z. Fu and Z. Peng, *Adv. Mater.*, 2017, **29**, 1701568.
339 V. S. Bryantsev, J. Uddin, V. Giordani, W. Walker, D. Addison and G. V. Chase, *J. Electrochem. Soc.*, 2012, **160**, A160–A171.
340 V. S. Bryantsev, V. Giordani, W. Walker, J. Uddin, I. Lee, A. C. T. van Duin, G. V. Chase and D. Addison, *J. Phys. Chem. C*, 2013, **117**, 11977–11988.
341 G. M. Veith, J. Nanda, L. H. Delmau and N. J. Dudney, *J. Phys. Chem. Lett.*, 2012, **3**, 1242–12427.
342 C. M. Burke, V. Pande, A. Khetan, V. Viswanathan and B. D. McCloskey, *Proc. Natl. Acad. Sci. U. S. A.*, 2015, **112**, 9293–9298.
343 X. Gao, Y. Chen, L. Johnson and P. G. Bruce, *Nat. Mater.*, 2016, **15**, 882–888.
344 W.-J. Kwak, D. Hirshberg, D. Sharon, H.-J. Shin, M. Afri, J.-B. Park, A. Garsuch, F. F. Chesneau, A. A. Frimer, D. Aurbach and Y.-K. Sun, *J. Mater. Chem. A*, 2015, **3**, 8855–8864.
345 T. Liu, M. Leskes, W. Yu, A. J. Moore, L. Zhou, P. M. Bayley, G. Kim and C. P. Grey, *Science*, 2015, **350**, 530–533.
346 H. D. Lim, H. Song, J. Kim, H. Gwon, Y. Bae, K. Y. Park, J. Hong, H. Kim, T. Kim, Y. H. Kim, X. Lepro, R. Ovalle-Robles, R. H. Baughman and K. Kang, *Angew. Chem., Int. Ed.*, 2014, **53**, 3926–3931.
347 Z. Liang and Y. C. Lu, *J. Am. Chem. Soc.*, 2016, **138**, 7574–7583.
348 B. J. Bergner, A. Schurmann, K. Peppler, A. Garsuch and J. Janek, *J. Am. Chem. Soc.*, 2014, **136**, 15054–15064.
349 X. Gao, Y. Chen, L. R. Johnson, Z. P. Jovanov and P. G. Bruce, *Nat. Energy*, 2017, **2**, 17118.
350 Y. Chen, S. A. Freunberger, Z. Peng, O. Fontaine and P. G. Bruce, *Nat. Chem.*, 2013, **5**, 489–494.
351 W. R. Torres, S. E. Herrera, A. Y. Tesio, Md Pozo and E. J. Calvo, *Electrochim. Acta*, 2015, **182**, 1118–1123.
352 M. J. Lacey, J. T. Frith and J. R. Owen, *Electrochem. Commun.*, 2013, **26**, 74–76.
353 L. Yang, J. T. Frith, N. Garcia-Araez and J. R. Owen, *Chem. Commun.*, 2015, **51**, 1705–1708.
354 S. Matsuda, K. Hashimoto and S. Nakanishi, *J. Phys. Chem. C*, 2014, **118**, 18397–18400.
355 D. Sun, Y. Shen, W. Zhang, L. Yu, Z. Yi, W. Yin, D. Wang, Y. Huang, J. Wang, D. Wang and J. B. Goodenough, *J. Am. Chem. Soc.*, 2014, **136**, 8941–8946.

356 D. Kundu, R. Black, B. Adams and L. F. Nazar, *ACS Cent. Sci.*, 2015, **1**, 510–515.
357 Q. Wang, D. Zheng, M. E. McKinnon, X.-Q. Yang and D. Qu, *J. Power Sources*, 2015, **274**, 1005–1008.
358 Y. Shao, F. Ding, J. Xiao, J. Zhang, W. Xu, S. Park, J.-G. Zhang, Y. Wang and J. Liu, *Adv. Funct. Mater.*, 2013, **23**, 987–1004.
359 X. Wu, W. Yu, K. Wen, H. Wang, X. Wang, C.-W. Nan and L. Li, *J. Energy Chem.*, 2021, **60**, 135–149.
360 D. Geng, N. Ding, T. S. A. Hor, S. W. Chien, Z. Liu, D. Wuu, X. Sun and Y. Zong, *Adv. Energy Mater.*, 2016, **6**, 1502164.
361 A. Cresce and K. Xu, *Carbon Energy*, 2021, **3**, 721–751.
362 D. Bin, Y. Wen, Y. Wang and Y. Xia, *J. Energy Chem.*, 2018, **27**, 1521–1535.
363 A. Eftekhari, *Adv. Energy Mater.*, 2018, **8**, 1801156.
364 D. Chao, W. Zhou, C. Ye, Q. Zhang, Y. Chen, L. Gu, K. Davey and S. Z. Qiao, *Angew. Chem., Int. Ed.*, 2019, **58**, 7823–7828.
365 Z. Hou, M. Dong, Y. Xiong, X. Zhang, Y. Zhu and Y. Qian, *Adv. Energy Mater.*, 2020, **10**, 1903665.
366 J. Huang, Z. Guo, Y. Ma, D. Bin, Y. Wang and Y. Xia, *Small Methods*, 2019, **3**, 1800272.
367 L. Tian and A. Yuan, *J. Power Sources*, 2009, **192**, 693–697.
368 F. Sauvage, L. Laffont, J. M. Tarascon and E. Baudrin, *J. Power Sources*, 2008, **175**, 495–501.
369 I. B. Stojković, N. D. Cvjetićanin and S. V. Mentus, *Electrochem. Commun.*, 2010, **12**, 371–373.
370 H. Kim, J. Hong, K. Y. Park, H. Kim, S. W. Kim and K. Kang, *Chem. Rev.*, 2014, **114**, 11788–11827.
371 F. Wang, Y. Lin, L. Suo, X. Fan, T. Gao, C. Yang, F. Han, Y. Qi, K. Xu and C. Wang, *Energy Environ. Sci.*, 2016, **9**, 3666–3673.
372 F. Wang, L. Suo, Y. Liang, C. Yang, F. Han, T. Gao, W. Sun and C. Wang, *Adv. Energy Mater.*, 2016, **7**, 1600922.
373 C. Cheng, Z. H. Li, X. Y. Zhan, Q. Z. Xiao, G. T. Lei and X. D. Zhou, *Electrochim. Acta*, 2010, **55**, 4627–4631.
374 C. Wessells, F. La Mantia, H. Deshazer, R. A. Huggins and Y. Cui, *J. Electrochem. Soc.*, 2011, **158**, A352.
375 J. Y. Luo, W. J. Cui, P. He and Y. Y. Xia, *Nat. Chem.*, 2010, **2**, 760–765.
376 A. Cresce, N. Eidson, M. Schroeder, L. Ma, Y. Howarth, C. Yang, J. Ho, R. Dillon, M. Ding, A. Bassett, J. Stanzione, R. Tom, T. Soundappan, C. Wang and K. Xu, *J. Power Sources*, 2020, **469**, 228378.
377 C. Lee, Y. Yokoyama, Y. Kondo, Y. Miyahara, T. Abe and K. Miyazaki, *Adv. Energy Mater.*, 2021, **11**, 2100756.
378 Q. Zheng, S. Miura, K. Miyazaki, S. Ko, E. Watanabe, M. Okoshi, C. P. Chou, Y. Nishimura, H. Nakai, T. Kamiya, T. Honda, J. Akikusa, Y. Yamada and A. Yamada, *Angew. Chem., Int. Ed.*, 2019, **58**, 14202–14207.
379 W. Li, J. R. Dahn and D. S. Wainwright, *Science*, 1994, **264**, 1115–1118.
380 W. Li and J. R. Dahn, *J. Electrochem. Soc.*, 1995, **142**, 1742–1746.
381 W. Li, W. R. McKinnon and J. R. Dahn, *J. Electrochem. Soc.*, 1994, **141**, 2310–2316.
382 L. Suo, O. Borodin, W. Sun, X. Fan, C. Yang, F. Wang, T. Gao, Z. Ma, M. Schroeder, A. von Cresce, S. M. Russell, M. Armand, A. Angell, K. Xu and C. Wang, *Angew. Chem., Int. Ed.*, 2016, **55**, 7136–7141.
383 Y. Yamada, K. Usui, K. Sodeyama, S. Ko, Y. Tateyama and A. Yamada, *Nat. Energy*, 2016, **1**, 16129.
384 S. F. Lux, L. Terborg, O. Hachmöller, T. Placke, H. W. Meyer, S. Passerini, M. Winter and S. Nowak, *J. Electrochem. Soc.*, 2013, **160**, A1694–A1700.
385 L. Suo, D. Oh, Y. Lin, Z. Zhuo, O. Borodin, T. Gao, F. Wang, A. Kushima, Z. Wang, H. C. Kim, Y. Qi, W. Yang, F. Pan, J. Li, K. Xu and C. Wang, *J. Am. Chem. Soc.*, 2017, **139**, 18670–18680.
386 M. R. Lukatskaya, J. I. Feldblyum, D. G. Mackanic, F. Lissel, D. L. Michels, Y. Cui and Z. Bao, *Energy Environ. Sci.*, 2018, **11**, 2876–2883.
387 L. Chen, J. Zhang, Q. Li, J. Vatamanu, X. Ji, T. P. Pollard, C. Cui, S. Hou, J. Chen, C. Yang, L. Ma, M. S. Ding, M. Garaga, S. Greenbaum, H.-S. Lee, O. Borodin, K. Xu and C. Wang, *ACS Energy Lett.*, 2020, **5**, 968–974.
388 J. Xie, Y. Guan, Y. Huang and Y.-C. Lu, *Chem. Mater.*, 2022, **34**, 5176–5183.
389 X. Hou, R. Wang, X. He, T. P. Pollard, X. Ju, L. Du, E. Paillard, H. Frielinghaus, L. C. Barnsley, O. Borodin, K. Xu, M. Winter and J. Li, *Angew. Chem., Int. Ed.*, 2021, **60**, 22812–22817.
390 C. Yang, J. Chen, T. Qing, X. Fan, W. Sun, A. von Cresce, M. S. Ding, O. Borodin, J. Vatamanu, M. A. Schroeder, N. Eidson, C. Wang and K. Xu, *Joule*, 2017, **1**, 122–132.
391 C. Yang, J. Chen, X. Ji, T. P. Pollard, X. Lu, C. J. Sun, S. Hou, Q. Liu, C. Liu, T. Qing, Y. Wang, O. Borodin, Y. Ren, K. Xu and C. Wang, *Nature*, 2019, **569**, 245–250.
392 J. Zhang, C. Cui, P.-F. Wang, Q. Li, L. Chen, F. Han, T. Jin, S. Liu, H. Choudhary, S. R. Raghavan, N. Eidson, A. von Cresce, L. Ma, J. Uddin, D. Addison, C. Yang and C. Wang, *Energy Environ. Sci.*, 2020, **13**, 2878–2887.
393 F. Wang, O. Borodin, M. S. Ding, M. Gobet, J. Vatamanu, X. Fan, T. Gao, N. Eidson, Y. Liang, W. Sun, S. Greenbaum, K. Xu and C. Wang, *Joule*, 2018, **2**, 927–937.
394 J. Chen, J. Vatamanu, L. Xing, O. Borodin, H. Chen, X. Guan, X. Liu, K. Xu and W. Li, *Adv. Energy Mater.*, 2019, **10**, 1902654.
395 P. Jiang, L. Chen, H. Shao, S. Huang, Q. Wang, Y. Su, X. Yan, X. Liang, J. Zhang, J. Feng and Z. Liu, *ACS Energy Lett.*, 2019, **4**, 1419–1426.
396 Y. Shang, N. Chen, Y. Li, S. Chen, J. Lai, Y. Huang, W. Qu, F. Wu and R. Chen, *Adv. Mater.*, 2020, **32**, e2004017.
397 D. Liu, L. Yuan, X. Li, J. Chen, R. Xiong, J. Meng, S. Zhu and Y. Huang, *ACS Appl. Mater. Interfaces*, 2022, **14**, 17585–17593.
398 Z. Ma, J. Chen, J. Vatamanu, O. Borodin, D. Bedrov, X. Zhou, W. Zhang, W. Li, K. Xu and L. Xing, *Energy Storage Mater.*, 2022, **45**, 903–910.
399 J. Xu, X. Ji, J. Zhang, C. Yang, P. Wang, S. Liu, K. Ludwig, F. Chen, P. Kofinas and C. Wang, *Nat. Energy*, 2022, **7**, 186–193.

400 M. Becker, R. S. Kuhnel and C. Battaglia, *Chem. Commun.*, 2019, **55**, 12032–12035.
401 S. Ko, Y. Yamada, K. Miyazaki, T. Shimada, E. Watanabe, Y. Tateyama, T. Kamiya, T. Honda, J. Akikusa and A. Yamada, *Electrochem. Commun.*, 2019, **104**, 106488.
402 P. Jaumaux, X. Yang, B. Zhang, J. Safaei, X. Tang, D. Zhou, C. Wang and G. Wang, *Angew. Chem., Int. Ed.*, 2021, **60**, 19965–19973.
403 Y. Shang, S. Chen, N. Chen, Y. Li, J. Lai, Y. Ma, J. Chen, F. Wu and R. Chen, *Energy Environ. Sci.*, 2022, **15**, 2653–2663.
404 Y. Wang, T. Wang, D. Dong, J. Xie, Y. Guan, Y. Huang, J. Fan and Y.-C. Lu, *Matter*, 2021, **5**, 162–179.
405 L. Droguet, A. Grimaud, O. Fontaine and J. M. Tarascon, *Adv. Energy Mater.*, 2020, **10**, 2002440.
406 O. Borodin, L. Suo, M. Gobet, X. Ren, F. Wang, A. Faraone, J. Peng, M. Olguin, M. Schroeder, M. S. Ding, E. Gobrogge, A. von Wald Cresce, S. Munoz, J. A. Dura, S. Greenbaum, C. Wang and K. Xu, *ACS Nano*, 2017, **11**, 10462–10471.
407 J. Vatamanu and O. Borodin, *J. Phys. Chem. Lett.*, 2017, **8**, 4362–4367.
408 M. S. Ding and K. Xu, *J. Phys. Chem. C*, 2018, **122**, 16624–16629.
409 N. Dubouis, P. Lemaire, B. Mirvaux, E. Salager, M. Deschamps and A. Grimaud, *Energy Environ. Sci.*, 2018, **11**, 3491–3499.
410 J. Lim, K. Park, H. Lee, J. Kim, K. Kwak and M. Cho, *J. Am. Chem. Soc.*, 2018, **140**, 15661–15667.
411 J. Zheng, G. Tan, P. Shan, T. Liu, J. Hu, Y. Feng, L. Yang, M. Zhang, Z. Chen, Y. Lin, J. Lu, J. C. Neuefeind, Y. Ren, K. Amine, L.-W. Wang, K. Xu and F. Pan, *Chem*, 2018, **4**, 2872–2882.
412 S. Han, *RSC Adv.*, 2019, **9**, 609–619.
413 Z. Li, R. Bouchal, T. Mendez-Morales, A. L. Rollet, C. Rizzi, S. Le Vot, F. Favier, B. Rotenberg, O. Borodin, O. Fontaine and M. Salanne, *J. Phys. Chem. B*, 2019, **123**, 10514–10521.
414 J. Hu, H. Guo, Y. Li, H. Wang, Z. Wang, W. Huang, L. Yang, H. Chen, Y. Lin and F. Pan, *Nano Energy*, 2021, **89**, 106413.
415 J. Xu and C. Wang, *J. Electrochem. Soc.*, 2022, **169**, 030530.
416 X. C. Tingzheng Hou, Lu Jiang and Cheng Tang, *J. Electrochem.*, 2022, **28**, 2219007.
417 G. H. Gu, J. Noh, I. Kim and Y. Jung, *J. Mater. Chem. A*, 2019, **7**, 17096–17117.
418 C. Gao, X. Min, M. Fang, T. Tao, X. Zheng, Y. Liu, X. Wu and Z. Huang, *Adv. Funct. Mater.*, 2021, **32**, 2108044.
419 H. Li, Z. Wang, N. Zou, M. Ye, R. Xu, X. Gong, W. Duan and Y. Xu, *Nat. Comput. Sci.*, 2022, **2**, 367–377.
420 M. H. S. Segler, M. Preuss and M. P. Waller, *Nature*, 2018, **555**, 604–610.
421 D. Pfau, J. S. Spencer, A. G. D. G. Matthews and W. M. C. Foulkes, *Phys. Rev. Res.*, 2020, **2**, 033429.
422 J. Hermann, Z. Schatzle and F. Noe, *Nat. Chem.*, 2020, **12**, 891–897.
423 B. Burger, P. M. Maffettone, V. V. Gusev, C. M. Aitchison, Y. Bai, X. Wang, X. Li, B. M. Alston, B. Li, R. Clowes, N. Rankin, B. Harris, R. S. Sprick and A. I. Cooper, *Nature*, 2020, **583**, 237–241.
424 V. L. Deringer, N. Bernstein, G. Csanyi, C. Ben Mahmoud, M. Ceriotti, M. Wilson, D. A. Drabold and S. R. Elliott, *Nature*, 2021, **589**, 59–64.
425 D. Montes de Oca Zapiain, J. A. Stewart and R. Dingreville, *npj Comput. Mater.*, 2021, **7**, 3.
426 B. Jiang, W. E. Gent, F. Mohr, S. Das, M. D. Berliner, M. Forsuelo, H. Zhao, P. M. Attia, A. Grover, P. K. Herring, M. Z. Bazant, S. J. Harris, S. Ermon, W. C. Chueh and R. D. Braatz, *Joule*, 2021, **5**, 3187–3203.
427 K. A. Severson, P. M. Attia, N. Jin, N. Perkins, B. Jiang, Z. Yang, M. H. Chen, M. Aykol, P. K. Herring, D. Fraggedakis, M. Z. Bazant, S. J. Harris, W. C. Chueh and R. D. Braatz, *Nat. Energy*, 2019, **4**, 383–391.
428 P. M. Attia, A. Grover, N. Jin, K. A. Severson, T. M. Markov, Y. H. Liao, M. H. Chen, B. Cheong, N. Perkins, Z. Yang, P. K. Herring, M. Aykol, S. J. Harris, R. D. Braatz, S. Ermon and W. C. Chueh, *Nature*, 2020, **578**, 397–402.
429 G. Rong, X. Zhang, W. Zhao, Y. Qiu, M. Liu, F. Ye, Y. Xu, J. Chen, Y. Hou, W. Li, W. Duan and Y. Zhang, *Adv. Mater.*, 2017, **29**, 1606187.
430 F. Wu and N. Yao, *Nano Energy*, 2015, **11**, 196–210.
431 L. Luo, B. Liu, S. Song, W. Xu, J. G. Zhang and C. Wang, *Nat. Nanotechnol.*, 2017, **12**, 535–539.
432 D. Liu, Z. Shadike, R. Lin, K. Qian, H. Li, K. Li, S. Wang, Q. Yu, M. Liu, S. Ganapathy, X. Qin, Q. H. Yang, M. Wagemaker, F. Kang, X. Q. Yang and B. Li, *Adv. Mater.*, 2019, **31**, e1806620.
433 B. J. Tremolet de Villers, S. M. Bak, J. Yang and S. D. Han, *Batteries Supercaps*, 2021, **4**, 778–784.
434 Y. Wu and N. Liu, *Chem*, 2018, **4**, 438–465.
435 Y. Ji, Z. W. Yin, Z. Yang, Y. P. Deng, H. Chen, C. Lin, L. Yang, K. Yang, M. Zhang, Q. Xiao, J. T. Li, Z. Chen, S. G. Sun and F. Pan, *Chem. Soc. Rev.*, 2021, **50**, 10743–10763.
436 A. M. Tripathi, W. N. Su and B. J. Hwang, *Chem. Soc. Rev.*, 2018, **47**, 736–851.
437 L. Zhang, T. Qian, X. Zhu, Z. Hu, M. Wang, L. Zhang, T. Jiang, J. H. Tian and C. Yan, *Chem. Soc. Rev.*, 2019, **48**, 5432–5453.
438 T. Herl and F. M. Matysik, *ChemElectroChem*, 2020, **7**, 2498–2512.
439 J. Z. Hu, N. R. Jaegers, M. Y. Hu and K. T. Mueller, *J. Phys.: Condens. Matter*, 2018, **30**, 463001.
440 H. Yang, P. Tang, N. Piao, J. Li, X. Shan, K. Tai, J. Tan, H.-M. Cheng and F. Li, *Mater. Today*, 2022, **57**, 279–294.
441 M. Yousaf, U. Naseer, A. Imran, Y. Li, W. Aftab, A. Mahmood, N. Mahmood, X. Zhang, P. Gao, Y. Lu, S. Guo, H. Pan and Y. Jiang, *Mater. Today*, 2022, **58**, 238–274.
442 J. Xie, J. Li, W. Mai and G. Hong, *Nano Energy*, 2021, **83**, 105780.
443 H. Bian, X. Wen, J. Li, H. Chen, S. Han, X. Sun, J. Song, W. Zhuang and J. Zheng, *Proc. Natl. Acad. Sci. U. S. A*, 2011, **108**, 4737–4742.
444 W. Yuan, B. Zhu, X. Y. Li, T. W. Hansen, Y. Ou, K. Fang, H. Yang, Z. Zhang, J. B. Wagner, Y. Gao and Y. Wang, *Science*, 2020, **367**, 428–430.

445 L. Xue, Y. Li, A. Hu, M. Zhou, W. Chen, T. Lei, Y. Yan, J. Huang, C. Yang, X. Wang, Y. Hu and J. Xiong, *Small Struct.*, 2022, **3**, 2100170.
446 M. G. Boebinger, J. A. Lewis, S. E. Sandoval and M. T. McDowell, *ACS Energy Lett.*, 2020, **5**, 335–345.
447 H. Li, S. Guo and H. Zhou, *J. Energy Chem.*, 2021, **59**, 191–211.
448 Y. Cheng, L. Zhang, Q. Zhang, J. Li, Y. Tang, C. Delmas, T. Zhu, M. Winter, M.-S. Wang and J. Huang, *Mater. Today*, 2021, **42**, 137–161.
449 J. Gao, M. Yoshio, L. Qi and H. Wang, *J. Power Sources*, 2015, **278**, 452–457.
450 T. Liu, L. Lin, X. Bi, L. Tian, K. Yang, J. Liu, M. Li, Z. Chen, J. Lu, K. Amine, K. Xu and F. Pan, *Nat. Nanotechnol.*, 2019, **14**, 50–56.
451 H. Bulter, F. Peters, J. Schwenzel and G. Wittstock, *Angew. Chem., Int. Ed.*, 2014, **53**, 10531–10535.
452 E. Ventosa, P. Wilde, A. H. Zinn, M. Trautmann, A. Ludwig and W. Schuhmann, *Chem. Commun.*, 2016, **52**, 6825–6828.
453 Y. Chen, Q. He, Y. Mo, W. Zhou, Y. Zhao, N. Piao, C. Liu, P. Xiao, H. Liu, B. Li, S. Chen, L. Wang, X. He, L. Xing and J. Liu, *Adv. Energy Mater.*, 2022, **12**, 2201631.
454 C. Niu, H. Lee, S. Chen, Q. Li, J. Du, W. Xu, J.-G. Zhang, M. S. Whittingham, J. Xiao and J. Liu, *Nat. Energy*, 2019, **4**, 551–559.
455 S. Chen, C. Niu, H. Lee, Q. Li, L. Yu, W. Xu, J.-G. Zhang, E. J. Dufek, M. S. Whittingham, S. Meng, J. Xiao and J. Liu, *Joule*, 2019, **3**, 1094–1105.
456 S. Chen, F. Dai and M. Cai, *ACS Energy Lett.*, 2020, **5**, 3140–3151.
457 P. A. Nelson, S. Ahmed, K. G. Gallagher and D. W. Dees, Argonne National Lab, 2019, ANL/CSE-19/2, DOI: **10.2172/1503280**.
458 J. Liu, Z. Bao, Y. Cui, E. J. Dufek, J. B. Goodenough, P. Khalifah, Q. Li, B. Y. Liaw, P. Liu, A. Manthiram, Y. S. Meng, V. R. Subramanian, M. F. Toney, V. V. Viswanathan, M. S. Whittingham, J. Xiao, W. Xu, J. Yang, X.-Q. Yang and J.-G. Zhang, *Nat. Energy*, 2019, **4**, 180–186.
459 L. Xu, Y. Lu, C. Z. Zhao, H. Yuan, G. L. Zhu, L. P. Hou, Q. Zhang and J. Q. Huang, *Adv. Energy Mater.*, 2020, **11**, 2002360.
460 M. Zhao, B. Q. Li, X. Q. Zhang, J. Q. Huang and Q. Zhang, *ACS Cent. Sci.*, 2020, **6**, 1095–1104.
461 R. Fang, S. Zhao, Z. Sun, D. W. Wang, H. M. Cheng and F. Li, *Adv. Mater.*, 2017, **29**, 1606823.
462 S. Xia, X. Wu, Z. Zhang, Y. Cui and W. Liu, *Chem*, 2019, **5**, 753–785.
463 D. W. McOwen, D. M. Seo, O. Borodin, J. Vatamanu, P. D. Boyle and W. A. Henderson, *Energy Environ. Sci.*, 2014, **7**, 416–426.
464 A. Abouimrane, J. Ding and I. J. Davidson, *J. Power Sources*, 2009, **189**, 693–696.
465 K. Matsumoto, K. Inoue, K. Nakahara, R. Yuge, T. Noguchi and K. Utsugi, *J. Power Sources*, 2013, **231**, 234–238.
466 C. Luo, Y. Li, W. Sun, P. Xiao, S. Liu, D. Wang and C. Zheng, *Electrochim. Acta*, 2022, **419**, 140353.
467 J. Han, L. Kiss, H. Mei, A. M. Remete, M. Ponikvar-Svet, D. M. Sedgwick, R. Roman, S. Fustero, H. Moriwaki and V. A. Soloshonok, *Chem. Rev.*, 2021, **121**, 4678–4742.

